Minimizing Residual Vibration of a Linear System Using Appropriately Shaped Forcing Functions

by

PETER HEINRICH MECKL

BSME, Northwestern University
(1981)

SUBMITTED TO THE DEPARTMENT OF
MECHANICAL ENGINEERING IN
PARTIAL FULFILLMENT OF THE
REQUIREMENTS FOR THE DEGREE OF

MASTER OF SCIENCE IN MECHANICAL ENGINEERING

at the

MASSACHUSETTS INSTITUTE OF TECHNOLOGY

May 1984

Signature of Author_____
Department of Mechanical Engineering
May 1984

Certified by_____
Warren Paul Seering
Thesis Supervisor

Accepted by_____
Warren Max Rohsenow
Chairman, Departmental Graduate Committee

Minimizing Residual Vibration of a Linear System Using Appropriately Shaped Forcing Functions

by

PETER HEINRICH MECKL

Submitted to the Department of Mechanical Engineering
May 1984 in partial fulfillment of the
requirements for the Degree of Master of Science in
Mechanical Engineering

ABSTRACT

This paper derives two alternative forcing functions to drive a dynamic system so as to generate minimal residual vibration, using open-loop control. A simple three-mass system with springs is used as an idealized model of a general dynamic system. First, the bang-bang function is derived, which gives time-optimal response. Formulas for determining the required number of switches and their location are developed. Second, a ramped sinusoid function is constructed, which has zero slope at beginning and end, whose harmonics can be added together for faster move times.

These two functions are then compared with respect to residual vibration amplitude in the presence of parameter errors, and with respect to move times to traverse the same displacement. A test fixture to evaluate these functions is described and experimental results are given. The effect of system damping is briefly explored and the importance of accurately determining the fundamental resonant frequency of the system is stressed. In practice, both functions achieve nearly an order-of-magnitude reduction in residual vibration amplitude as compared to a square wave forcing function.

Thesis Supervisor: Warren Paul Seering
Title: Associate Professor of Mechanical Engineering

Dedicated to my loving parents ...

ACKNOWLEDGEMENTS

This paper describes research done at the Artificial Intelligence Laboratory of the Massachusetts Institute of Technology. Support for the laboratory's artificial intelligence research is provided in part by the Office of Naval Research contract N00014-77-C-0389 and in part by the System Development Foundation.

I would like to extend my sincere gratitude to Dr. Warren Seering, who inspired me to come up with answers, rather than give me his own. I wish to thank Ken Pasch for the many brainstorming sessions late into the night which often bore the seed of a new approach. And I sincerely thank the members of the Acoustics and Vibration/Machine Dynamics Laboratory and those of the Artificial Intelligence Laboratory for their suggestions and the many times they have listened to my problems and helped me find new solutions. I also extend heartfelt thanks to my friend Marie for her infinite patience while I was completing this document.

Table of Contents

Table 1.1: Definition of Symbols

$\mathbf{A}$:	state matrix
A_l:	weighting coefficients of ramped sinusoids
$\mathbf{b}$:	control input weighting vector
b_1,b_2:	viscous damping coefficients
B_l:	dimensionless weighting coefficients of ramped sinusoids
c_1,c_2,c_3,c_4:	integrating constants of adjoint system
C_1,C_2,C_3:	modal weighting coefficients of u
da:	residual acceleration half-amplitude of m_1
da^*:	dimensionless residual acceleration half-amplitude of m_1
f:	friction opposing force
F:	peak force exerted on mass m_3
F^*:	dimensionless force
$\mathcal{F}(\omega)$:	Fourier transform of forcing function
$\mathcal{F}^*(\omega)$:	dimensionless Fourier transform magnitude
i:	motor current
I_r,I_{rl}:	dimensionless integral expressions
j:	imaginary number: $j = \sqrt{-1}$
J,J_1,J_2,J_3:	rotational inertias
k:	subscript for resonant frequencies
k_1,k_2:	stiffness
K,K_1,K_2:	rotational stiffnesses
K_t:	motor torque constant
l:	index of ramped sinusoid terms
L:	max number of ramped sinusoid terms added
m:	subscript for switch times
m_1,m_2,m_3:	masses
n:	number of states
N:	number of masses
SF:	scale factor to normalize ramped sinsoid series
t:	time
t':	time $t > T_f$
t_1,t_2,...:	bang-bang switch times

T_f: final time required to move the distance x_f

T_s: time required to move x_f when forced by square wave

T: motor torque

u: forcing function exerted on m_3

u_1,u_2,u_3: modal forcing function inputs

$\mathbf{x}$: state vector

$\mathbf{x}^o$: initial state vector

x_1,x_2,x_3: positions of m_1,m_2,m_3 respectively

x_f: final distance traveled by m_1

x_r: position of rigid body mode

$\dot{x}_1$: velocity of m_1

$\ddot{x}_1$: acceleration of m_1

$\dot{x}_1^*$: dimensionless velocity of m_1

$\ddot{x}_1^*$: dimensionless acceleration of m_1

y_1,y_2,y_3: modal coordinate positions

$\dot{y}_1,\dot{y}_2,\dot{y}_3$: modal coordinate velocities

$\ddot{y}_1,\ddot{y}_2,\ddot{y}_3$: modal coordinate accelerations

z: variable for boundary value problem

z': first time derivative of z

z'': second time derivative of z

z^{IV}: fourth time derivative of z

α,α_l: dimensionless characteristic number

β: weighting coefficient in switching function

γ: weighting coefficient in switching function

Γ: ratio of ramped sinusoid to square wave move time

ς: damping ratio

η: adjoint system coordinate vector

η^o: initial adjoint system vector

λ,λ_l: characteristic numbers for ramped sinusoids

φ: damping phase angle

ϕ_1,ϕ_2: phase angles in switching function

Φ,Φ_l:	characteristic function
Φ_l^*:	dimensionless characteristic function
ω_2:	fundamental resonant frequency
ω_3:	second natural frequency
ω_{d2}:	damped natural frequency
ωdt_1:	difference between $\omega T_f/2$ and ωt_1
ωdt_2:	difference between $\omega T_f/2$ and ωt_2
ω_r:	ratio of second natural frequency to fundamental
ωt:	dimensionless time
ωt_1,ωt_2,...:	dimensionless bang-bang switch times
ωT_f:	dimensionless final time
ωT_s:	dimensionless square wave final time

Table 1.2: Definition of Dimensionless Parameters

$$B_l = \frac{T_f^2 A_l}{F}$$

$$da^* = \frac{(m_1 + m_2 + m_3)\, da}{F}$$

$$F^* = \frac{F}{(m_1 + m_2 + m_3) x_f \omega_2^2}$$

$$\mathcal{F}^*(\omega) = \frac{|\mathcal{F}(\omega)|}{F T_s}$$

$$I_r^* = \frac{I_r}{T_f^3}$$

$$I_{rl}^* = \frac{I_{rl}}{T_f^5}$$

$$x^* = \frac{x}{x_f}$$

$$\dot{x}^* = \frac{\dot{x}}{x_f \omega_2}$$

$$\ddot{x}^* = \frac{\ddot{x}}{x_f \omega_2^2}$$

$$\alpha = \lambda T_f$$

$$\Phi_l^* = \lambda_l^2 \Phi_l$$

$$\omega_r = \frac{\omega_3}{\omega_2}$$

$$\omega dt_1 = \omega T_f/2 - \omega t_1$$

$$\omega dt_2 = \omega T_f/2 - \omega t_2$$

$$\omega t = \omega_2 t$$

$$\omega t_1 = \omega_2 t_1, \quad \omega t_2 = \omega_2 t_2, \ \ldots$$

$$\omega T_f = \omega_2 T_f$$

$$\omega T_s = \omega_2 T_s$$

Chapter 1.

Introduction

Industrial robots have been proposed to perform simple assembly tasks but in order to compete with human labor they need to operate more quickly and more accurately. Subject to design constraints, robots could be moved faster, but with the low first mode resonant frequencies found on most production robots, this would lead to excessive structural vibration, which would persist at the end of the move. One could stiffen the structural elements of the manipulator but this would invariably mean larger actuators at higher cost. The solution proposed here is to appropriately shape the forcing function generated by the actuator so as to minimize the amplitude of residual vibration at the end of a move. In this way, the manipulator can be moved from point to point as fast as the actuators allow and come to rest at the end of the move without any time wasted waiting for the endpoint to settle.

Throughout this analysis, strictly open loop control will be used. The rationale is to study the endpoint vibration problem separately from the control problem to gain insight into the characteristics of appropriately shaped forcing functions which attenuate residual vibration. Such functions can then be employed in a closed loop control system designed to reduce the effect of disturbances and parameter variations.

Previous work has been done in this area of open loop vibration control, mainly for reorientation of satellites and spacecraft. Both distributed and lumped models

have been used to describe the systems. Usually the concern is residual vibration of elastic appendages such as antennae or solar panels after the system undergoes a rotation and stops. Of paramount importance is the accuracy of the reorientation, not necessarily the speed.

Several papers have proposed solutions to this problem by appropriately shaping the forcing function. Aspinwall [1] uses a finite Fourier expansion for the forcing function and then proceeds to pick coefficients to reduce the peaks of the frequency spectrum at discrete points. This only eliminates a few of the peaks and leaves some modes excited. In addition, the resulting move time for a given peak force is longer than it could be with proper selection of a time-optimal forcing function. Swigert [2] succeeds in deriving an appropriate shaped torque which not only minimizes residual vibration but also minimizes the effect of parameter variations which change the modal frequencies. But, again, the forcing function is not time-optimal for the given peak torque. Sangveraphunsiri and Book [3] actually use a time-optimal bang-bang function to control a simple flexible arm with one vibrating mode. But the numerical procedure to determine the switch times is cumbersome and does not always converge, even in this simple case. An alternative approach will be discussed here which easily extends to systems with many vibrating modes.

Another approach has been to use closed loop control to achieve the desired response of spacecraft by feeding back discrete modal components. Lin [4] investigates four alternative methods to derive output variable feedback. Meirovitch [5], Balas [6][7], Turner [8], and Caglayan [9] present techniques that permit representing an infinitely dimensional distributed system by decoupled modal components. Gran [10], Joshi [11], Skelton [12], and Gibson [13] describe methods for reducing the order of the state estimator which is required to obtain all the modes. Sesak [14], Balas [15], and Strunce [16] present suppression techniques which reduce some of the modeling errors of the state estimator. Johnson [17], Benhabib [18] and Potter [19] use adaptive control to improve the lumped parameter model of the spacecraft. Book [20] uses a frequency domain, distributed parameter model to update a low

order modal state variable model in a conventional state variable control design. Gupta and Lyons [21] use frequency shaping techniques to prevent excitation of unmodeled modes. All of these methods control at least some of the vibration modes in a structure with varying degrees of success. The major drawback of these closed-loop control schemes is that they require considerable computation in real time and can only deal with vibration after it is sensed, which means invariably sub-time-optimal response.

In this paper, two types of functions will be derived which reduce residual vibration while, in addition, driving the system as quickly as possible. A multi-switch bang-bang function will be developed to achieve time-optimal control. Then a series of harmonics of ramped sinusoids will be derived which bound the vibration at the end of the move. These two functions are compared in terms of residual vibration amplitude due to parameter variations and in total time to complete the move. A test fixture to verify the utility of these functions is described and experimental results are presented. Comparisons are made between simulation results and experimental data and the effect of damping present in the real system is briefly considered. Finally, precise determination of the actual fundamental frequency gives forcing functions which produce considerably less residual vibration.

Chapter 2.

Time-Optimal Bang-Bang Solution

2.1. Model

In order to derive the appropriate time-optimal solution to the problem of residual vibration, it is first necessary to establish a model of the system under investigation. A three mass, two spring model is used here as a simple representation of a three-axis cartesian robot (Fig. 2.1).

The main source of vibration in such a manipulator is the moving structure. In the model, the lumped masses represent the inertias of the moving parts, while the springs represent the stiffness of the structure. Such a model is designed to study the problem of moving the endpoint using the actuator farthest removed from it,

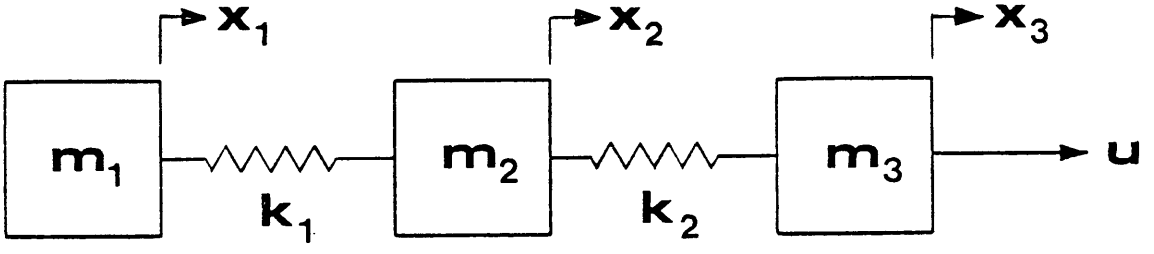

Figure 2.1: Model

with the intermediate links contributing the lumped masses and springs. Damping is initially neglected to provide a worst case vibration amplitude and to simplify the analysis.

In order to provide general results which apply for any set of parameters, all the variables of interest have been nondimensionalized. Table 1.1 defines all the symbols used throughout this paper, including the parameters which are used to nondimensionalize. Table 1.2 gives expressions defining all the dimensionless parameters.

For a system which can be represented by this simple model, and which consists of actuators with peak force limits, a bang-bang solution is time-optimal. This means the fastest response time is achieved when the actuator always generates peak force of either positive or negative magnitude. This idea was put in practice long before it was rigorously proven to be optimal by mathematicians, notably Bellman [22] and La Salle [23]. They showed that such a function will be time-optimal only for certain types of systems, namely those for which all the modes are controllable at all times. This condition is satisfied by the model chosen here since the springs transfer the driving force to all the masses. Controllability is rigorously proven for this system in Appendix A. Thus for this system the bang-bang function will provide optimal move times with zero residual vibration.

2.2. Number of Switches

Having narrowed the choice of candidate functions to a set which always maintains peak force, all that remains to be determined is the number of switches and their precise timing. For a system with all real poles, at most $n-1$ switches are necessary to reach the final state, where n is the system order, here simply twice the number of masses. This can be rigorously proven [24]. But no general statement can be made about a system which has complex poles and oscillatory behavior. Therefore it is necessary to look at the specifics of the system being studied here

in an attempt to determine the fewest switches needed to arrive at the endpoint without residual vibration. Such a determination is much simpler to make if the three-mass system is broken into its modal components. Since damping is absent, this can always be done using an appropriate coordinate transformation [25][26]. For three masses, the result is three subsystems, one the rigid body mode in pure translation, the other two in pure oscillation at frequencies ω_2 and ω_3. A new set of three independent differential equations in the new modal coordinates y_1, y_2, y_3 now fully describes the system,

$$\ddot{y}_1 = u_1 = C_1 u \tag{2.1}$$

$$\ddot{y}_2 + \omega_2^2 y_2 = u_2 = C_2 u \tag{2.2}$$

$$\ddot{y}_3 + \omega_3^2 y_3 = u_3 = C_3 u \tag{2.3}$$

where u_1, u_2, and u_3 are related to the applied forcing function u by the constants C_1, C_2, and C_3.

Solutions to these equations can be illustrated graphically using phase planes for each subsystem, plotting y_1 vs. $\dot{y}_1$ for equation (2.1) and ωy vs. $\dot{y}$ for equations (2.2) and (2.3). For translation, phase plots become parabolas, as shown in Fig. 2.2(a), while for oscillation, they are circles with centers at $-1/\omega$ or $+1/\omega$ depending on whether the applied force is negative or positive (Fig. 2.2(b)).

As Fig. 2.2(a) makes clear, the fastest way to arrive at any desired destination for pure translation is to switch once at the halfway point. Symmetry is required to stop the system at the end of the move. This suggests letting the system build up maximum speed before reversing the force and slowing it down. However, if both of the other two subsystems are also to be stopped at the end of the move, Figure 2.2(b) suggests something more is necessary. Because positive velocity must cause a positive change in position, the circles in these phase plots are traversed clockwise. The trajectory starts at the origin and, if vibration is to be stopped, must return to the origin. Each revolution represents one resonant period, $\omega t = 2\pi$.

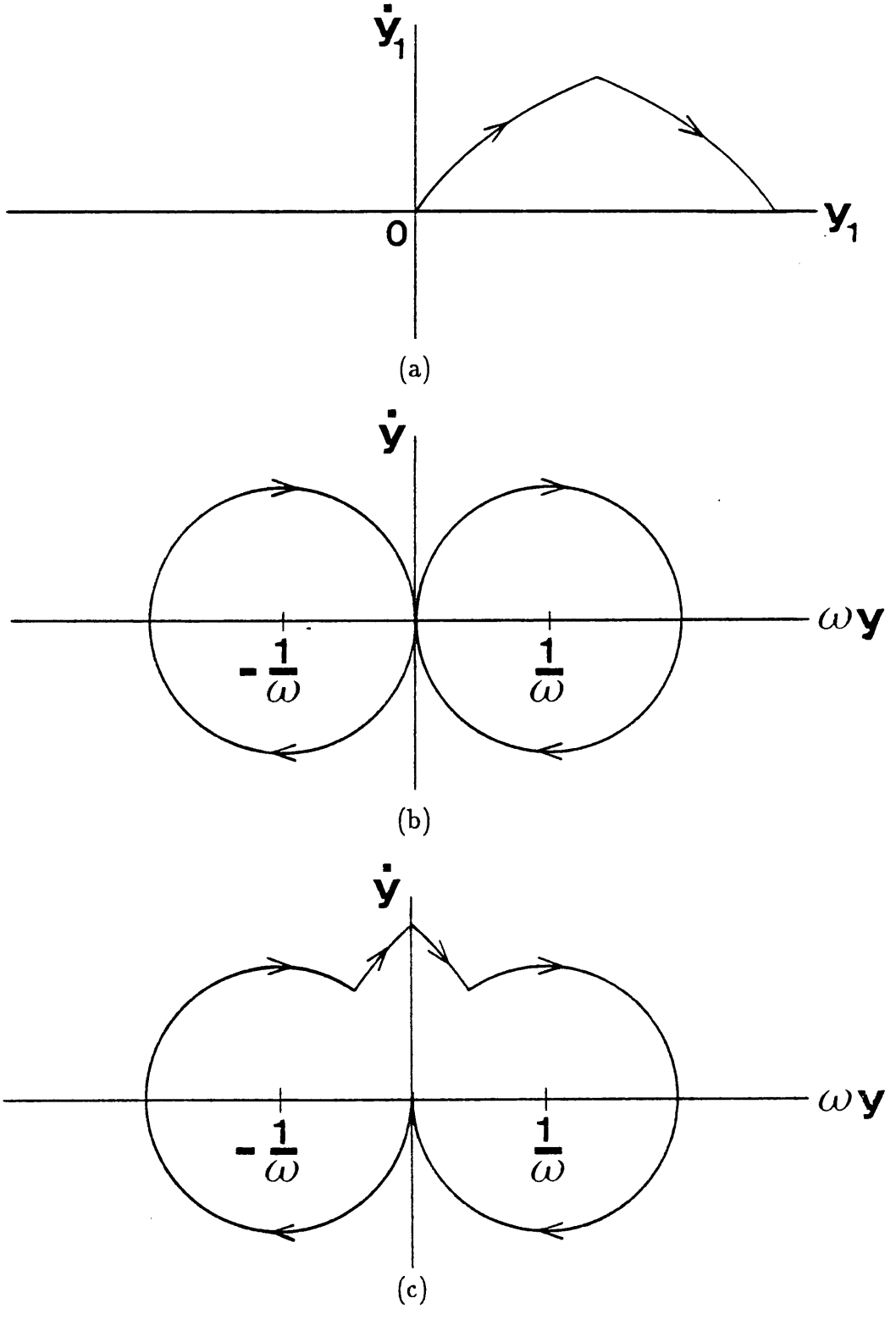

Figure 2.2: Phase Plane Plots:(a) Translation.(b) Oscillation.(c) Multiple Switches.

If the force is switched only once, it must be done when both oscillating subsystems are at the origin so that during the second half of the move, an identical rotation occurs about the second center to arrive back at the origin at the end of the move. In order to satisfy this requirement, the total travel time T_f must be such that a whole number of rotations occurs about each center for each oscillating system. Thus, ωT_f must be an integral multiple of 4π, since at least two rotations are required, one about each center. Then T_f must be an integral multiple of both $4\pi/\omega_2$ and $4\pi/\omega_3$ for a square wave to return the system to the origin without residual vibration. Clearly this will only occur for very few combinations of T_f, $4\pi/\omega_2$, and $4\pi/\omega_3$.

For a general move, one method to arrive at the origin of each subsystem is to switch more frequently. This can be visualized in the phase plane, noting that time is represented as the angle of rotation about the force points. If two additional switches occur symmetrically about the center switch, which must occur on the $\dot{y}$-axis, the required combination of total angles traveled on each arc can be adjusted to any T_f. This is shown in Fig. 2.2(c). With more than one oscillating subsystem, each can be made to return to the origin if one set of switches is introduced for each mode considered. With symmetry about the $\dot{y}$-axis, each switch is accompanied by its reflected twin about $t = T_f/2$. Thus every additional oscillating mode must introduce one more pair of switches symmetrical about the midpoint. For one translating mode and $N-1$ oscillating modes, where N is the number of lumped masses, a minimum of $2(N-1)+1 = 2N-1$ switches is necessary to bring the system to rest. This is exactly the number which is required , in general, for a non-oscillating system.

2.3. Calculation of Switch Times

The desired bang-bang function thus requires 5 switches for the three-mass model. Those switch times must be determined in order to uniquely define the

forcing function. In the time-optimal control literature, two distinctly different methods of locating the switch points are discussed. One technique is to determine the forcing function directly as a function of the system states, which allows a state-variable feedback control system design. This is usually done with reference to the phase plane by locating the switching surfaces. Such a determination is relatively simple for a second-order system of complex poles or some simple third and fourth-order systems with real poles. Bushaw [27] treats the second-order case while Ryan [28] deals with several third and fourth-order systems. Athanassiades and O. Smith [29] derive equations for the switching hypersurfaces of higher-order systems with real poles, and then use a nonlinear computer to determine the switches in real time based on the current system state. Feedback of the actual position locates a point in phase space with respect to these switching surfaces which specifies the sign of the control force. Another approach is to determine a set of equations as functions of the switch times. F. Smith [30] and Lee [31] use a nonphase space method to generate this set of transcendental equations whose solution gives the switch times. These are then solved to generate each new switch time based on current initial conditions measured on the real system. Thus the system operates as a series of open-loop control intervals, updated to compensate for variations in the real system at every switch. Unfortunately, these sets of equations are difficult to solve in general for higher-order systems. An easier derivation follows from the modal decomposition.

The modal equations can be used to derive expressions for the 5 switch times as well as the total travel time T_f in terms of the desired move distance. Since the resultant forcing function can be considered as a sum of step functions each delayed in time and alternating in sign and since the system is linear, the total response is simply the sum of responses for each step. Referring to the second mode differential equation,

$$\ddot{y}_2 + \omega_2^2 y_2 = 1 \tag{2.4}$$

$$y_2(0) = 0,\ \dot{y}_2(0) = 0$$

and solving gives

$$y_2(t) = \frac{1}{\omega_2^2}(1 - \cos\omega_2 t). \tag{2.5}$$

This expression gives the response to a single step. With the switch times numbered in ascending order for increasing time ($t_1 < t_2 < t_3 = T_f/2 < t_4 < t_5 < t_6 = T_f$), the total response at time $t' > T_f$ is given by

$$\begin{aligned} y_2(t') = \frac{1}{\omega_2^2}\Big[&\big(1 - \cos\omega_2 t'\big) - 2\big(1 - \cos\omega_2(t' - t_1)\big) + 2\big(1 - \cos\omega_2(t' - t_2)\big) \\ &- 2\big(1 - \cos\omega_2(t' - T_f/2)\big) + 2\big(1 - \cos\omega_2(t' - t_4)\big) \\ &- 2\big(1 - \cos\omega_2(t' - t_5)\big) + \big(1 - \cos\omega_2(t' - T_f)\big)\Big] = 0 \end{aligned} \tag{2.6}$$

where $y_2(t') = 0$ for all time $t' > T_f$ implies that no more oscillation occurs at the end of the move. Simplifying yields:

$$\begin{aligned} &\cos\omega_2 t'\big[1 - 2\cos\omega_2 t_1 + 2\cos\omega_2 t_2 - 2\cos(\omega_2 T_f/2) \\ &\qquad + 2\cos\omega_2 t_4 - 2\cos\omega_2 t_5 + \cos\omega_2 T_f\big] \\ &+ \sin\omega_2 t'\big[-2\sin\omega_2 t_1 + 2\sin\omega_2 t_2 - 2\sin(\omega_2 T_f/2) \\ &\qquad + 2\sin\omega_2 t_4 - 2\sin\omega_2 t_5 + \sin\omega_2 T_f\big] = 0. \end{aligned} \tag{2.7}$$

For this to be true for all t', both expressions in brackets must be zero. Thus,

$$\begin{aligned} &1 - 2\cos\omega_2 t_1 + 2\cos\omega_2 t_2 - 2\cos(\omega_2 T_f/2) \\ &\quad + 2\cos\omega_2 t_4 - 2\cos\omega_2 t_5 + \cos\omega_2 T_f = 0 \end{aligned} \tag{2.8}$$

$$\begin{aligned} &- 2\sin\omega_2 t_1 + 2\sin\omega_2 t_2 - 2\sin(\omega_2 T_f/2) \\ &\quad + 2\sin\omega_2 t_4 - 2\sin\omega_2 t_5 + \sin\omega_2 T_f = 0. \end{aligned} \tag{2.9}$$

The same result follows for the third mode, with ω_2 replaced by ω_3:

$$\begin{aligned} &1 - 2\cos\omega_3 t_1 + 2\cos\omega_3 t_2 - 2\cos(\omega_3 T_f/2) \\ &\quad + 2\cos\omega_3 t_4 - 2\cos\omega_3 t_5 + \cos\omega_3 T_f = 0 \end{aligned} \tag{2.10}$$

$$- 2\sin\omega_3 t_1 + 2\sin\omega_3 t_2 - 2\sin(\omega_3 T_f/2)$$
$$+ 2\sin\omega_3 t_4 - 2\sin\omega_3 t_5 + \sin\omega_3 T_f = 0 \qquad (2.11)$$

For a system consisting of N masses, these equations can be written down simply by inspection,

$$\cos\omega_k t_0 - 2\cos\omega_k t_1 + 2\cos\omega_k t_2 - \cdots$$
$$- 2\cos\omega_k t_{2N-1} + \cos\omega_k t_{2N} = 0 \qquad (2.12)$$

$$\sin\omega_k t_0 - 2\sin\omega_k t_1 + 2\sin\omega_k t_2 - \cdots$$
$$- 2\sin\omega_k t_{2N-1} + \sin\omega_k t_{2N} = 0 \qquad (2.13)$$

for $2 \leq k \leq N$, since $\omega_1 = 0$. Using $t_0 = 0$ eliminates one of the unknowns. From the symmetry considerations cited earlier,

$$t_N = t_{2N}/2 = T_f/2 \qquad (2.14)$$

and

$$t_m = t_{2N} - t_{2N-m} = T_f - t_{2N-m} \qquad (N+1 \leq m < 2N). \qquad (2.15)$$

Since the expressions in sin and cos give the same information, there will be $N-1$ transcendental equations in t_m, $N-1$ linear symmetry constraints and one expression for the central switch point. This gives a total of $2N-1$ equations in $2N$ unknowns. One more equation is needed to relate T_f to x_f, the final move distance. This can be obtained from the rigid body mode, summing responses as before for the individual steps.

Since all three masses move together in the rigid body mode, x_r represents the distance moved by a rigid body of total mass $(m_1 + m_2 + m_3)$. The equation to be solved is

$$\ddot{x}_r = \frac{F}{(m_1 + m_2 + m_3)} \qquad (2.16)$$

with initial conditions

$$x_r(0) = 0,\ \dot{x}_r(0) = 0$$

and x_r is given by

$$x_r(t) = \frac{Ft^2}{2(m_1 + m_2 + m_3)}. \tag{2.17}$$

For the combined steps,

$$x_r(T_f) = \frac{F}{2(m_1 + m_2 + m_3)}\Big[T_f^2 - 2(T_f - t_1)^2 + 2(T_f - t_2)^2 - 2(T_f - T_f/2)^2 + 2(T_f - t_4)^2 - 2(T_f - t_5)^2\Big]. \tag{2.18}$$

Since $x_r(T_f)$ is defined to be x_f, the resultant expression relating x_f and T_f is:

$$(m_1 + m_2 + m_3)x_f = \frac{F}{2}\Big[T_f^2 - 2(T_f - t_1)^2 + 2(T_f - t_2)^2 - 2(T_f - T_f/2)^2 + 2(T_f - t_4)^2 - 2(T_f - t_5)^2\Big]. \tag{2.19}$$

In general, this equation can be written as

$$(m_1 + m_2 + \cdots + m_N)x_f = \frac{F}{2}\Big[(t_{2N} - t_0)^2 - 2(t_{2N} - t_1)^2 + 2(t_{2N} - t_2)^2 - \cdots - 2(t_{2N} - t_{2N-1})^2\Big] \tag{2.20}$$

where again $t_0 = 0$ and $t_{2N} = T_f$.

Thus in general $2N$ equations in $2N$ unknown switch times result, where N equations are simultaneous nonlinear equations that must be solved numerically, and N equations are linear and simply involve substitution into the nonlinear equations.

For generality, these equations can also be nondimensionalized. Thus in terms of dimensionless switch times ωt_1,ωt_2, $\omega T_f/2$,ωt_4,ωt_5, and ωT_f, equations (2.8) and (2.9) now become

$$1 - 2\cos\omega t_1 + 2\cos\omega t_2 - 2\cos(\omega T_f/2) + 2\cos\omega t_4 - 2\cos\omega t_5 + \cos\omega T_f = 0 \tag{2.21}$$

$$- 2\sin\omega t_1 + 2\sin\omega t_2 - 2\sin(\omega T_f/2) + 2\sin\omega t_4 - 2\sin\omega t_5 + \sin\omega T_f = 0 \tag{2.22}$$

while equations (2.10) and (2.11) require the ratio $\omega_r = \omega_3/\omega_2$ to yield:

$$1 - 2\cos\omega_r\omega t_1 + 2\cos\omega_r\omega t_2 - 2\cos(\omega_r\omega T_f/2) + 2\cos\omega_r\omega t_4 - 2\cos\omega_r\omega t_5 + \cos\omega_r\omega T_f = 0 \tag{2.23}$$

$$-2\sin\omega_r\omega t_1 + 2\sin\omega_r\omega t_2 - 2\sin(\omega_r\omega T_f/2) + 2\sin\omega_r\omega t_4 - 2\sin\omega_r\omega t_5 + \sin\omega_r\omega T_f = 0. \tag{2.24}$$

The linear equations are analogous:

$$\omega t_N = \omega t_{2N}/2 = \omega T_f/2 \tag{2.25}$$

and

$$\omega t_m = \omega t_{2N} - \omega t_{2N-m} = \omega T_f - \omega t_{2N-m} \qquad (N+1 \le m < 2N). \tag{2.26}$$

The expression in x_f and T_f, (eq. 2.19), can be nondimensionalized by multiplying by ω_2^2 and using ωT_s, the dimensionless move time when the system masses are rigidly connected and excited by a single cycle of a square wave:

$$\omega T_s = \omega_2\sqrt{4(m_1 + m_2 + m_3)x_f/F}. \tag{2.27}$$

Thus equation (2.19) becomes

$$\left[\omega T_f^2 - 2(\omega T_f - \omega t_1)^2 + 2(\omega T_f - \omega t_2)^2 - 2(\omega T_f - \omega T_f/2)^2 + 2(\omega T_f - \omega t_4)^2 - 2(\omega T_f - \omega t_5)^2\right] = (\omega T_s)^2/2. \tag{2.28}$$

Note that the calculation of the dimensionless switch times depends only on the dimensionless parameters ω_r and ωT_s. The ratio ω_r characterizes the system resonances, while ωT_s indicates the relative force applied to the combined system inertia over a given displacement. The dimensionless force F^*, given by

$$F^* = \frac{F}{(m_1 + m_2 + m_3)x_f\omega_2^2}, \tag{2.29}$$

is related to ωT_s by

$$F^* = 4/(\omega T_s)^2. \tag{2.30}$$

The above expressions in the dimensionless switch times can be further simplified using a new choice of variables. Since the switches occur symmentrically about $\omega T_f/2$, instead of using the absolute switch times ωt, use the difference between $\omega T_f/2$ and ωt. Thus, $\omega dt_1 = \omega T_f/2 - \omega t_1$ and $\omega dt_2 = \omega T_f/2 - \omega t_2$. Because of symmetry, the differences for ωt_4 and ωt_5 are simply the negative of those above. Using these substitutions, both equations (2.21) and (2.22) become

$$-2\cos\omega dt_1 + 2\cos\omega dt_2 + \cos(\omega T_f/2) - 1 = 0 \tag{2.31}$$

and both equations (2.23) and (2.24) become

$$-2\cos\omega_r\omega dt_1 + 2\cos\omega_r\omega dt_2 + \cos(\omega_r\omega T_f/2) - 1 = 0 \tag{2.32}$$

while equation (2.28) becomes

$$-2\omega dt_1^2 + 2\omega dt_2^2 + (\omega T_f/2)^2 - (\omega T_s/2)^2 = 0. \tag{2.33}$$

Since the linear constraints have already been incorporated into these equations, there are now only 3 unknowns and 3 nonlinear equations to solve for them.

2.4. Bounding the Solution

Since the determination of the switch times requires that a set of nonlinear equations be solved numerically, an initial guess of solutions must be generated. From time-optimal control theory, a necessary condition for optimal switch times can be derived which will bound the solution set about $T_f/2$ and a reasonable guess for T_f can be obtained directly from x_f. To apply the optimality condition, it is necessary to write the system equations as a set of first-order differential equations. This will give a matrix equation of the form

$$\dot{\mathbf{x}} = \mathbf{A}\,\mathbf{x} + \mathbf{b}\,u \tag{2.34}$$

where $\mathbf{A}$ is an $n \times n$ square matrix, $\mathbf{b}$ is an $n \times 1$ column vector, and $\mathbf{x}$ is an $n \times 1$ column vector of state variables, n representing the number of states, here twice N. The necessary optimality condition is derived by Lee and Markus in [32] and specifies that

$$u(t) = \text{sgn}\{\eta(t)\mathbf{b}\} \tag{2.35}$$

where

$$\dot{\eta}(t) = -\eta\mathbf{A} \tag{2.36}$$

and $\eta(t)$ is the $1 \times n$ adjoint state row vector.

The signum operator sgn[ ] specifies the algebraic sign of the expression within brackets. The resulting equation for $u(t)$ is given by

$$u(t) = \text{sgn}\Big[c_1 \sin\omega_2(t+\phi_1) + c_2 \sin\omega_3(t+\phi_2) + c_3 t + c_4\Big] \tag{2.37}$$

where the sinusoid frequencies ω_2 and ω_3 correspond to the system resonant frequencies and the c's and ϕ's are arbitrary constants.

Since the switches will occur symmetrically about $T_f/2$, some of these constants can be determined. Wherever $u(t)$ switches its sign, the argument has a zero. Thus for symmetry, both sinusoids and the ramp component must be zero at $T_f/2$. This gives

$$\phi_1 = \phi_2 = -T_f/2 \tag{2.38}$$

and

$$c_4 = -\frac{T_f}{2}c_3 \tag{2.39}$$

from which $u(t)$ can be rewritten, factoring out c_1 since it will not affect the location of the zeros:

$$u(t) = \text{sgn}\Big[\sin\omega_2(t - T_f/2) + \beta \sin\omega_3(t - T_f/2) + \gamma(t - T_f/2)\Big] \tag{2.40}$$

Nondimensionally, this can be rewritten as:

$$u(t) = \text{sgn}\Big[\sin(\omega t - \omega T_f/2) + \beta \sin\omega_r(\omega t - \omega T_f/2) + \gamma(\omega t - \omega T_f/2)\Big] \tag{2.41}$$

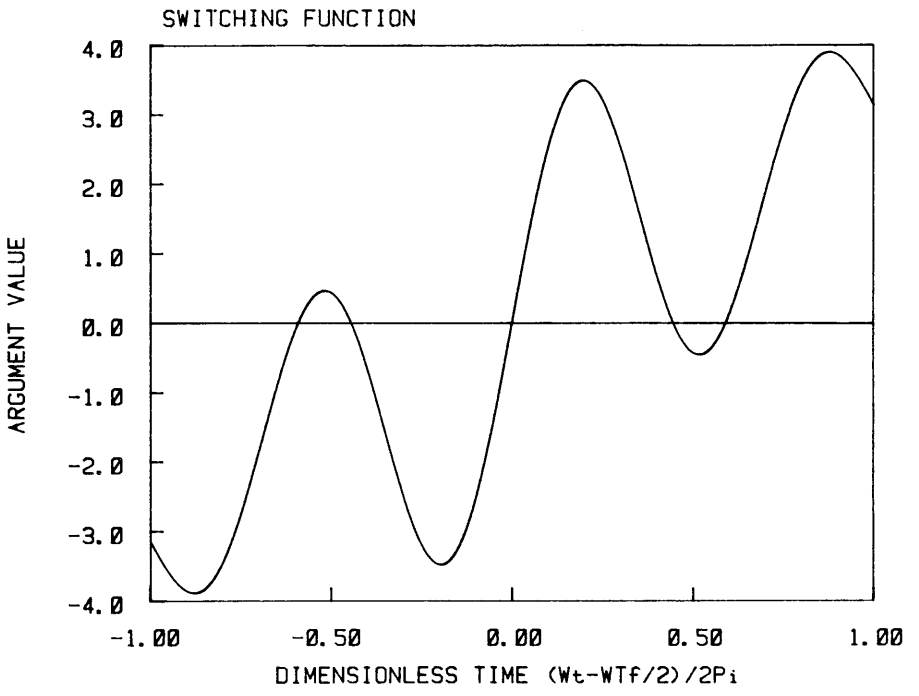

Figure 2.3: Switching Function

The above expressions do not uniquely define $u(t)$ since arbitrary constants remain which would be specified by the desired final state. However, a plot of this switching function can give some insight into the approximate locations of the switch times. Appropriate values of β and γ can be chosen which will give 5 switches clustered about $\omega T_f/2$ as required. Such a plot is shown in Fig. 2.3, given with respect to dimensionless time $(\omega t - \omega T_f/2)$, with $\omega_r = 1.5$.

Notice that the switches occur in a band about $\omega T_f/2$ whose width is one period of the dominant oscillation of the curve. Thus at worst, the switches ωt_m will lie in a region $\omega T_f/2 \pm \pi$, or t_m will occur within $T_f/2 \pm \pi/\omega_2$. The particular value of ω_r for the system in question will determine the period of the superimposed oscillation which actually fixes the intermediate zero crossings. Picking initial guesses for $\omega t_1 = \omega T_f/2 - \frac{\pi}{2}$ and $\omega t_2 = \omega T_f/2 - \frac{\pi}{2\omega_r}$ or correspondingly $t_1 = T_f/2 - \frac{\pi}{2\omega_2}$ and $t_2 = T_f/2 - \frac{\pi}{2\omega_r\omega_2}$ gives good convergence to the final solution. For higher order systems, analogous expressions can be derived for $u(t)$ by determining the ratios of higher system resonant frequencies with respect to ω_2.

It remains to determine an initial guess for T_f. Since the best any system can do is undergo pure translation without any energy going into oscillation, a lower limit on T_f results if all masses move together as one. Then

$$x_f/2 = \frac{F}{2(m_1 + m_2 + m_3)}(T_f/2)^2 \tag{2.42}$$

from which

$$T_f = \sqrt{4(m_1 + m_2 + m_3)x_f/F} = T_s\,. \tag{2.43}$$

This expression can be generalized to any number of masses simply by summing all the m's, and can be nondimensionalized simply by multiplying by ω_2. Thus enlightened guesses for all the switch times can be made to ensure rapid and accurate convergence of the numerical solution to the system of nonlinear equations. A three-dimensional Newton method was used here to obtain solutions to the switch times.

2.5. Response

To determine the response curves for any forcing function, a Runge-Kutta-Merson method was used to solve the differential equations and simulate the dynamic system. Specifying the values of ω_r and ωT_s is sufficient to uniquely determine dimensionless response. For these simulations, values were chosen so that $\omega_r = 1.5$ and $\omega T_s = 70$. The acceleration response of m_1 was used to indicate residual vibration of the endpoint mass. All parameters in the response plots are expressed in dimensionless form, so all the time histories have dimensionless ωt as the independent variable. A bang-bang forcing function switching five times for the three-mass system is shown in Fig. 2.4(a). System response as indicated by the acceleration curve is shown in Fig. 2.4(b). The residual vibration is indeed eliminated as expected.

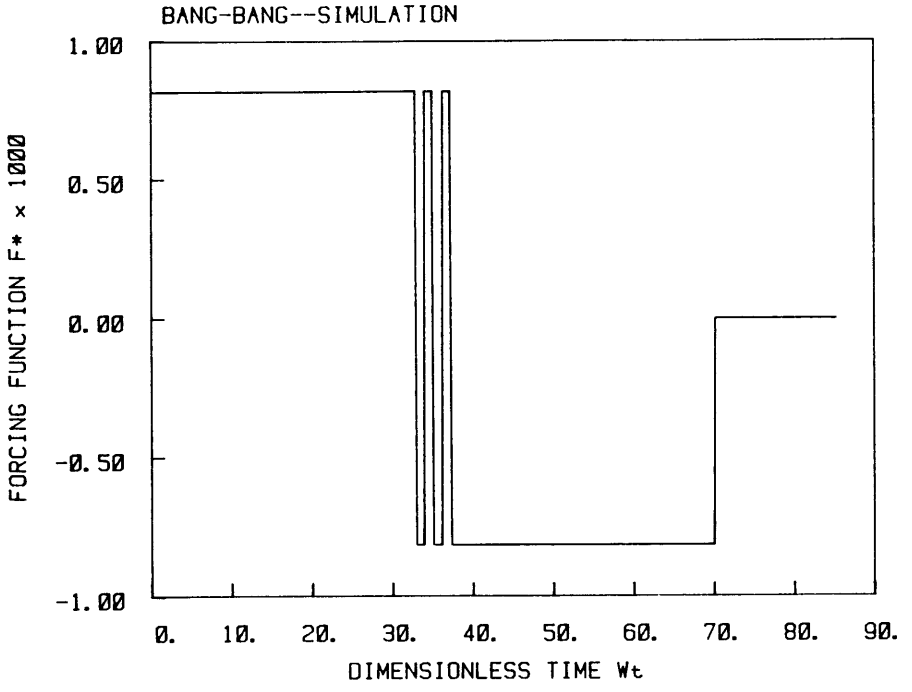

(a)

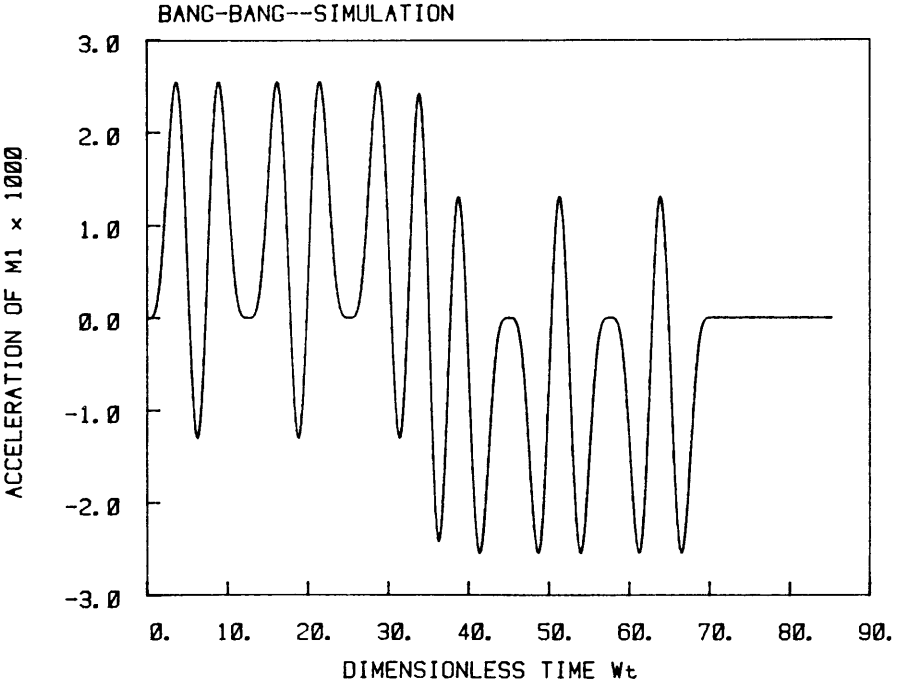

(b)

Figure 2.4: Bang-Bang Response:(a) Forcing Function.(b) Acceleration Response.

Chapter 3.

Ramped Sinusoid Solution

3.1. Motivation

Even though the bang-bang solution is time-optimal, it excites system resonances throughout the move to reach the destination as quickly as possible. To minimize any detrimental effects which this vibration might cause, another forcing function was developed in an attempt to minimize excitation of system resonances during the move while reaching the destination reasonably quickly.

To appreciate the motivation behind this development, a look at the frequency spectra of some typical functions is instructive. Any forcing function which starts and stops abruptly will have many frequency components in its spectrum because of these sudden discontinuities. A single cycle of a square wave is a good example. We examined the spectra of three functions symmetric in time about the midpoint: a single cycle of a square wave, a single cycle of a sine wave, and a function constructed of versed sine waves. (A versed sine function is defined as $1-\cos$.) These waveforms are shown in Fig. 3.1. The square wave contains significant components over a wide band of frequencies. The sine wave has less energy in higher frequency components but still excites a wide range of frequencies because of its abrupt jump at beginning

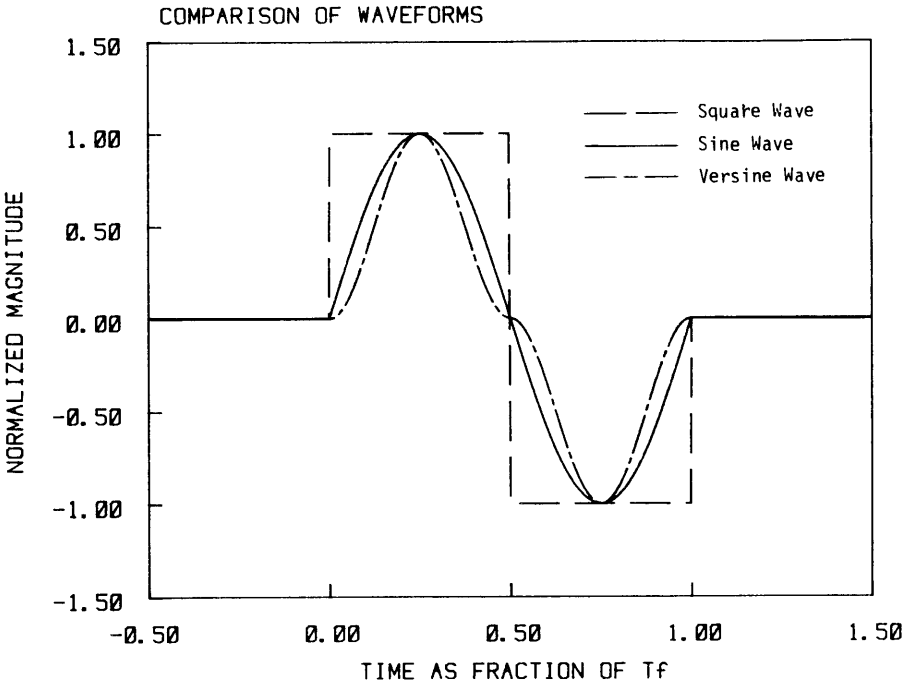

Figure 3.1: Shapes of Typical Forcing Functions

and end. The versed sine function, given by

$$u(t) = \begin{cases} \frac{F}{2}(1 - \cos 4\pi \frac{t}{T_f}) & 0 < t < T_f/2 \\ -\frac{F}{2}(1 - \cos 4\pi \frac{t}{T_f}) & T_f/2 < t < T_f \end{cases} \tag{3.1}$$

starts and stops with zero slope, which narrows the frequency spectrum of significant energy.

3.2. Derivation of Function

The frequency spectra of the aforementioned functions suggest that if the function begins and ends with zero slope, it is less likely to excite resonances because it has no discontinuities in slope. This is the motivation behind cam design methods. In fact, a cam-shaped forcing function was developed by H. Makino [33] to drive the SCARA robot arm. However, no attempt was made to tailor this function to the dynamics of the system to minimize both move time and residual vibration. If

a function having a narrow band of low frequency components could be derived, it should be possible to establish a forcing function which only excites frequencies well below the resonance of the system. It might even be possible to combine harmonics of this function and still maintain frequencies of excitation below the resonant frequency, or tailor the sum of harmonics in such a way that any higher excitation frequencies do not occur at resonance.

To achieve a function which has zero magnitude and slope at beginning and end requires specifying four boundary conditions to a fourth-order boundary value problem. Such an equation is obtained when describing a system of two masses connected by a spring undergoing translation. The purpose here is simply to derive a function from this boundary-value problem, not to describe the dynamic behavior of this system. For this reason, the parameter which would normally represent the resonant frequency is determined so as to satisfy the boundary conditions on the function.

The differential equation which leads to the desired characteristic functions is

$$z^{IV} + \lambda^2 z'' = 0 \tag{3.2}$$

with end conditions:

$$z(0) = 0, \qquad z(T_f) = 0$$
$$z'(0) = 0, \qquad z'(T_f) = 0.$$

Using the initial conditions, the solution becomes:

$$z(t) = \frac{c_1}{\lambda^2}(\lambda t - \sin \lambda t) + \frac{c_2}{\lambda^2}(1 - \cos \lambda t) \tag{3.3}$$

Making use of the final conditions, two equations in c_1 and c_2 result whose determinant must be zero for a nontrivial solution for c_1 and c_2. Thus,

$$\begin{vmatrix} \frac{1}{\lambda^2}(\lambda T_f - \sin \lambda T_f) & \frac{1}{\lambda^2}(1 - \cos \lambda T_f) \\ \frac{1}{\lambda}(1 - \cos \lambda T_f) & \frac{1}{\lambda} \sin \lambda T_f \end{vmatrix} = 0 . \tag{3.4}$$

This leads to

$$\lambda T_f \sin \lambda T_f + 2\cos \lambda T_f - 2 = 0 \tag{3.5}$$

or, representing $\lambda T_f = \alpha$,

$$\alpha \sin \alpha + 2\cos \alpha - 2 = 0. \tag{3.6}$$

Two sets of characteristic numbers α_l result from this equation. For l even, $\alpha_l = l\pi$. Between these values lies another set which can only be determined numerically and will be denoted simply by α_l. Thus, the characteristic numbers are given by:

$$\begin{aligned} \lambda_l &= \alpha_l / T_f, \qquad \text{l odd} \\ \lambda_l &= l\pi / T_f, \qquad \text{l even.} \end{aligned} \tag{3.7}$$

These characteristic numbers give rise to two sets of characteristic functions which will be denoted by $\Phi_l(t)$:

$$\begin{aligned} \Phi_l(t) &= \frac{1}{\lambda_l^2}\left[\lambda_l(t - T_f/2) - \sin \lambda_l t + \frac{\lambda_l T_f}{2}\cos \lambda_l t\right] \qquad \text{l odd} \\ \Phi_l(t) &= \frac{1}{\lambda_l}(1 - \cos \lambda_l t) \qquad \text{l even.} \end{aligned} \tag{3.8}$$

The second of these functions is simply the versed sine function discussed in Sec. 3.1. The first represents a function which can be classified as a ramped sinusoid. A graph of its characteristic shape with $l = 1$ is shown in Fig. 3.2. Notice that it has odd symmetry about $T_f/2$ which makes it particularly convenient as a forcing function. Higher order functions simply compress more sinusoids into the same time interval— $0 < t < T_f$. Since this function peaks at a value other than 1, it must be normalized using an appropriate scale factor which will be denoted by SF.

Using one cycle of the ramped sinusoid with $l = 1$ in the computer simulation with $\omega_r = 1.5$ and $\omega T_s = 70$ gives encouraging results, as shown in the acceleration response curve of Fig. 3.3(b). Residual vibration is very nearly eliminated. However, for the same peak force as the bang-bang, response time is increased by 45 %. If more terms of higher characteristic number could be added so that the resulting function approximates a square wave, the speed of response would improve considerably, as long as the resultant frequency spectrum does not contain high energies at system resonant frequencies.

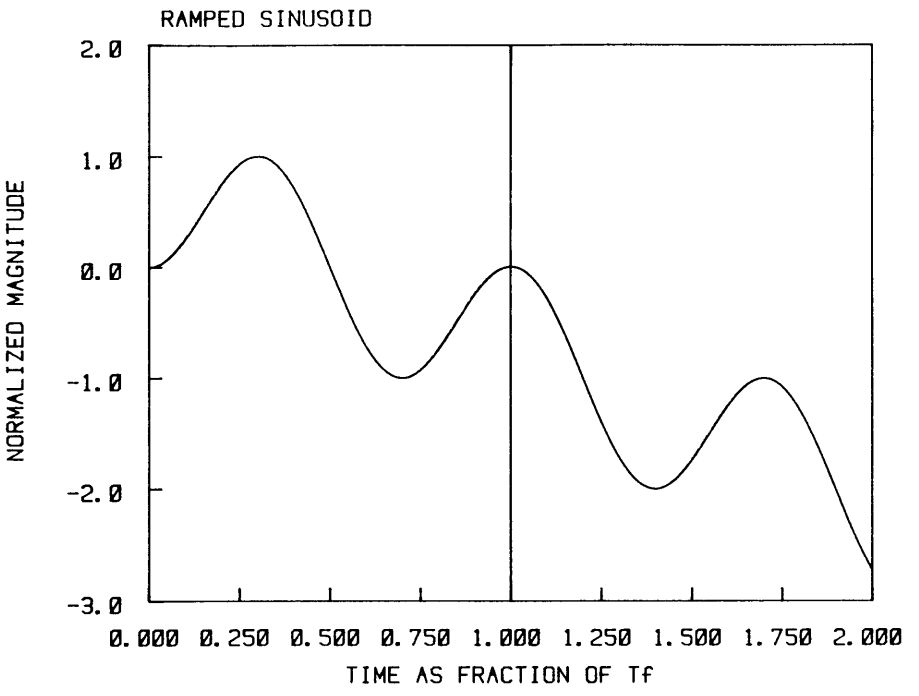

Figure 3.2: Characteristic Shape of Ramped Sinusoid Function

3.3. Least-Squares Fit to a Square Wave

A least-squares approximation to the square wave can be constructed by minimizing the square of the error between the desired square wave of height F and a finite sum of weighted ramped sinusoids. The weighting coefficients A_l must be determined, where l now refers to an index number for all ramped sinusoid components and may be either even or odd. The expression to be minimized is

$$\int_0^{T_f/2}\Big[F-\sum_{l=1}^{L}A_l\Phi_l(t)\Big]^2\,dt+\int_{T_f/2}^{T_f}\Big[-F-\sum_{l=1}^{L}A_l\Phi_l(t)\Big]^2\,dt=\min\,. \tag{3.9}$$

Differentiating with respect to A_r,

$$\int_0^{T_f/2}\Big[F-\sum_{l=1}^{L}A_l\Phi_l(t)\Big]\Phi_r(t)\,dt-\int_{T_f/2}^{T_f}\Big[F+\sum_{l=1}^{L}A_l\Phi_l(t)\Big]\Phi_r(t)\,dt=0 \tag{3.10}$$

and rearranging gives:

$$\sum_{l=1}^{L}A_l\underbrace{\int_0^{T_f}\Phi_l(t)\Phi_r(t)\,dt}_{I_{rl}}=F\underbrace{\left[\int_0^{T_f/2}\Phi_r(t)\,dt-\int_{T_f/2}^{T_f}\Phi_r(t)\,dt\right]}_{I_r} \tag{3.11}$$

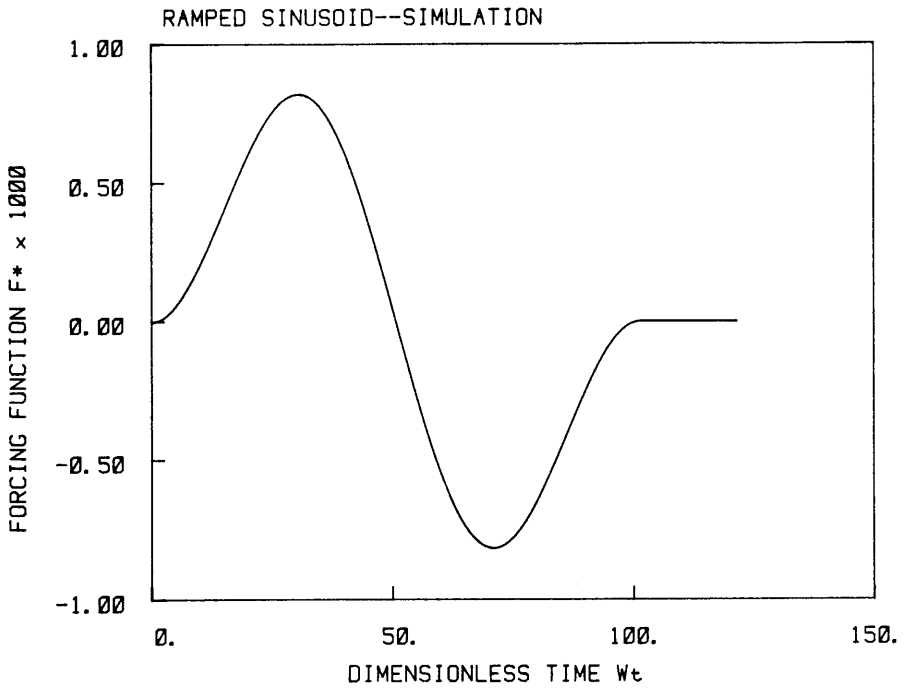

(a)

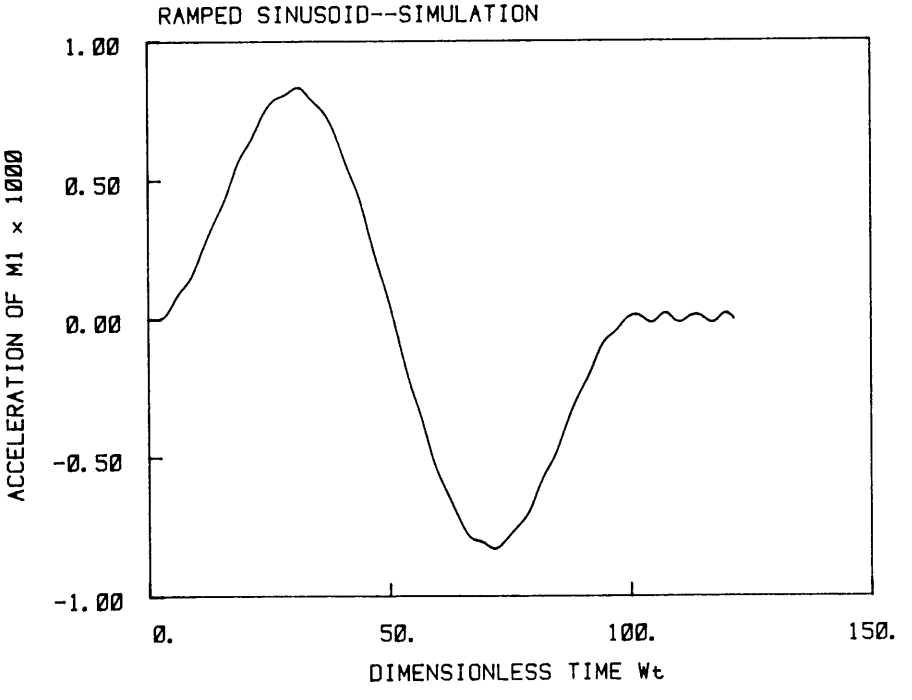

(b)

Figure 3.3: Ramped Sinusoid Response:(a)Forcing Function.(b)Acceleration Response.

These integrals can be evaluated to give:

$$I_{rl} = \frac{-T_f^5}{\alpha_l^2 - \alpha_r^2}\left\{\frac{\alpha_r}{\alpha_l^4}\left[\frac{\alpha_l^3}{12} + \left(\frac{\alpha_l^2}{2} - 1\right)\sin\alpha_l + \alpha_l\cos\alpha_l + \frac{\alpha_l}{2}(\cos\alpha_l - 1)\right]\right.$$
$$\left. - \frac{\alpha_l}{\alpha_r^4}\left[\frac{\alpha_r^3}{12} + \left(\frac{\alpha_r^2}{2} - 1\right)\sin\alpha_r + \alpha_r\cos\alpha_r + \frac{\alpha_r}{2}(\cos\alpha_r - 1)\right]\right\} \quad (r \neq l) \quad (3.12)$$

$$I_{rl} = \frac{T_f^5}{\alpha_l^5}\left\{\frac{\alpha_l}{4} + \frac{5}{24}\alpha_l^3 + \frac{1}{4}\left[(\alpha_l/2)^2 - 1\right]\sin 2\alpha_l + \left(\alpha_l^2/2 - 2\right)\sin\alpha_l\right.$$
$$\left. + \frac{\alpha_l}{4}\cos 2\alpha_l + 2\alpha_l\cos\alpha_l\right\} \quad (r = l) \quad (3.13)$$

$$I_r = \frac{T_f^3}{\alpha_r^3}\left[-\left(\frac{\alpha_r}{2}\right)^2 + 2\cos(\frac{\alpha_r}{2}) + \alpha_r\sin(\frac{\alpha_r}{2}) - \cos\alpha_r - \frac{\alpha_r}{2}\sin\alpha_r - 1\right] \quad (3.14)$$

The resulting matrix expression to solve for the A_l's is

$$[I_{rl}]\,[A_l] = F\,[I_r] \quad (3.15)$$

Eliminating the excess T_f's and solving for $B_l = T_f^2 A_l/F$ gives the dimensionless form of this expression:

$$[B_l] = [I_{rl}^*]^{-1}\,[I_r^*] \quad (3.16)$$

where $I_{rl}^* = I_{rl}/T_f^5$ and $I_r^* = I_r/T_f^3$.

All of the foregoing integral expressions do not depend on T_f directly but only on the combination $\alpha = \lambda T_f$. Thus they can be evaluated in general, independent of the system specifications. Then B_l can be determined simply by solving the linear matrix equation for the desired number of terms L. The aim is to determine an expression for $u(t)$:

$$u(t) = \frac{1}{SF}\sum_{l=1}^{L} A_l\Phi_l(t)\,. \quad (3.17)$$

Defining a dimensionless characteristic function as

$$\Phi_l^*(t) = \lambda_l(t - T_f/2) - \sin\lambda_l t + \frac{\lambda_l T_f}{2}\cos\lambda_l t \quad (3.18)$$

allows $u(t)$ to be written in terms of B_l as

$$u(t) = \frac{F}{SF} \sum_{l\ 1}^{L} \frac{B_l}{\alpha_l^2} \Phi_l^*(t) \tag{3.19}$$

where again a scale factor SF is necessary to normalize the function. Thus, all that is required to uniquely define $u(t)$ is that the value of T_f be inserted into $\Phi_l^*(t)$. This is easily done for a given x_f simply by solving the differential equation of motion for the rigid body mode:

$$\ddot{x}_r = \frac{F}{(m_1 + m_2 + m_3)SF} \sum_{l=1}^{L} \frac{B_l}{\alpha_l^2} \Phi_l^*(t)\,. \tag{3.20}$$

Solving and replacing $\Phi_l^*(t)$ gives

$$T_f = \sqrt{\frac{-12(m_1 + m_2 + m_3)x_f}{\frac{F}{SF}\sum_{l=1}^{L} B_l/\alpha_l}} \tag{3.21}$$

which can be rewritten as

$$T_f = \Gamma T_s \tag{3.22}$$

where Γ is given by

$$\Gamma = \sqrt{\frac{-3}{\frac{1}{SF}\sum_{l=1}^{L} B_l/\alpha_l}} \tag{3.23}$$

With B_l determined, any number of terms of ramped sinusoids can be added together to approach the shape of a square wave. The shapes of the resulting forcing functions with $L = 11$ and $L = 15$ are shown in Fig. 3.4. only odd series are shown since the even components contribute little to the overall curve due to their asymmetry about $T_f/2$. A typical acceleration response curve for $L = 11$ is shown in Fig. 3.5(b). Significant residual vibration is generated, but response time has been reduced.

3.4. Determination of Number of Terms

Since the response depends on the shape of the forcing function, adjusting the maximum number of ramped sinusoid terms added together will have an effect on

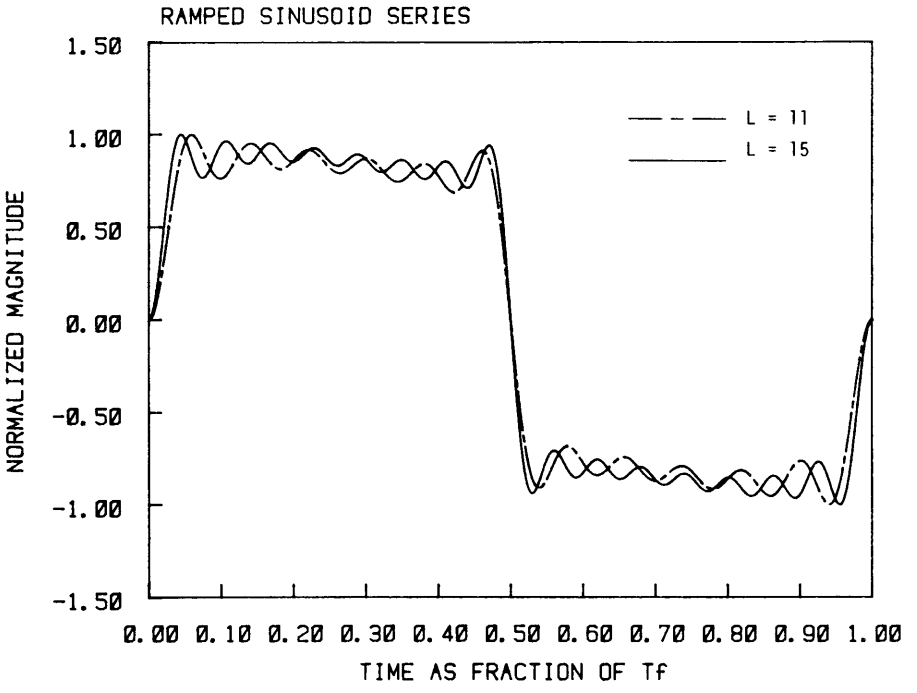

Figure 3.4: Two Ramped Sinusoid Series: $L = 11$ and $L = 15$

both move time and residual vibration. Ideally, only as many terms should be combined as will minimize move time while satisfying the vibration requirement. Clearly the more terms used the closer the function approximates a square wave and the faster the response. The problem is that higher harmonics of the ramped sinusoid introduce excitation at higher frequencies. This may bring the excitation frequencies closer to the system resonances. Preferably, any frequencies excited by the forcing function will lie well below the lowest system resonance. An alternate approach would be to allow excitation frequencies over a wider range, some exceeding system resonance, while making sure that the actual resonant frequencies are not excited. It is conceivable that the latter effect could be achieved by leaving out some of the terms in the ramped sinusoid series. However, since each term in the series contains contributions at several frequencies, a suitable algorithm to determine which terms to include is difficult to establish. Therefore, only the total number of terms was adjusted in the hopes of achieving both minimum vibration and minimum move time in a simpler way.

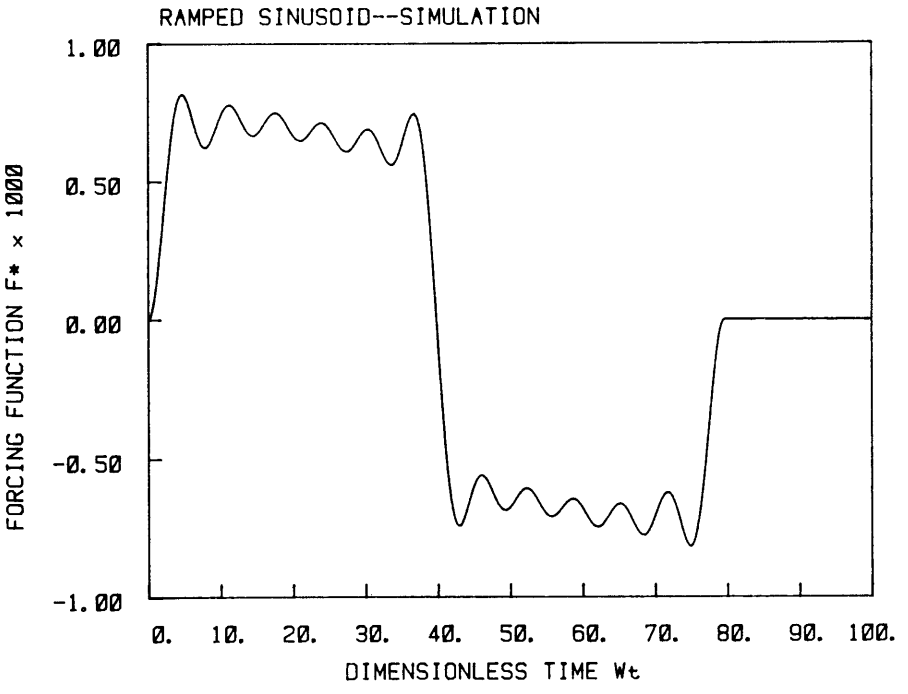

(a)

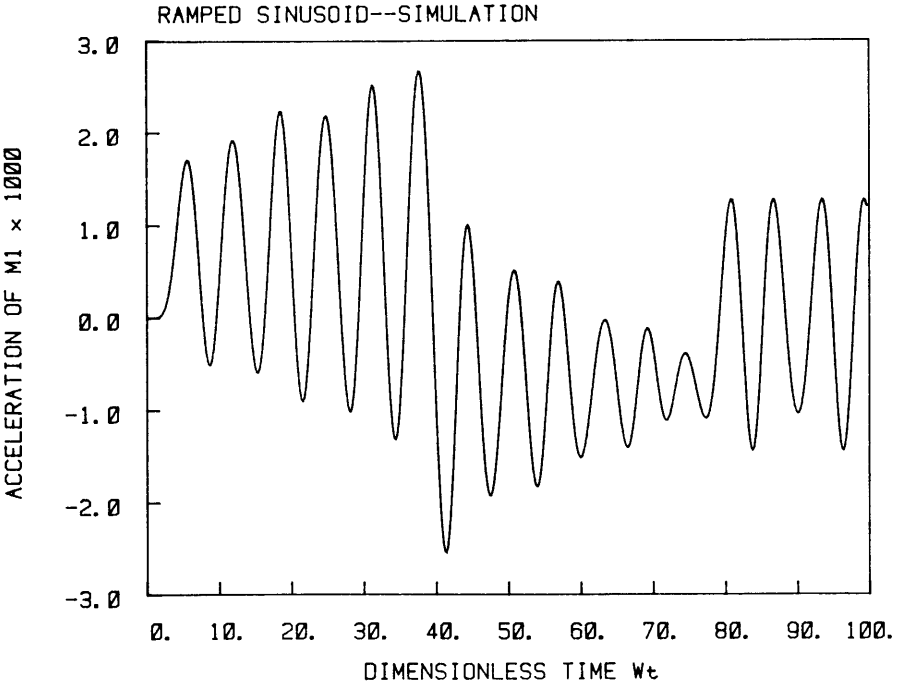

(b)

Figure 3.5: Ramped Sinusoid Series Response ($L = 11$):(a)Forcing Function. (b)Acceleration Response.

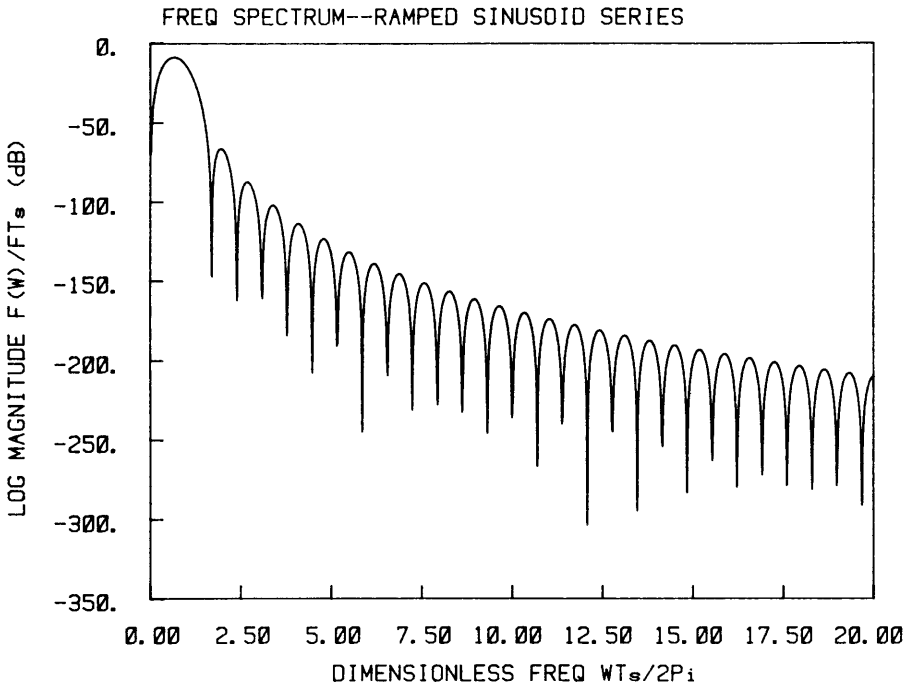

Figure 3.6: Frequency Spectrum of a Single Ramped Sinusoid

A look at the frequency spectra of sums of ramped sinusoids will help determine the maximum number of terms allowed without inducing residual vibration. The frequency spectrum of a single ramped sinusoid is shown in Fig. 3.6. A detailed derivation may be found in Appendix B. Both the log magnitude scale and the frequency scale are given in dimensionless coordinates. In this way, their dependence on system parameters can be readily investigated. The parameter T_s used to nondimensionalize ω represents the move time when the system masses are rigidly connected and excited by a single cycle of a square wave as the forcing function. It is given by

$$T_s = \sqrt{4(m_1 + m_2 + m_3)x_f/F}\,. \tag{3.24}$$

Thus, the units on the abscissa represent the frequency ω as a multiple of T_s, while the units on the ordinate represent the dimensionless magnitude ratio $|\mathcal{F}(\omega)|/(FT_s)$. Given the value of T_s corresponding to the desired masses, peak force, and move distance, the magnitude ratio at particular frequencies can be uniquely determined. If the lowest system resonant frequency occurs at a point in the spectrum where

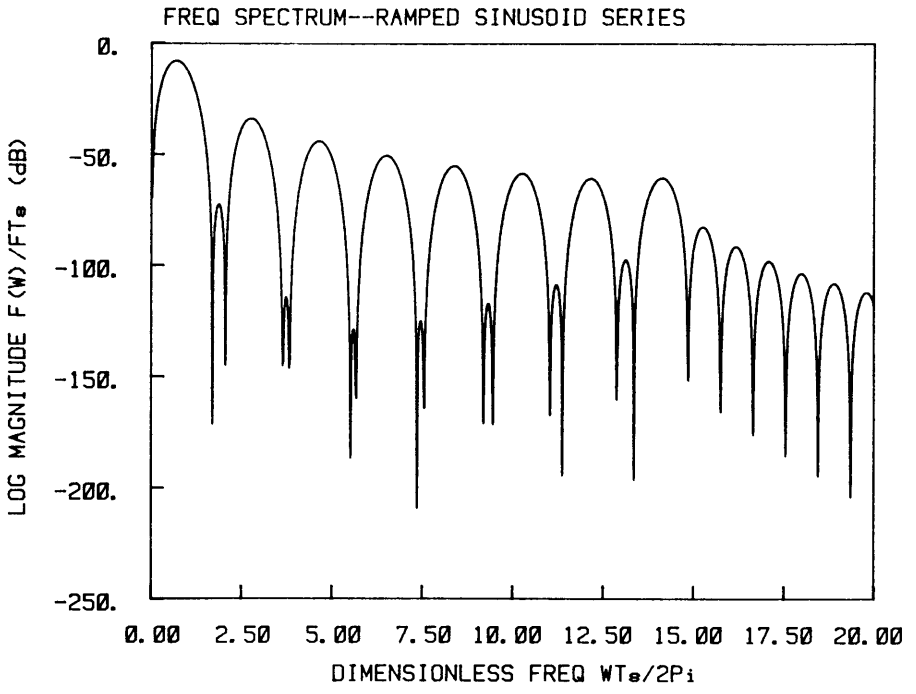

Figure 3.7: Frequency Spectrum of 15-term Ramped Sinusoid Series

the magnitude of the frequency components has sufficiently tapered off, then a minimum of residual vibration is to be expected.

As long as the forcing function only excites frequencies well below the fundamental system resonance, that function is acceptable. But an equally satisfactory solution is possible if the forcing function has a local minimum excitation at the frequency corresponding to resonance. This requires a trough in the frequency spectrum at the appropriate frequency. Such troughs actually exist in the spectra of sums of ramped sinusoids, as shown by Fig. 3.7, which shows the frequency spectrum for a 15-term series. Since the addition of higher harmonic terms to the series will contribute energy at higher frequencies, the requirement that resonance occur above these excitation frequencies would severely limit the total number of terms allowed. If the resonant frequency can fall in such a trough in the spectrum, then more terms can be added which introduce excitation at frequencies above resonance where their effect is minimal. When more terms are combined to form the forcing function, more energy can be transferred to the system and the move time

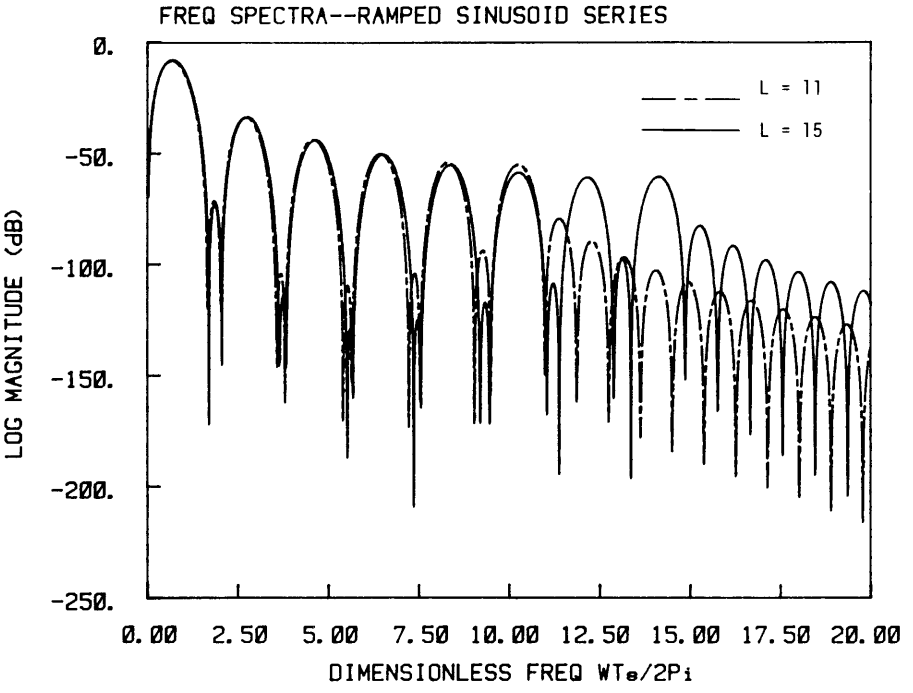

Figure 3.8: Comparison of Frequency Spectra: $L = 11$ and $L = 15$

is correspondingly reduced. Thus, taking advantage of these troughs allows faster response while minimizing residual vibration. Fortunately, the regions of frequency where excitation is minimal have a finite width; they are not merely a single point. Thus precise placement of the trough with respect to the system natural frequencies is not critical.

A comparison of frequency spectra of two different series of ramped sinusoids indicates an additional advantage. Figure 3.8 shows the spectra of an 11-term and a 15-term series. It is clear that series with more terms have troughs at very nearly the same locations as series with fewer terms. Thus, if the resonant frequency falls in a trough for a series with 11 terms, it will fall equally well into the trough for a series of 15 terms. So the higher-order series will have minimal excitation at resonance while reaching the end state in less time. This suggests that, when resonance occurs in a spectral trough, many terms can be added without detrimental effects on residual vibration. In fact, the vibration may decrease when adding more terms if the height of the trough decreases for a larger number of terms. This phenomenon is

also evident in Fig. 3.8. At first this seems counterintuitive since one would expect higher excitation using more terms. But the important concept here is the phase of the added components in the frequency domain. If at some frequency the sign of the contribution from the added term is opposite that of the existing frequency component, the net effect will be attenuation of the frequency spectrum at that frequency. Thus it can happen that using more terms not only reduces response time but also reduces residual vibration.

The foregoing observations lead to a method for determining the appropriate forcing function for a given set of masses, peak force, and move distance. First, the parameter T_s is evaluated corresponding to a desired move distance. This will calibrate the nondimensionalized frequency spectrum for each sum of sinusoids. Then the system resonant frequencies are located in each of the spectra. The largest number of terms is desired for the forcing function, so that L is chosen for which the frequency spectrum indicates a magnitude below a certain threshold level for each of the resonant frequencies. The threshold level is determined by an acceptable level of residual vibration in the simulation. For a structure having several resonant frequencies, the spectral magnitudes at resonance for the appropriate forcing function must all be lower than the threshold level. With this criterion met, a forcing function composed of the appropriate number of ramped sinusoid terms will provide fast response time while minimizing residual vibration.

Chapter 4.

Comparison

4.1. Square Wave Residual Vibration Amplitude

The two important goals of the forcing functions used here are fast move time and negligible residual vibration. Since these goals are generally incompatible, a compromise must be made between them. A certain amount of suboptimality has to be accepted in order to stay within a maximum vibration envelope. Since neither of the functions derived here can be practically expected to have zero residual vibration, a measure of vibration attenuation is necessary. Since the square wave contains many dominant frequency components, the residual vibration in response to this forcing function would provide a convenient worst-case comparison for expected vibration. But since the vibration amplitude can depend on many of the system parameters, it is instructive to nondimensionalize so as to identify the actual functional dependencies.

A dimensional analysis indicates that residual vibration amplitude, symbolized by da^* and defined as half the peak-to-peak dimensionless residual acceleration response, depends only on the values of two independent dimensionless parameters. Two parameters of particular convenience in this study are ω_r and ωT_s. The value of ω_r characterizes the system by indicating the relationship between resonant frequencies. The value of ωT_s indicates the effect of peak force input and desired move distance x_f. When the system and force input are fixed, different values

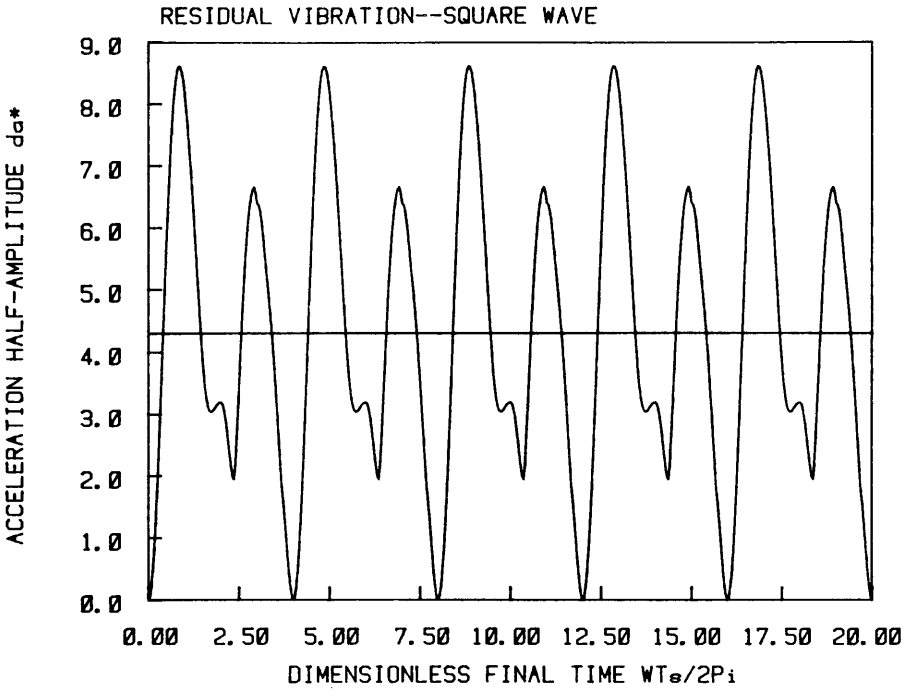

Figure 4.1: Square Wave Residual Amplitude vs. ωT_s

of ωT_s represent different move distances. It is now possible to plot da^* against both of these parameters in turn to develop some insight into the nature of square wave vibration. Shown in Fig. 4.1 is the residual amplitude da^* against ωT_s, with $\omega_r = 1.5$. The amplitude takes on the same peak values periodically and dips to zero periodically as the move time is increased. This is understandable, since the phase plane analysis indicated that zero vibration is possible with only one switch whenever ωT_s is an integral multiple of both 4π and $4\pi/\omega_r$. For $\omega_r = 1.5$, this requires that ωT_s be an integral multiple of both 4π and $8\pi/3$, which is satisfied for multiples of 8π, or at every 4 periods of 2π.

The effect of ω_r on da^* is even more interesting. Using values of ωT_s corresponding to the peaks of Fig. 4.1 gives plots of da^* against ω_r which all have the same general shape suggested in Fig. 4.2, for which $\omega T_s = 10\pi$. The interesting phenomenon is that all these curves converge to the same value of da^* at large enough ω_r, namely $da^* = 4.0$. Thus for $\omega_r > 4$, the residual vibration amplitude is practically independent of ω_r. In the range $1 < \omega_r < 2$, however, residual vibration

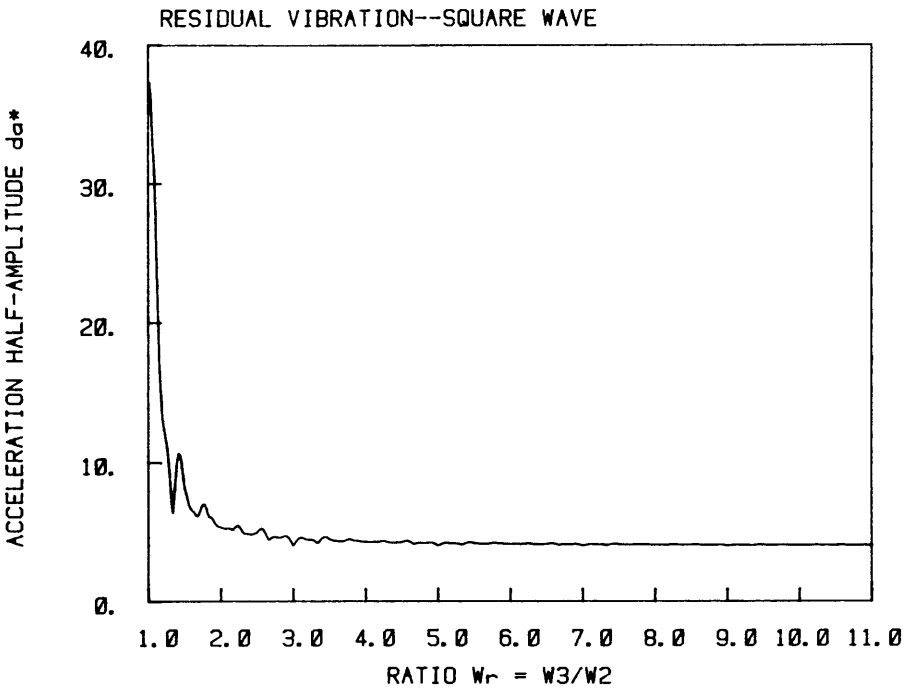

Figure 4.2: Square Wave Residual Amplitude vs. ω_r

is very sensitive to ω_r, and most real systems are characterized by values of ω_r in this range. Therefore, the baseline vibration amplitude should depend on ω_r for true comparison. To indicate the variation of square wave amplitude with move time, a mean value over several periods of Fig. 4.1 is used, with $\omega_r = 1.5$. This mean amplitude measures 4.30 and can be considered the worst-case residual vibration amplitude to compare with the mean values of other forcing functions over the range of move times at the same $\omega_r = 1.5$.

4.2. Bang-Bang Residual Vibration – Switching Errors

With a baseline residual amplitude well defined, it is now possible to investigate the degree of vibration attenuation using each of the chosen functions. Theoretically, the bang-bang function has zero residual vibration. But in practice, switch time errors and variations in system parameters will adversely affect resid-

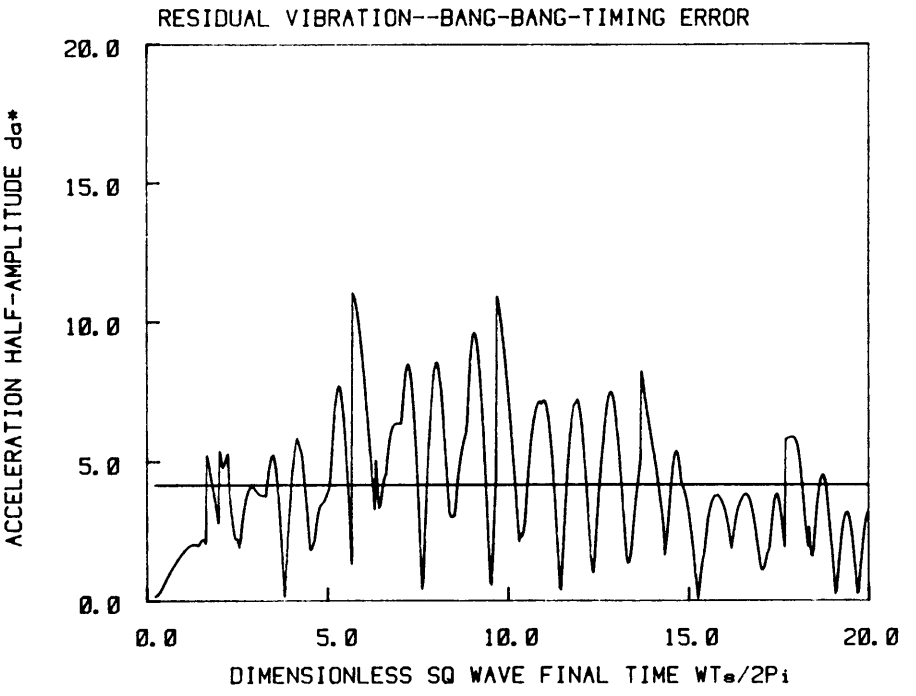

Figure 4.3: Bang-Bang Residual Amplitude–Switching Errors

ual vibration. Parameter variations will also affect the ramped sinusoid functions and hence the sensitivity of both functions to these deviations can be readily compared. Switching errors, however, only affect the bang-bang function so these will be explored first.

To simulate errors in switching, the bang-bang function was first determined with switch times appropriate for $\omega_r = 1.5$, and then these switch times were increased by 10 %. The effect on residual vibration is shown in Fig. 4.3, which plots the dimensionless residual amplitude of the bang-bang function with incorrect switches against ωT_s. Notice the significant increase in vibration, whose mean amplitude of 4.16 is now of the same order of magnitude as the square wave mean amplitude. Thus, the residual vibration in response to the bang-bang function is very sensitive to errors in the switch times.

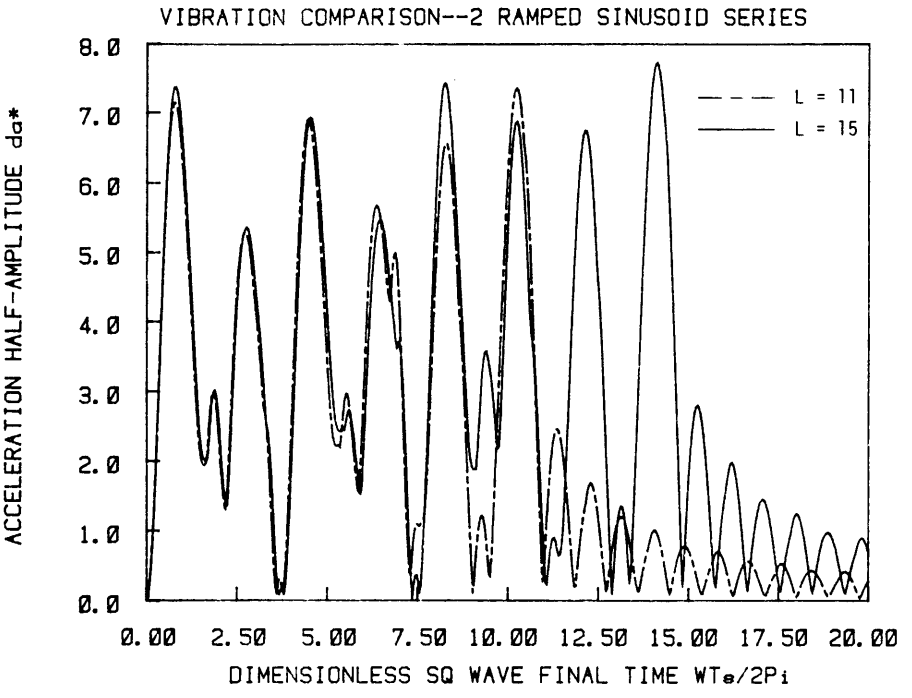

Figure 4.4: Effect of L on Ramped Sinusoid Residual Amplitude

4.3. Ramped Sinusoid Residual Vibration – Effect of L

For the ramped sinusoid functions, adding terms which contribute excitation at resonance will adversely affect the residual vibration. Choice of L, the maximum number of terms added in the series, thus plays an important role in determining residual vibration. It is instructive to look more closely at the vibration amplitudes of some ramped sinusoid functions having the same L over the entire range of moves. Two different series are compared in Fig. 4.4, using $L = 11$ and $L = 15$. The residual vibration amplitude is again given as a function of ωT_s. The shapes of the curves bear a striking resemblance to the square wave amplitude curve, with slightly lower peak amplitudes and a significant drop-off at higher values of ωT_s. This resemblance is understandable since more terms more closely approximate a square wave. A more useful observation to facilitate selection of L comes from a comparison of this plot with the frequency spectra for these two series in Fig. 3.8.

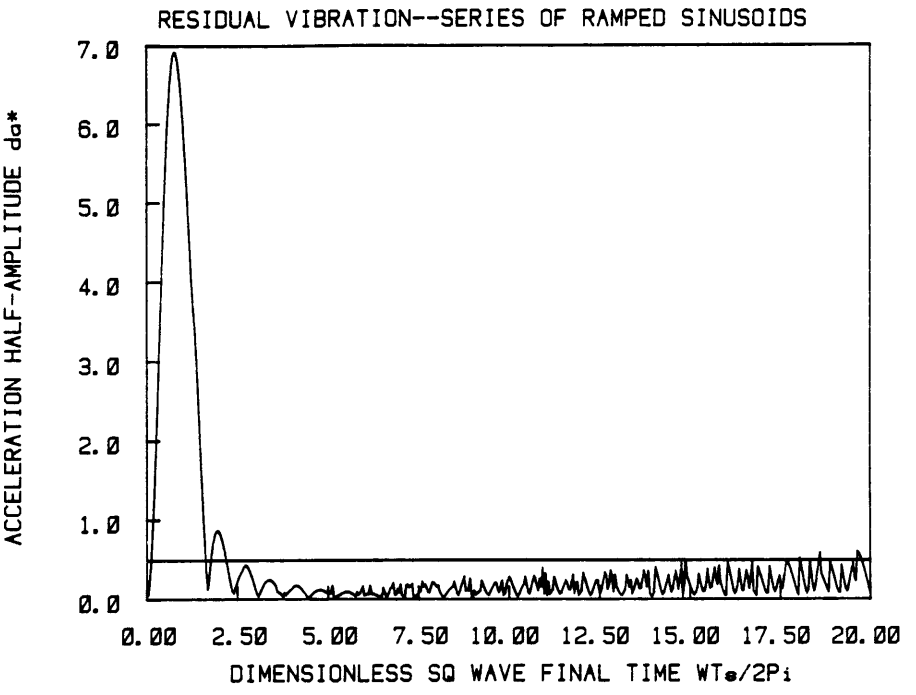

Figure 4.5: Ramped Sinusoid Residual Amplitude–L selected for each ωT_s

At each value of ωT_s where the residual vibration curve peaks, the corresponding frequency spectrum of each series also peaks. This correlation suggests that the frequency spectra alone can be used as reliable criteria to select the number of terms for a given move distance.

If L is chosen so that the spectral magnitude at all system resonant frequencies is held below -120 dB, the mean residual amplitudes in response to these ramped sinusoid functions is less than 11.5 % of the mean square wave amplitude. This is verified in Fig. 4.5, which shows the residual amplitude for the ramped sinusoid functions over the range of ωT_s. Notice that these functions do considerably better for $\omega T_s > 3\pi$, where the mean amplitude is less than 10 % of mean square wave amplitude. Since at particular values of ωT_s even a square wave will have zero amplitude, infinitely many terms could be added together at those ωT_s's without contributing to residual vibration. Therefore, an upper bound must be set on the number of terms to be added, here chosen as 15.

An important observation on these selected functions is in order. A direct

comparison of vibration amplitudes for the square wave and the ramped sinusoid series at a given ωT_s indicates an important fact. Wherever the square wave produces minimal residual vibration, the chosen ramped sinusoid series produces larger vibration amplitude. This suggests that for various moves, it would be wiser to use simply the square wave without resorting to the increased complexity of shaping the ramped sinusoids. Of course, the issue is to develop an appropriate algorithm which picks the correct type of function depending on the desired move and the allowable residual vibration. This problem does not appear with the bang-bang functions since ideally they always improve on square wave response by eliminating all residual vibration.

4.4. Residual Vibration with Parameter Errors – Comparison

To investigate the effect of uncertain or slightly varying system parameters, both sets of functions were determined for a particular set of parameters and tested using slightly altered parameters. Again the mean ramped sinusoid residual vibration amplitude was limited to 11.5 % of that of the square wave. In this work, the parameter change was achieved by decreasing the fundamental resonant frequency ω_2 by 10 % in the simulation. The effect of this variation on the residual vibration amplitude of the two functions is shown in Figure 4.6. Again, amplitudes are given over a range of values of ωT_s. Clearly evident is the increase in vibration for both functions due to the parameter change. But more important is the relatively larger effect of parameter changes on the bang-bang function, causing larger vibration amplitudes over a greater portion of the operating regime than the ramped sinusoids. In fact, with a mean amplitude of 2.5 compared to the ramped sinusoid mean amplitude of 0.9, the bang-bang produces almost three times as much residual vibration on average as does the ramped sinusoid. Thus, even though ideally the bang-bang function is both time-optimal and vibration-free, in practice it is very sensitive to

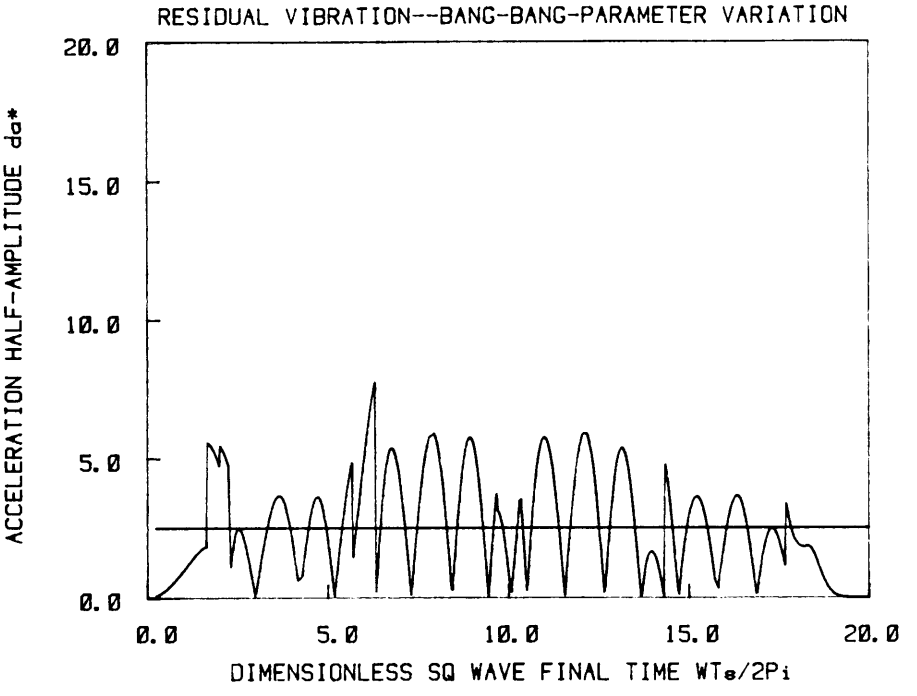

(a)

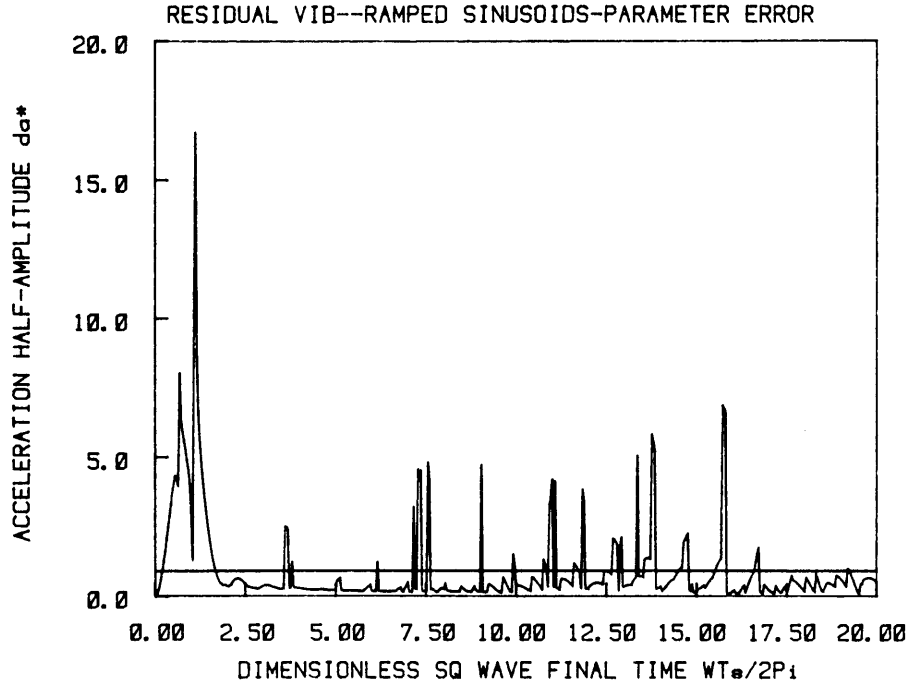

(b)

Figure 4.6: Residual Amplitudes With Parameter Errors:(a)Bang-Bang. (b)Ramped Sinusoid.

any imperfections in parameter measurements or drift. In comparison, the series of ramped sinusoid functions are less sensitive to these parameter variations.

4.5. Move Times Compared

It remains to be seen whether the ramped sinusoids give sufficiently fast response times. Since the bang-bang function is time-optimal, comparing move times for the two functions will indicate how close the ramped sinusoid comes to optimal time response. The ramped sinusoid series are chosen to limit mean residual amplitude to 11.5 % of the mean square wave amplitude, as before. Dimensionless move time is obtained by dividing ωT_f of either function by ωT_s of the square wave function, the minimum time if the system were a rigid body, free of any vibration. As pointed out before, ωT_s also indicates the choice of peak force F and move distance x_f. Thus a plot of T_f/T_s as a function of ωT_s indicates relative move times over a range of move distances for each function. With ramped sinusoid series chosen to limit vibration amplitudes as before, move times at comparable values of ωT_s for both functions are given in Fig. 4.7.

The bang-bang move time rises and falls periodically, approaching the minimum square wave move time at all moves where the square wave has zero residual vibration. Between these points, compensation for vibration requires longer move times, their relative maximum value decreasing with larger ωT_s. There are five regions where the bang-bang function takes considerably longer to complete the move. Here, the only switch times which satisfy the equations have correspondingly large final times. This may indicate that true optimal solutions here require more switches, or perhaps an asymmetric set of switches, if they are to completely eliminate residual vibration. Certainly, if the governing equations for the switch times are correct, then no other solutions exist. This is indicated at some length in Appendix C. However, since the resulting switches do not lie within the specified band about $\omega T_f/2$, it seems likely that an error exists in the analysis which does

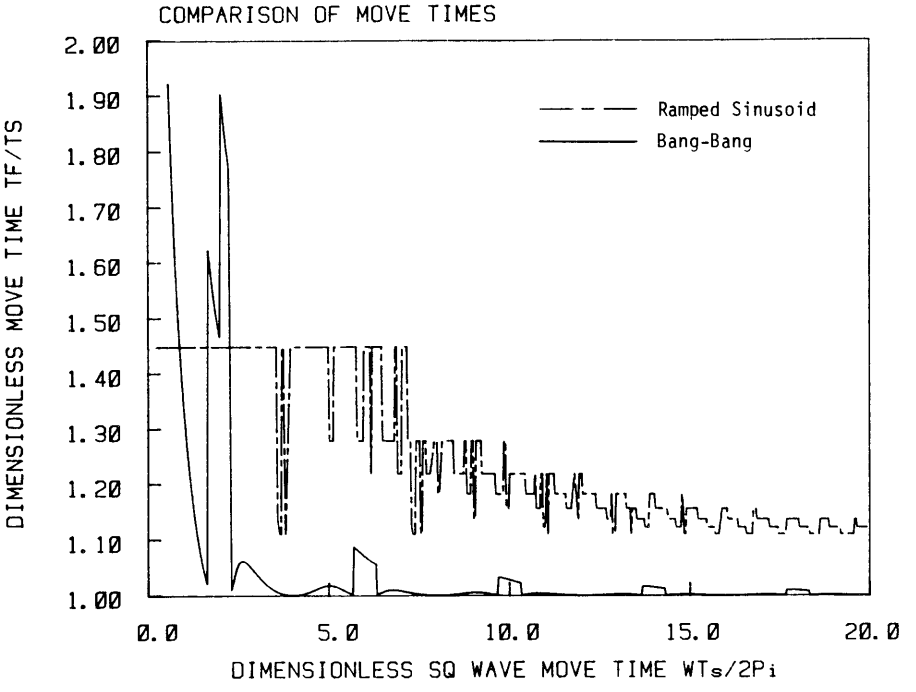

Figure 4.7: Comparison of Move Times

not give optimal solutions in these regions.

The ramped sinusoid move time depends on the number of terms in the series, and hence exhibits step discontinuities. Particularly at short moves or very low resonant frequencies, the ramped sinusoid series are suboptimal. But at large enough values of ωT_s, their move time is only 25 % higher than that of the bang-bang function. Thus, at certain moves, the ramped sinusoid forcing functions provide both minimum residual vibration and fast move times. Except for the regions noted above, the bang-bang function gives generally faster response for a wider range of moves.

Chapter 5.

Design of Test Fixture

In order to evaluate these analytical predictions, a test fixture was designed and built. It had to satisfy two important specifications:

1. Closely represent an undamped three-mass, two-spring system; and
2. Accurately duplicate the desired forcing functions.

To achieve these aims, a series of design choices had to be made to ensure predictable experimental results.

First, a rotational model was chosen rather than a translational one. This eliminated the need for a transmission, such as a ball screw, to convert rotation of an electric motor into translation along a track. Of course, a linear motor could have been used but these proved complicated to configure and much too costly. Reduction of sliding friction would also have required an additional shaft and sliding roller bearings to keep the system damping sufficiently low. Using a rotating setup, a simple set of low-friction ball bearings supports the shaft and inertias. An added advantage of a rotating system is its compact size since larger moves can be simulated by several rotations rather than a lengthy track.

A photograph of the final configuration is shown in Fig. 5.1. It consists of a DC permanent magnet motor coupled to a system of two aluminum shafts acting as springs and two steel disks as rotating inertias. The combined inertia of the rotor and the coupling represent the third inertia. Steel disks and aluminum shafts were used in order to achieve sufficiently low resonant frequencies, typical of those

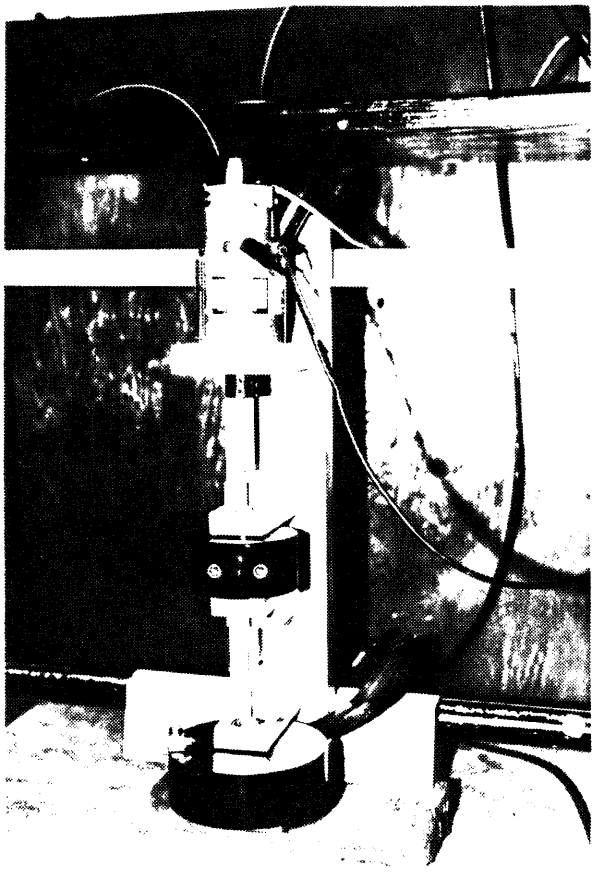

Figure 5.1: Rotational Vibration Test Fixture

in current robot designs. An important factor in the resonance calculation was the respective diameters of the shafts and disks. Sufficiently large values of J, the inertia, and small values of K, the stiffness, were necessary to achieve a fundamental resonant frequency at 20 Hz. And since both J and K vary as the fourth power of the diameter, the disks had to be made large, in this case 4 in. and 6 in. respectively, and the shaft diameter had to be made small, here only 1/4 in, to establish fundamental resonance at 20 Hz. Fortunately, this makes the inertia of the shafts so small as to be negligible compared to the lumped inertias of the disks. The inertia of the bearings would be a larger contribution but since they were mounted on a stiff portion of the shaft very near the large inertial masses that contribution could also be ignored. Hence, the lumped parameter model is fairly accurate. Although the 20 Hz fundamental mode could be achieved, the very low inertia of the rotor and coupling brought the calculated higher resonant frequency up to 130 Hz.

The resonant modes of interest are vibration modes in torsion. In order to accurately represent the features of the mathematical model, all other vibration modes had to be isolated from these torsional modes. This required that the bending mode occur at a sufficiently high frequency so as not to be detected in the region of interest up to about 150 Hz. Because of the 2 in. width of the disks, supporting each of them on one side with only one bearing would result in a large enough moment arm to induce bending of the thin shafts at frequencies as low as 21 Hz. The only solution to this problem was to support both disks on both sides. This brought the bending mode frequency up to 1500 Hz, far enough out of the desired frequency window to be ignored.

To eliminate any nonlinear effects due to slipping in the couplings, a clamp-type coupling was used which effectively makes the motor shaft, coupling, aluminum shaft assembly one rigid member. In addition, the shaft was machined in one piece, again to prevent any slippage between sections. In order to isolate those sections of the shaft which are to act like torsional springs, intermediate sections

were made about twice as thick to increase the stiffness of those sections by an order of magnitude. In this way, the lumped parameter model still holds. The disks were to be clamped onto the shaft also, but this presented an assembly problem, since the bearing mounts are on both sides of the disks. The solution was to split the disks and clamp them onto the thick portions of the shaft. For added stiffness in the transverse direction, angular contact ball bearings support the shaft with preloads of 10 lb. to minimize clearance between the balls and races. The preload is achieved using wavy washers compressed against retaining rings. Figure 5.2 shows details of the stepped shaft, split disk, and bearing mounting. The result of all these efforts is a test fixture which closely conforms to a linear, lumped model. Now an actuator had to be found which could accurately duplicate the forcing functions. The critical parameter is the rise time of the torque output of the motor. In order to switch accurately at the switching rates required by the bang-bang function, a rise time on the order of 1 msec is required. Since the torque and current are proportional,

$$T = K_t i \tag{5.1}$$

this requires that the current in the motor rise rapidly and hold its peak value regardless of motor speed. All DC motors, however, generate a back emf voltage proportional to motor speed. For a step voltage input, as the motor speed increases the back emf voltage increases and the current decreases with smaller net voltage in the circuit. To maintain current irrespective of motor speed requires that the current to the motor be controlled. Thus a transconductance current amplifier is required to generate a step change in current which generates a step change in torque according to (5.1). A slight problem with this technique is that all motors have some inductance which resists any outside imposition of current. However, if this inductance is sufficiently small, the current amplifier essentially overrides the inductance. The effect is similar to prescribing the velocity of a mass, which can be done as long as the mass is very small. Therefore, a low inductance, permanent magnet DC motor was chosen in conjunction with a current amplifier. The combination generates a current output having approximately 0.25 msec rise time, quite

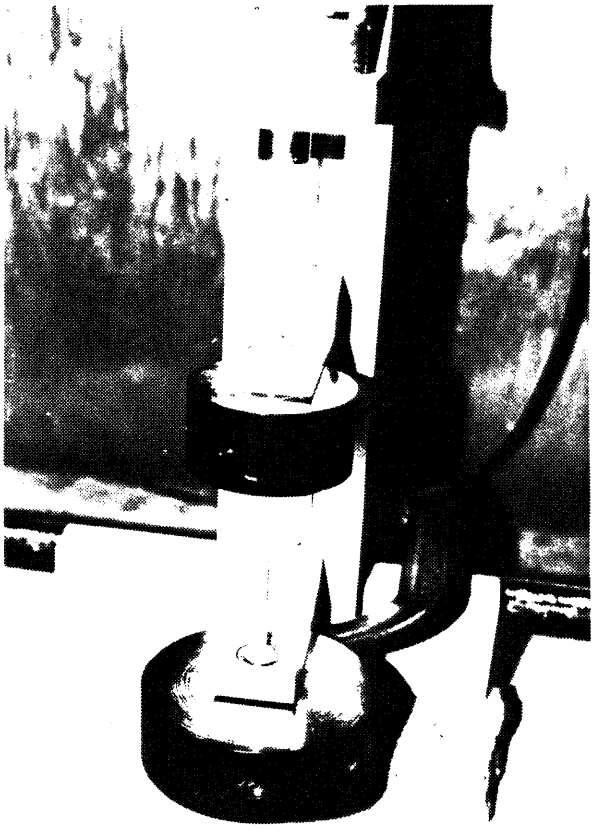

Figure 5.2: Detail of Shaft, Disk, and Bearing Mounting

satisfactory in duplicating the switching bang-bang forcing function.

The actual forcing function waveforms are generated via software in a DEC PDP-11/44 computer, converted to analog voltages using a Datel D/A Converter, and the current amplifier generates a current waveform proportional to the voltage waveform. This current produces a corresponding torque in the motor which drives the system. An accelerometer mounted tangentially on the largest disk, farthest away from the motor, senses the acceleration of the end disk. A triaxial accelerometer was chosen since it can be mounted flush on a face whose normal does not coincide with the sensing direction (Fig. 5.3). This permits tangential measurements of acceleration which can easily be converted to torsional acceleration. Both this signal and a voltage equivalent of the motor current generated by the current amplifier are fed into the computer, via the Datel A/D Converter, where the data is subsequently plotted. A block diagram schematic of the experimental setup is shown in Fig. 5.4.

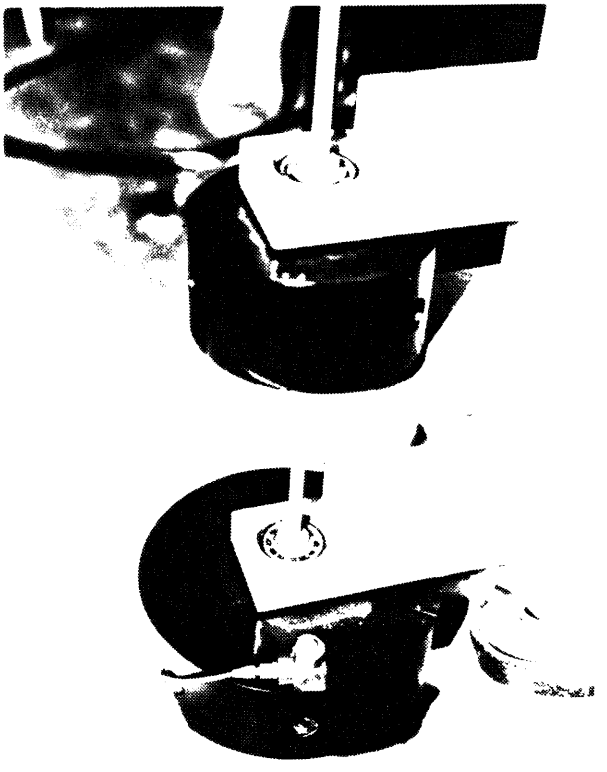

Figure 5.3: Accelerometer Mounting

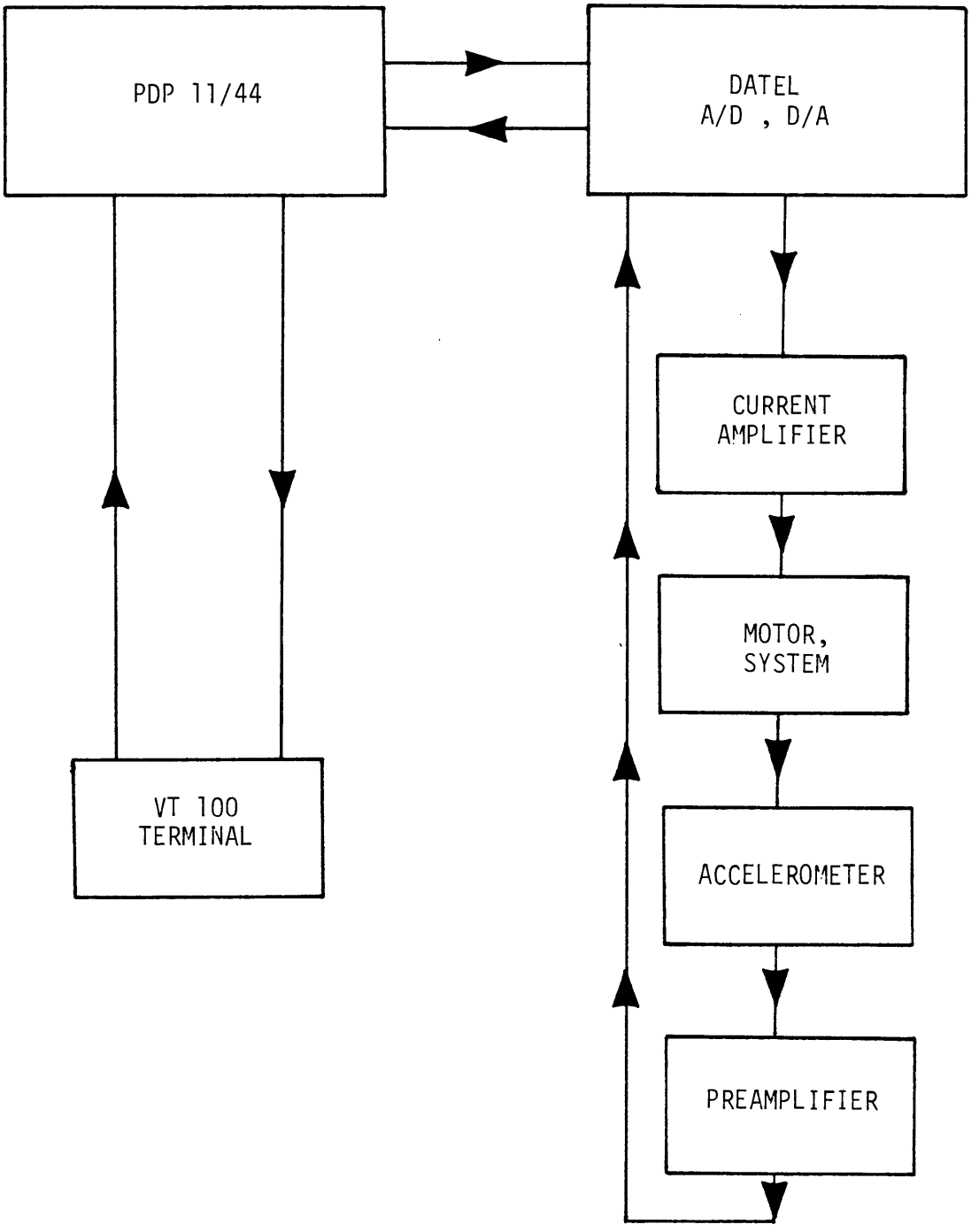

Figure 5.4: Block Diagram of Experiment

Chapter 6.

Experimental Results

Before actual tests could be performed using the forcing functions under consideration, an accurate transfer function of the experimental system had to be obtained. This would pinpoint the actual resonant frequencies and take into account the effects of system damping and slight parameter deviations. A Hewlett-Packard 5423A Structural Dynamics Analyzer was used to generate the transfer function. The disks were impacted tangentially with an impact hammer whose force transducer measures the impact input to the system while the accelerometer measures acceleration output. Figure 6.1 shows the details of the impacting procedure. Transfer functions were generated for three cases, by impacting each disk and the motor coupling in turn while measuring the acceleration at the impact points. As the modal analysis verifies, the higher resonance is only dominant in the smallest inertia, the motor, since both the large disks are near nodes for that mode. The fundamental resonance is readily visible at all three impact points. Thus, the best location to determine the system transfer function is at the motor coupling. Figure 6.2 shows the resulting frequency response plot. Pronounced peaks are evident at about 19.5 Hz and 117.3 Hz, values which are a bit lower than expected owing to the inertia of the motor coupling and the presence of damping in the real system.

The values of these resonant frequencies, together with inertia figures of the three masses, were used in the ideal model representation to generate the appro-

Figure 6.1: Details of Impacting Technique

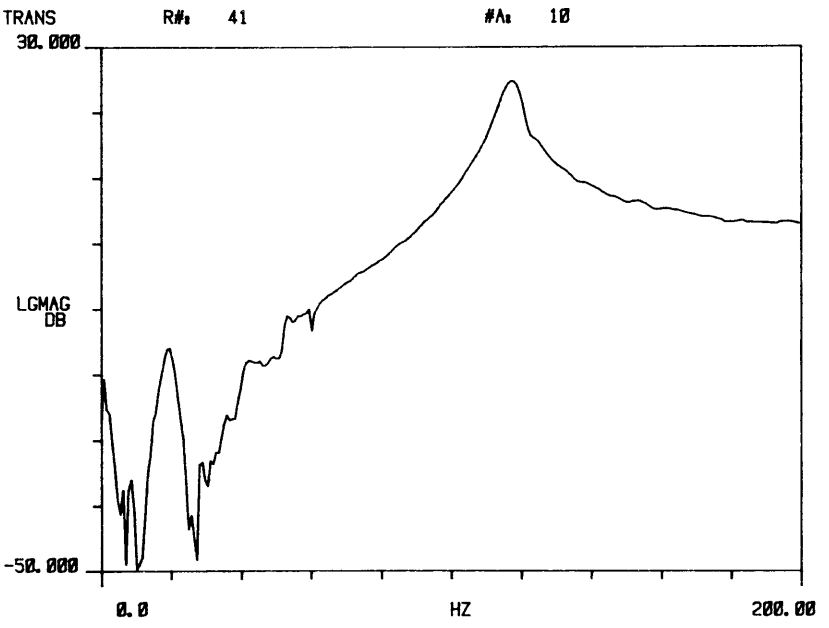

Figure 6.2: Magnitude of Frequency Response

priate forcing functions. The model along with the system parameters is shown in Fig. 6.3. Results of initial tests for an angular rotation of 29 degrees are shown in Figures 6.4 to 6.7. The tests were run with a peak motor torque of 3 lb-in. Each figure shows the current, i.e. torque, waveform in (a) and below it in (b) the accelerometer output. Figure 6.4 shows the response to a square wave input. Figures 6.5 and 6.6 show two bang-bang responses, a 5-switch and a 3-switch respectively. The 5-switch function treats the system as having two significant resonant frequencies and ideally eliminates vibration at both frequencies. The simpler 3-switch function gives slightly larger residual vibration amplitude of the fundamental resonance, but shows no increase in higher frequency vibration since the end mass barely sees the resonance at 117 Hz. This can be seen in Fig. 6.6. Notice that both bang-bang functions reduce residual vibration to 15 % of the square wave vibration at that move angle. And even though considerable vibration still exists throughout the move, the bang-bang function does prevent the large increase in vibration which occurs halfway through the square wave response.

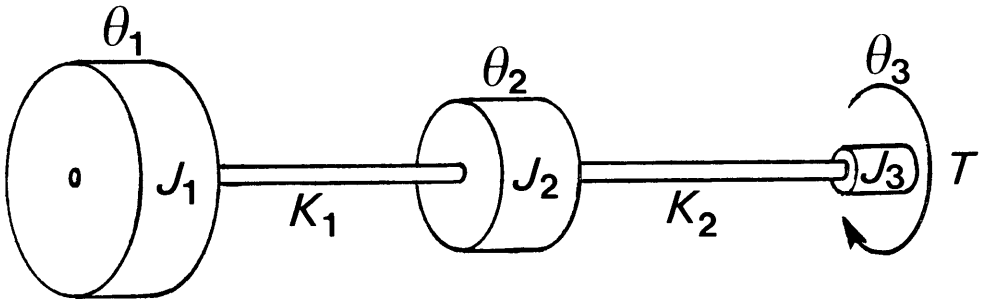

$J_1 = 0.161$ lb·in·sec^2

$J_2 = 0.0292$

$J_3 = 0.001424$

$\omega_2 = 19.5$ hz

$\omega_3 = 117.3$

$T = 3.0$ lb·in

Figure 6.3: Idealized Model of Test System and Parameters

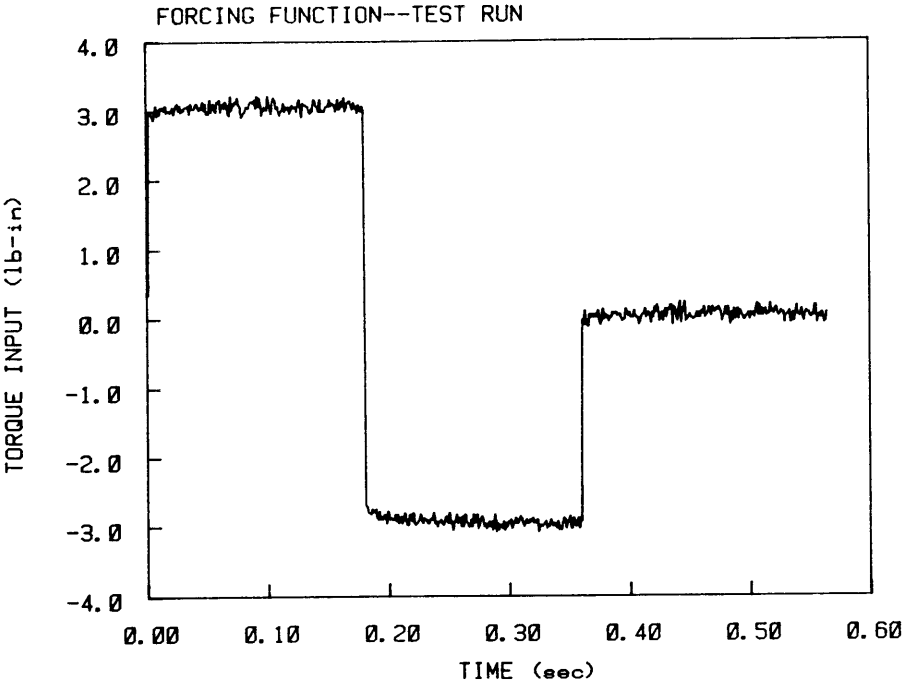

(a)

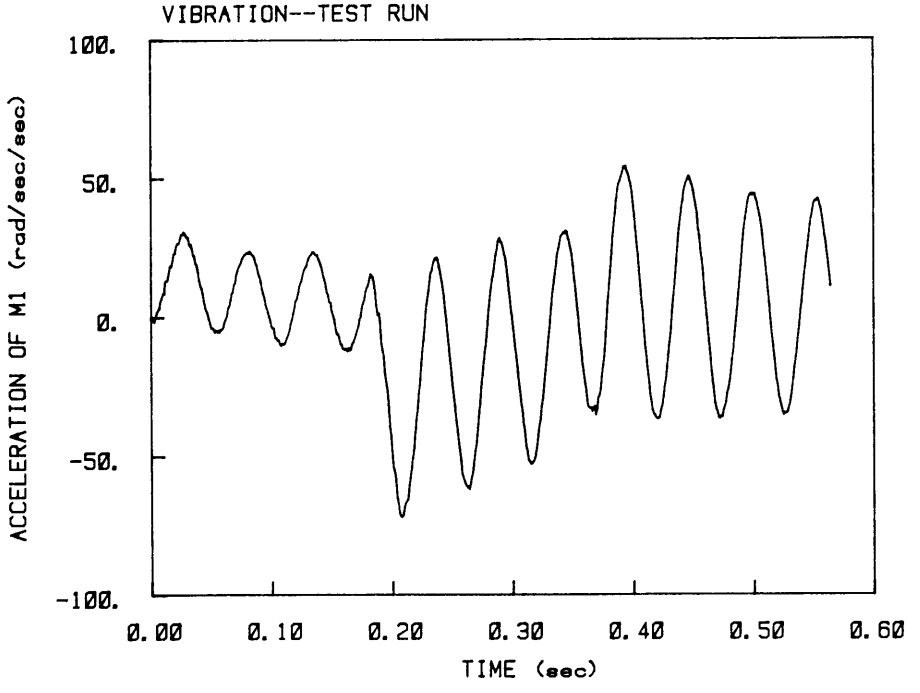

(b)

Figure 6.4: Square Wave Response:(a)Torque Input.(b)Acceleration Response.

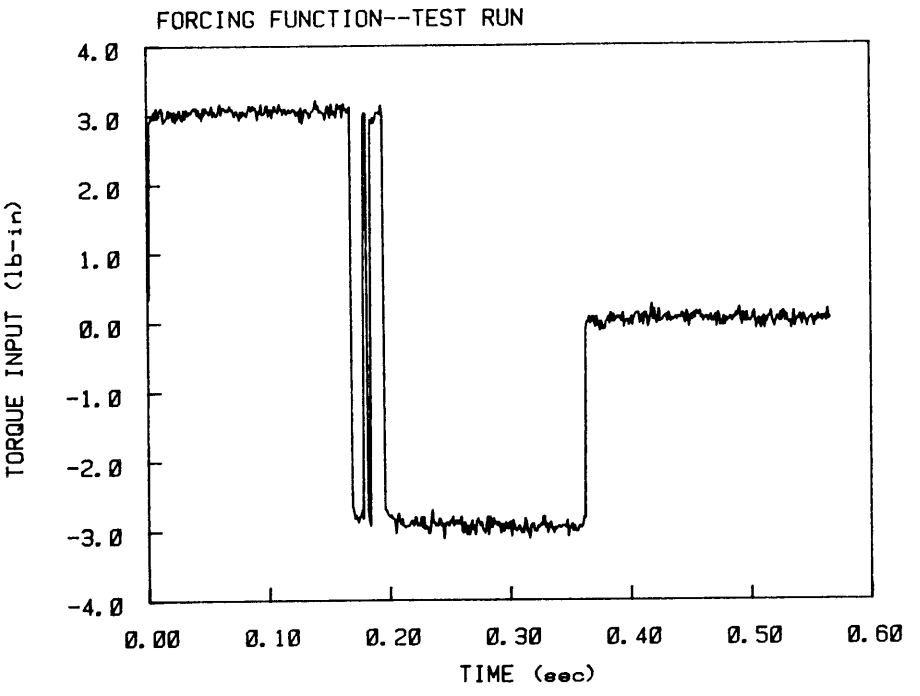

(a)

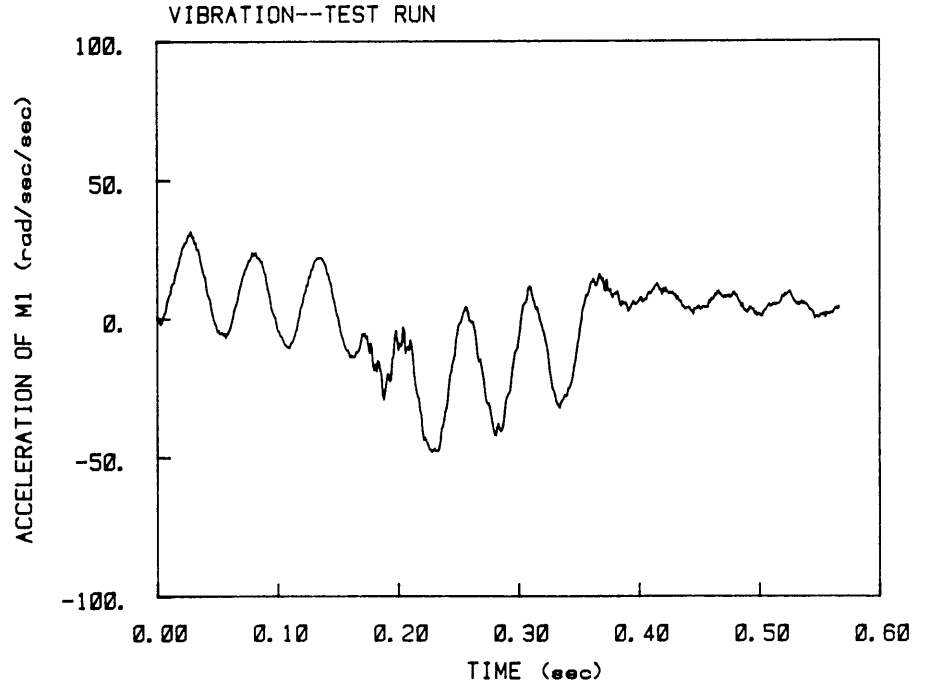

(b)

Figure 6.5: 5-Switch Bang-Bang Response:(a)Torque Input.(b)Acceleration Response.

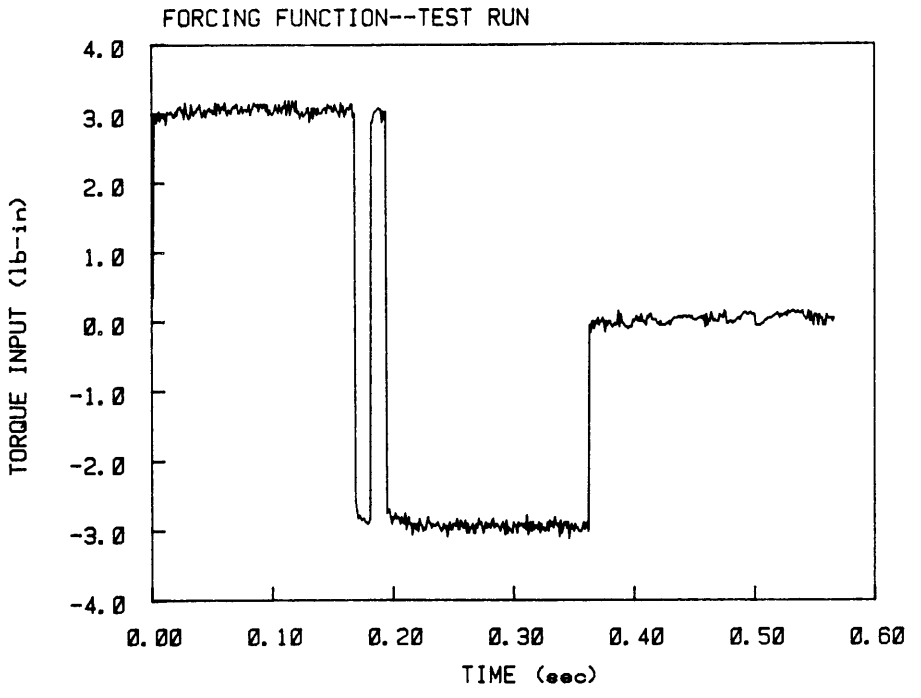

(a)

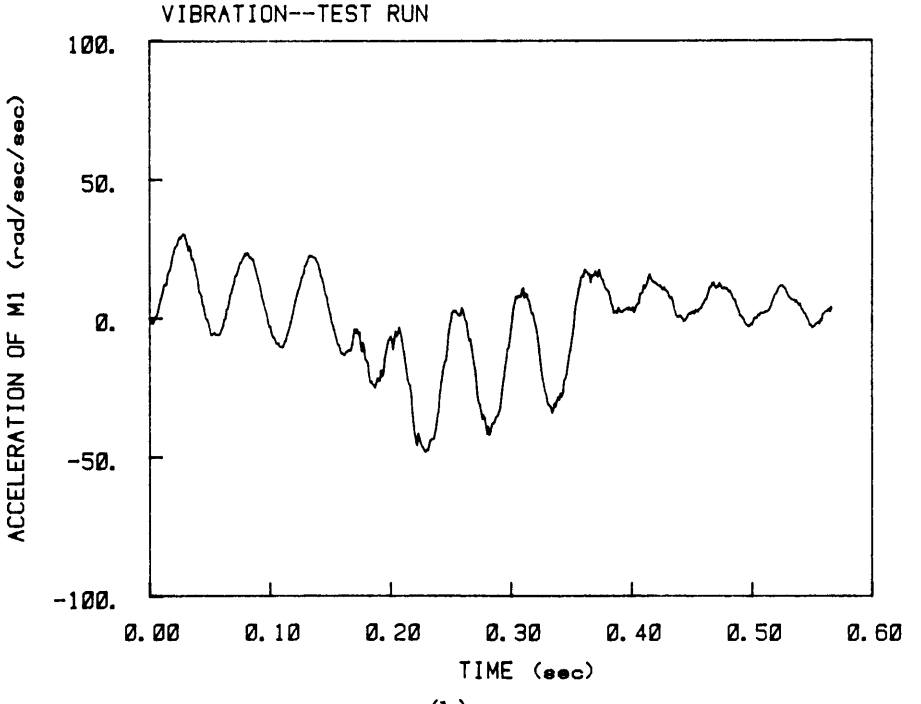

(b)

Figure 6.6: 3-Switch Bang-Bang Response:(a)Torque Input.(b)Acceleration Response.

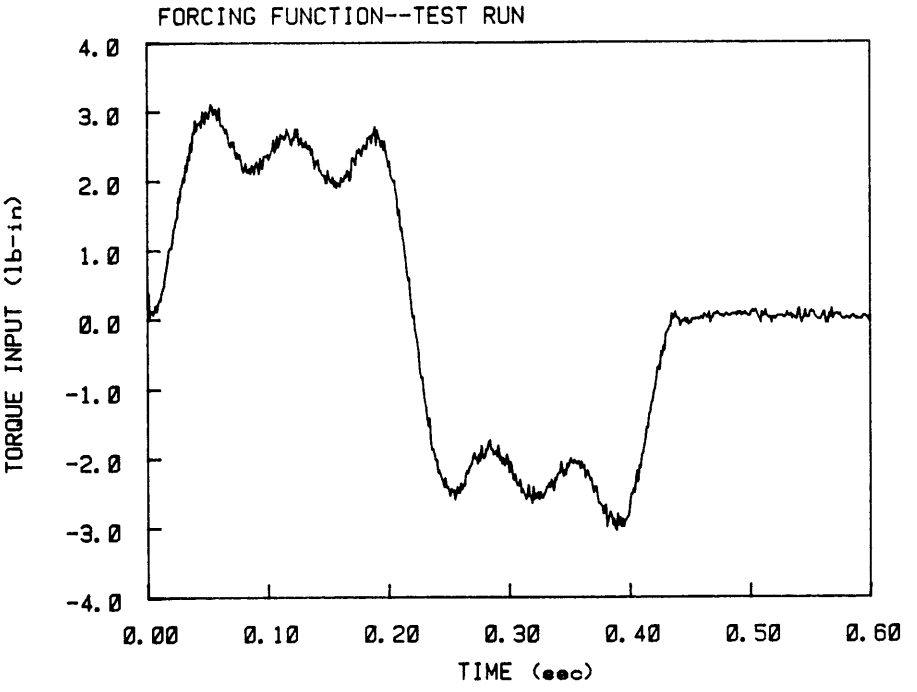

(a)

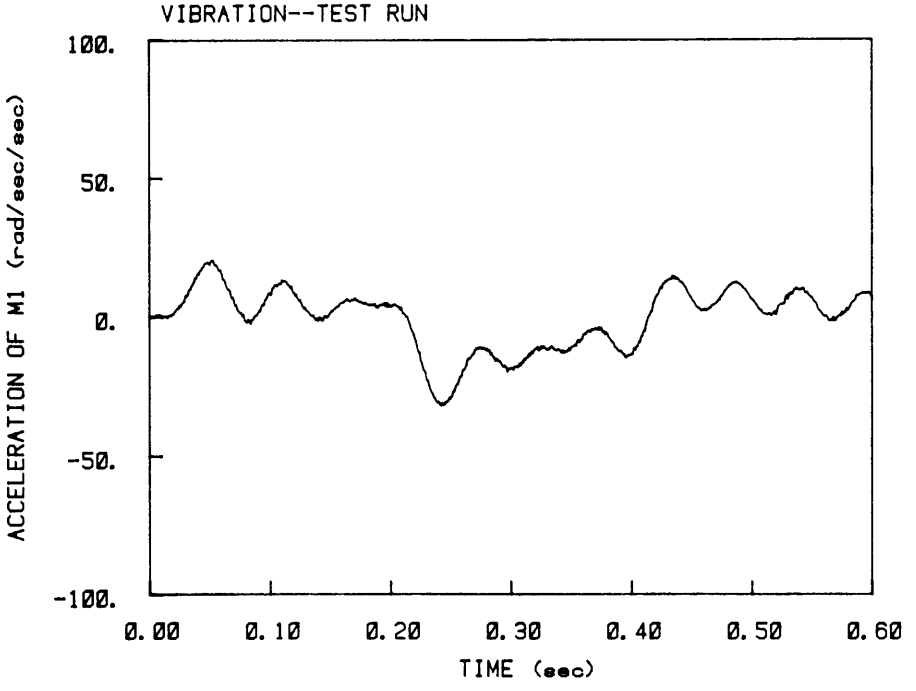

(b)

Figure 6.7: Ramped Sinusoid Response:(a)Torque Input.(b)Acceleration Response.

The ramped sinusoid forcing functions used in these tests were selected by choosing an appropriate L for each move angle. For this 29 degree rotation,the frequency domain criterion chose a 5-term series. The forcing function and corresponding acceleration response are shown in Fig. 6.7. Compared to the optimal time of 0.36 sec for the bang-bang function to rotate 29 degrees, this ramped sinusoid series takes almost 0.44 sec, nearly 22 % longer. However, it does produce less residual vibration, only 12.5 % of the corresponding square wave amplitude. In addition, the vibration amplitude present throughout the move has been reduced by 75 %, in comparison with either the square wave or the bang-bang functions. Therefore, if vibration attenuation throughout the move is important, this ramped sinusoid function gives satisfactory response, at the expense of fast move times.

A few comments about the response plots are in order. The current signals show some high-frequency noise around the desired forcing function signal. It is unclear where this comes from but it appears to be at megahertz frequencies, which suggests it might be radio frequencies interfering with instrument signals. It definitely does not indicate fluctuations in the current to the motor since its electrical impedance filters out all such high frequencies.

The acceleration curves also are less than ideal since the preamplifier used for the accelerometer cuts off low frequencies. This is particularly evident for the bang-bang forcing function. The actual signal shows some decay at each step transition, while the simulated results predict natural oscillation about constant levels corresponding to the step functions comprising the bang-bang function. Thus, the instrumentation is unable to exactly duplicate the expected response functions.

The foregoing response characteristics for a 29 degree rotation look promising, but only represent vibration attenuation at one particular move. Only composite data over a range of moves can indicate whether these are isolated results or truly represent favorable vibration characteristics of the two chosen functions. Therefore, a set of response data was collected for each of the functions under investigation to determine residual vibration for rotations between 1 degree and 200 degrees, at

1 degree increments.

The residual vibration amplitudes for the square wave over the range of move angles again provides a worst-case mean amplitude against which the selected function responses can be compared. Figure 6.8(a) shows the plot of actual residual vibration amplitudes, showing the characteristic rising and falling observed earlier (see Sec. 4.1). The periodicity of this fluctuation increases with move angle since angular displacement is related to the square of the move time. In terms of move time, the periodicity of the peaks would be constant. These results provide a mean square wave amplitude in the actual system of 23.5 rad/sec^2.

To indicate how well the assumed system model predicts experimental results, a plot of theoretical square wave residual amplitude is shown in Fig. 6.8(b). The locations of the peaks and valleys do not coincide, suggesting that some of the assumed system parameters are in error. And even though a constant peak amplitude is predicted, actual amplitudes decrease with move angle. This is probably a result of inherent system damping, which reduces the vibration amplitude at larger moves, and results in a lower mean level of vibration. This is borne out when comparing the predicted mean amplitude of 32.2 rad/sec^2 with the actual mean amplitude of 23.5 rad/sec^2. The discrepancies between the model and the actual system are also responsible for the small, nonzero residual vibration which occurs at angles where theory predicts zero vibration.

Having obtained a measured mean square wave amplitude, it is now possible to assess the degree of vibration attenuation for the two functions over a range of moves. Figures 6.9(a) and 6.10(a) show the measured residual amplitudes for the 5-switch bang-bang function and the ramped sinusoid series, respectively. Both functions excite significant residual vibration at certain moves. The mean amplitude of 20.7 rad/sec^2 for the bang-bang function suggests only a 12 % reduction over the square wave. The ramped sinusoid functions, on the other hand, show better improvement, reducing mean amplitude to 7.1 rad/sec^2, a 70 % improvement, giving mean vibration only 30 % of that for the square wave.

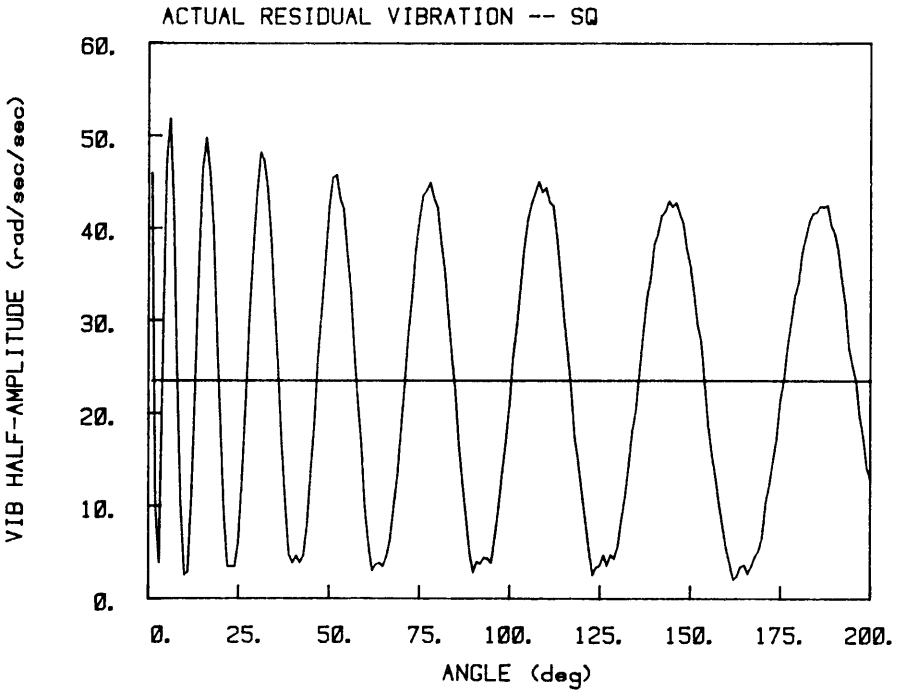

(a)

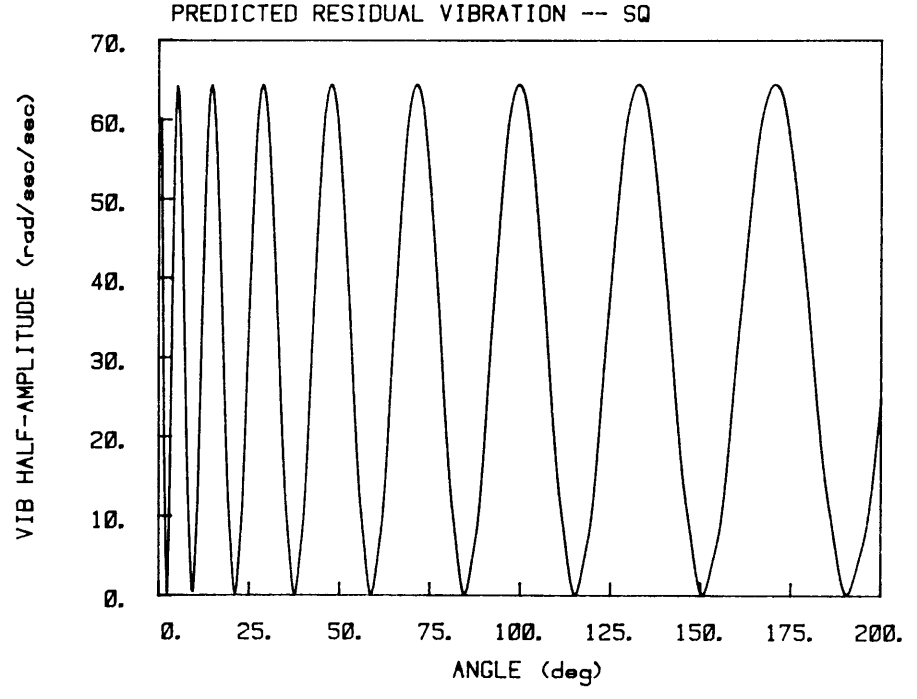

(b)

Figure 6.8: Square Wave Vibration:(a)Actual Vibration.(b)Predicted Vibration.

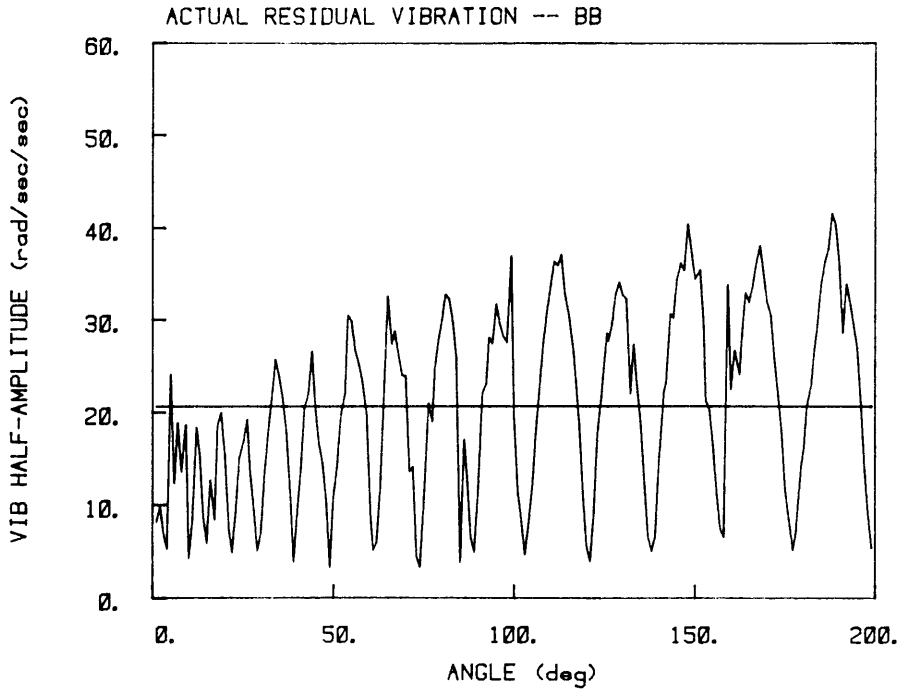

(a)

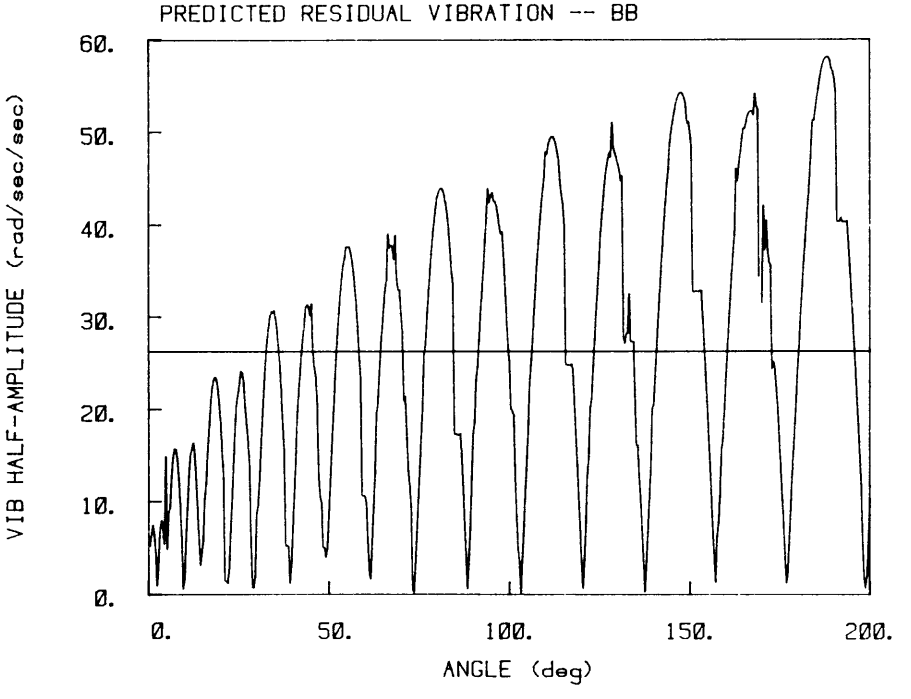

(b)

Figure 6.9: Bang-Bang Vibration:(a)Actual Vibration.(b)Predicted Vibration.

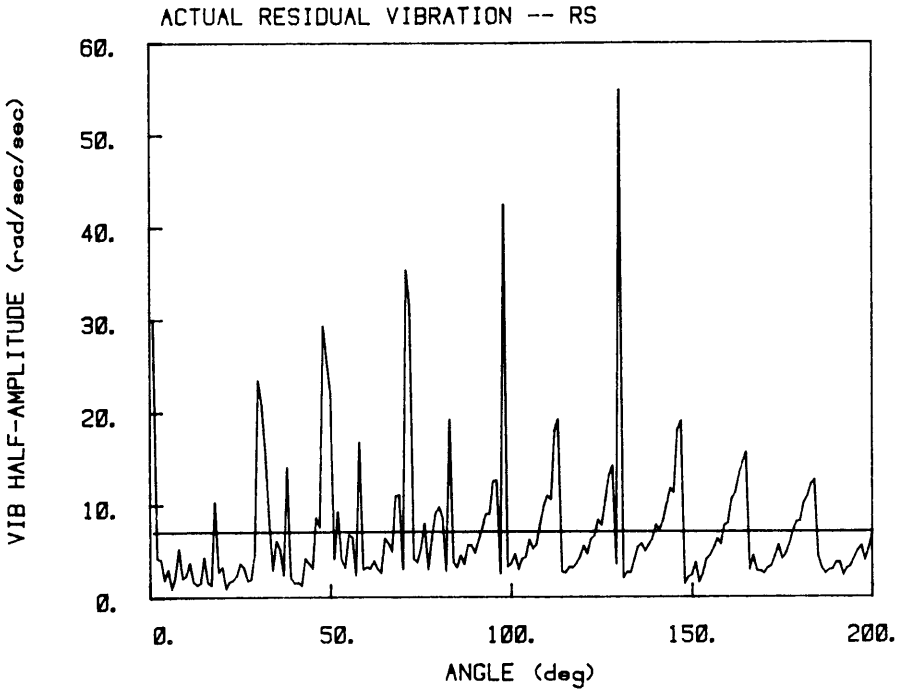

(a)

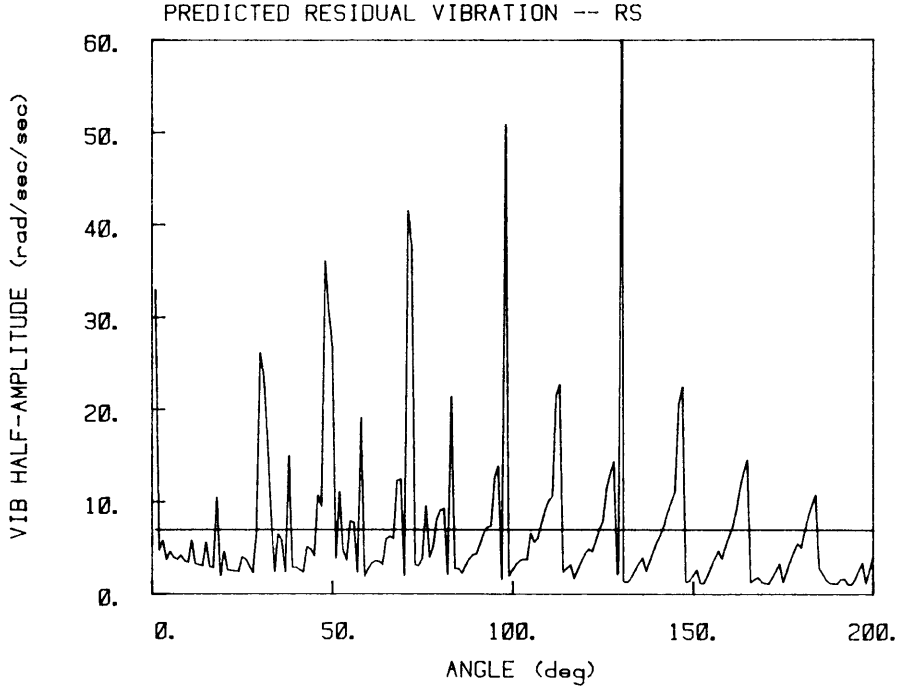

(b)

Figure 6.10: Ramped Sinusoid Vibration:(a)Actual Vibration.(b)Predicted Vibration.

Since the square wave residual vibration plot suggests parameter errors, a plot predicting amplitudes in the presence of errors in ω_2 will provide an appropriate comparison with the actual amplitude plots for the bang-bang and ramped sinusoid functions. Figures 6.9(b) and 6.10(b) show theoretical residual amplitudes when simulated ω_2 is 4 % smaller than that used to generate the forcing functions (see Sec. 4.4). Actual and predicted curves have similar attributes. The more frequent periodicity of the bang-bang plot as compared to the square wave plot is substantiated. And the spikes seen in the actual ramped sinusoid residual amplitude curve are in the predicted curve with parameter errors. This supports the contention that the system model is in error. Attempts to improve the theoretical model will be discussed in the next two chapters; chapter 7 treats the damping problem, while chapter 8 discusses parameter adjustments.

Chapter 7.

Damping

7.1. Viscous Damping

It is clear from the experimental results that the system model adopted here does not adequately describe all the dynamics in the real system. Since the exact shape of the bang-bang function is determined by switches which must be exactly tuned to system parameters, an accurate model is especially important for the bang-bang functions. Experimental results show that residual vibration remains which can be attributed to the discrepancies between the actual system and the ideal model upon which the switch times are based. One of the more significant deficiencies in the model is its assumption of zero damping. Any real system has some damping, even if it be small. To evaluate this effect, a small amount of damping was introduced into the simulation. Actual system parameters were used to generate system reponse to a 5-switch bang-bang function. Figure 7.1 shows this response when some viscous damping is assumed to act between the masses. Because of the decay in the vibration amplitude, the system is always at a different place when switching occurs than it would be without damping. Thus when the system arrives at the endpoint where the forcing function is removed, it has a position other than zero and hence has a residual acceleration that leads to continued vibration. Seen in the phase plane portraits discussed earlier, the effect of damping is to diminish the radius of rotation and give inward spirals. At every switch, the system has

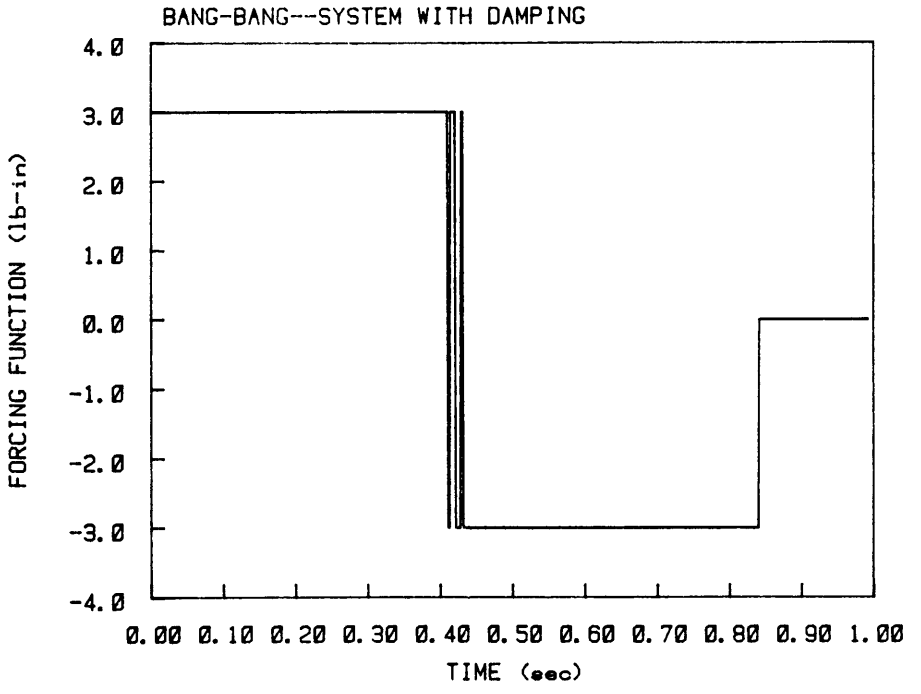

(a)

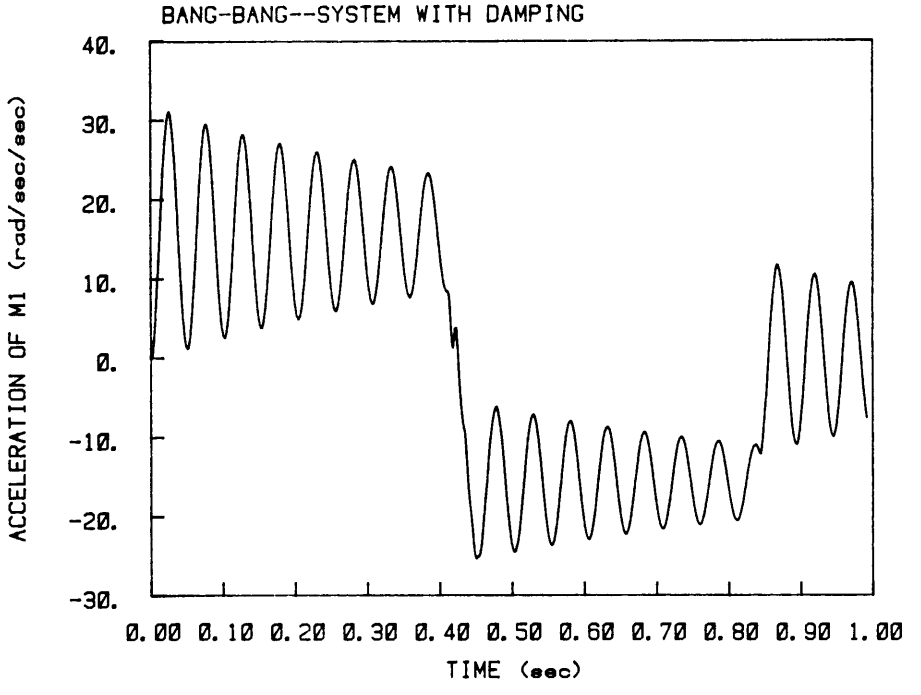

(b)

Figure 7.1: Bang-Bang Response in the Presence of Viscous Damping.(a)Torque Input.(b)Acceleration Response.

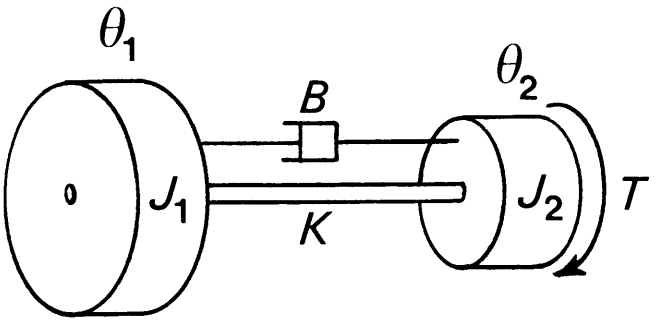

$$\zeta = 0.026265$$

Figure 7.2: Idealized System Model with Viscous Damping

moved closer toward the center of the spirals and these radial deviations cause the system to miss the origin at the end of the move and continue oscillating about the origin. A set of asymmetric switches is necessary to eliminate residual vibration.

A new set of switches can be derived in the same way as the original symmetric switches were derived, this time including the effect of damping. Since the equations become more complex with damping, a simpler two-mass system makes it easier to develop the formulation for the switch times. A lower-order model is a good approximation here since the real system as viewed from the end mass behaves very much like a system with a single resonance. It does not, however, apply in general for any real system. The model used here, with viscous dampers between the masses, is shown in Fig. 7.2.

The first step in deriving a new set of switches is to decouple the system into its natural modes. This cannot always be done in general except when the damping matrix can be written as a linear combination of the mass and stiffness matrices. Since the two-mass system has only one damping term and one stiffness term, the

two can be related by a weighting constant, thereby permitting modal decoupling. The result is a set of two modal equations, one in translation, the other in damped oscillation:

$$\ddot{y}_1 = C_1 u \tag{7.1}$$

$$\ddot{y}_2 + 2\zeta\omega_2\dot{y} + \omega_2^2 y_2 = C_2 u \tag{7.2}$$

Since the order of the system is unchanged with damping, a set of three switches should still enable the system to come to rest at the endpoint. Solving (7.2) and setting the response to zero at time t' greater than the final time T_f yields two conditions on the switch times:

$$\begin{aligned}\cos\varphi - 2e^{\zeta\omega_2 t_1}\cos(\omega_{d2}t_1 - \varphi) + 2e^{\zeta\omega_2 t_2}\cos(\omega_{d2}t_2 - \varphi) \\ - 2e^{\zeta\omega_2 t_3}\cos(\omega_{d2}t_3 - \varphi) + e^{\zeta\omega_2 T_f}\cos(\omega_{d2}T_f - \varphi) = 0\end{aligned} \tag{7.3}$$

$$\begin{aligned}\sin\varphi + 2e^{\zeta\omega_2 t_1}\sin(\omega_{d2}t_1 - \varphi) - 2e^{\zeta\omega_2 t_2}\sin(\omega_{d2}t_2 - \varphi) \\ + 2e^{\zeta\omega_2 t_3}\sin(\omega_{d2}t_3 - \varphi) - e^{\zeta\omega_2 T_f}\sin(\omega_{d2}T_f - \varphi) = 0\end{aligned} \tag{7.4}$$

where φ is the phase angle and ω_{d2} is the damped natural frequency given by $\omega_{d2} = \omega_2\sqrt{1-\zeta^2}$. Since three switch times and the final time T_f must be determined, two more equations are necessary to uniquely define these values. One expression is actually the basis for the symmetry constraints obtained in the undamped case. It is a linear expression relating the three switch times and can be derived simply by specifying that the end velocity be zero. This requires that the integral of the acceleration curve be zero at time T_f, or since acceleration and input force are related, it requires that the integral of the three-switch forcing function be zero at T_f. This leads to another equation:

$$t_1 - t_2 + t_3 - T_f/2 = 0 \tag{7.5}$$

Notice that the requirement that $t_2 = T_f/2$, which specifies the central switch, combined with (7.5) leads to the symmetry relations used in the undamped analysis.

With damping, this central switch point is no longer correct and (7.5) becomes a simple relation between t_1, t_2, and t_3 without any implications of symmetry.

A final expression relating the switch times and T_f to the final move distance x_f can be obtained in the same way as before using the same rigid body mode:

$$(m_1 + m_2)x_f = \frac{F}{2}\left[T_f^2 - 2(T_f - t_1)^2 + 2(T_f - t_2)^2 - 2(T_f - t_3)^2\right] \qquad (7.6)$$

The four equations (7.3) to (7.6) are sufficient to solve for t_1, t_2, t_3, and T_f numerically. The problem is in determining appropriate initial guesses to ensure convergence to the correct optimal set of switches. As in the undamped case, a switching function can be derived but this time no symmetry constraints exist to solve for some of the unknown constants. A new approach is necessary.

As verified in the earlier analysis, the type of system under investigation gives time-optimal response when forced with a bang-bang function. For such a system, the necessary optimality condition is also unique. Thus if a method could be found to solve for the arbitrary constants in the switching function, the result would be a unique solution to the switch times. The necessary condition on the forcing function $u(t)$ is given by

$$u(t) = \text{sgn}\{\eta(t)\,\mathbf{b}\} \qquad (7.7)$$

where $\eta(t)$ satisfies the adjoint system given by

$$\dot{\eta}(t) = -\eta\,\mathbf{A}. \qquad (7.8)$$

The solution to $\eta(t)$ is

$$\eta(t) = \eta^o \left(e^{-\mathbf{A}^T t}\right)^T \qquad (7.9)$$

and $u(t)$ is given by

$$u(t) = \text{sgn}\left\{\eta^o \left(e^{-\mathbf{A}^T t}\right)^T \mathbf{b}\right\} \qquad (7.10)$$

In order to uniquely define $u(t)$, the initial conditions of the adjoint system η^o must be known. This vector can only be determined if it can be related to the initial

conditions of the actual system $\mathbf{x}^o$. To arrive at this relationship, the solution to the original system must be obtained. The final state at time T_f is given by:

$$\mathbf{x}(T_f) = e^{\mathbf{A}T_f}\,\mathbf{x}^o + e^{\mathbf{A}T_f}\int_0^{T_f} e^{-\mathbf{A}t}\,\mathbf{b}\,u(t)\,dt \tag{7.11}$$

Assuming the final state to be the origin,

$$\mathbf{x}(T_f) = 0, \tag{7.12}$$

the result for $\mathbf{x}^o$ is given by

$$\mathbf{x}^o = -\int_0^{T_f} e^{-\mathbf{A}t}\,\mathbf{b}\,u(t)\,dt \tag{7.13}$$

In this case, the final state is not exactly the origin since a final displacement of x_f is desired. But a simple shift of scales gives as initial conditions $-x_f$ position and zero velocity. Substituting (7.10) into (7.13) gives

$$\mathbf{x}^o = -\int_0^{T_f} e^{-\mathbf{A}t}\,\mathbf{b}\,\mathrm{sgn}\left\{\eta^o\left(e^{-\mathbf{A}^T t}\right)^T\mathbf{b}\right\}\,dt \tag{7.14}$$

This is the desired relationship between the initial conditions of the original system and the adjoint system. We need the inverse of this relation. Knudsen [34] shows that such an inverse does indeed exist and is unique and then proceeds to give a numerical iteration scheme to converge on η^o given $\mathbf{x}^o$. With this vector uniquely determined, $u(t)$ is uniquely determined and the precise locations of the optimal switch times can be found.

Since this scheme involves lengthy computations, it would be useful to determine if the newly derived switches actually help reduce residual vibration in the experimental system. An arbitrary set of switches which satisfy the simultaneous equations (7.3)–(7.6), even if suboptimal, can at least suggest the usefulness of this method. A forcing function consisting of such arbitrary switches (Fig. 7.3) was tested in a computer simulation with encouraging results, as shown by the response plot in Fig. 7.4. The angular rotation is 158.6 degrees. In this case,

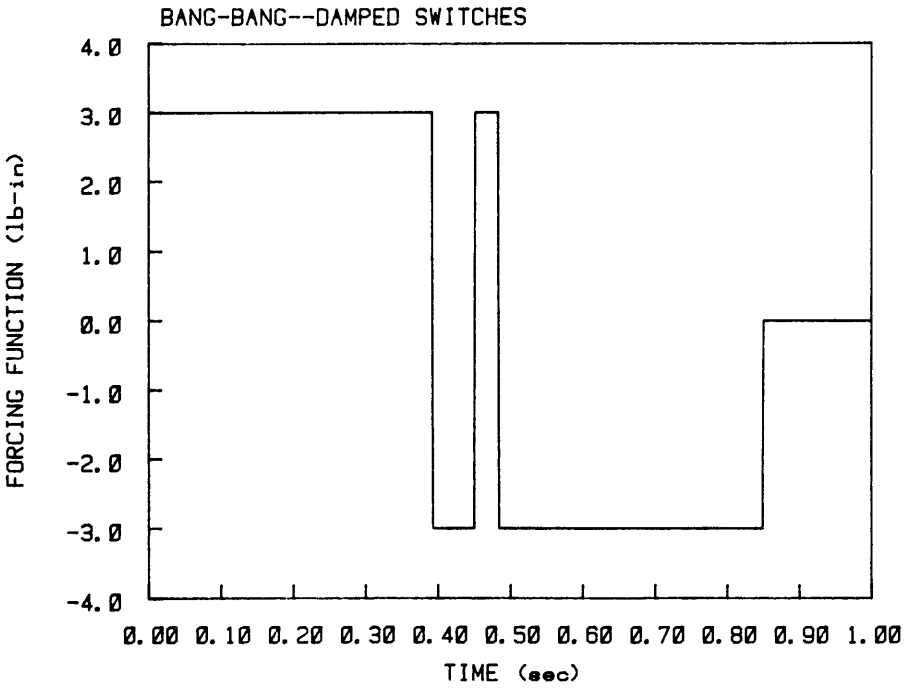

Figure 7.3: Bang-Bang Function with Damped Switches

the higher frequency residual vibration remains, since only a 3-switch function was used. But the dominant fundamental vibration has been eliminated.

A determination of the damped switch times for the real system requires a knowledge of the equivalent viscous damping in the system. Figure 7.5 shows a transient response for the large end inertia when impacted with an impact hammer. The amplitude appears to decay exponentially. Fitting an exponential curve to this plot gives a viscous damping ratio of 0.026. The forcing function with appropriate switching for this damping ratio gives vibration response for the real system as shown in Fig. 7.6(b). Notice that residual vibration still exists and has an even larger amplitude than that in response to the 5-switch bang-bang function of Fig. 7.6(a), derived without regard to damping. Clearly this is not the way to achieve better response for the bang-bang function.

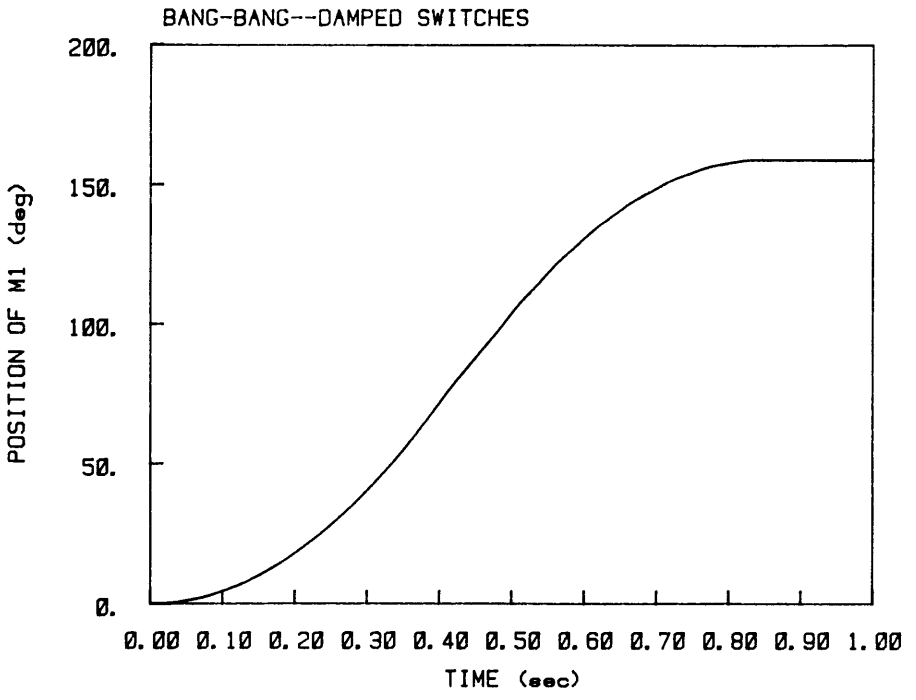

(a)

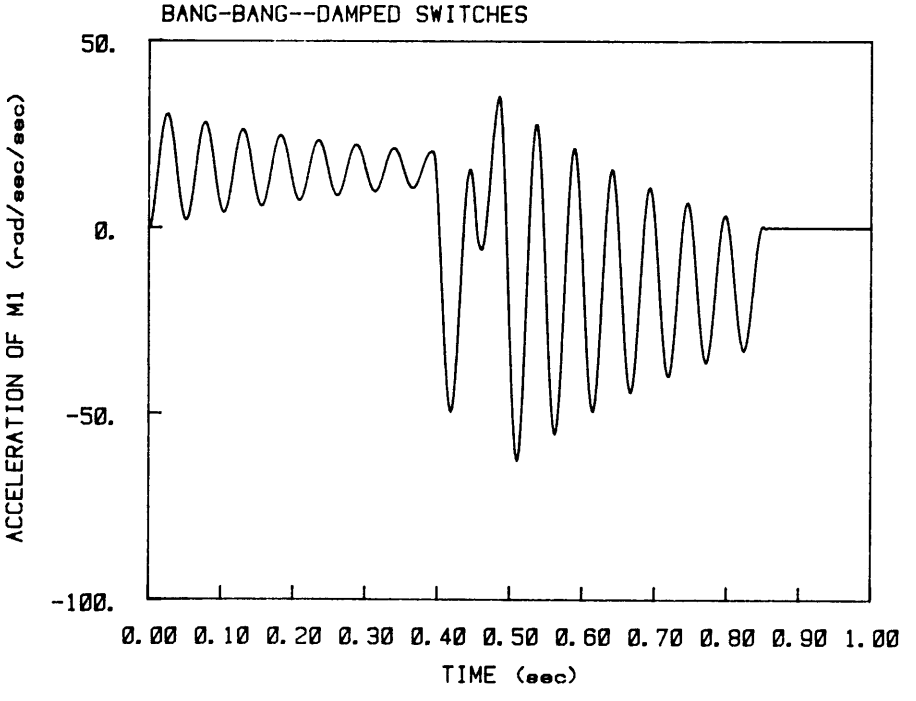

(b)

Figure 7.4: Simulated Damped Bang-Bang Response:(a)Position.(b)Acceleration.

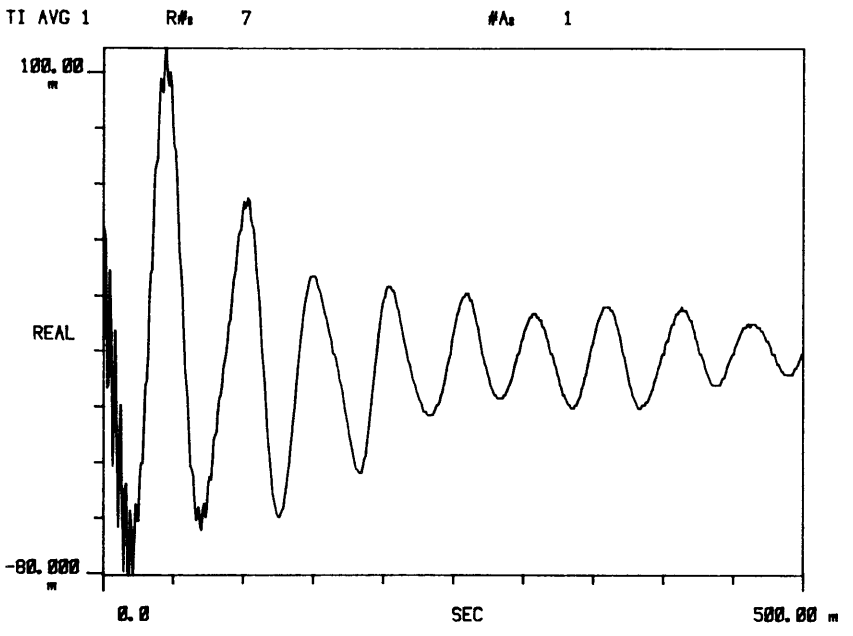

Figure 7.5: Experimental Transient Response

7.2. Friction Damping

One possible explanation for this degraded response is the inadequacy of the viscous damping model to correctly characterize the experimental system. The dissipation is most likely due to friction, both in the bearings and in the brushes of the motor. In addition, the viscous dampers between masses totally ignore dissipation between the system and ground, which is where most of it originates in the real system. Figure 7.7 shows a new model with friction between each of the masses and ground. This represents the dissipation in the motor brushes and the bearings. Since the bang-bang function appears to be more sensitive, the effect of friction on bang-bang response will again be investigated in a simulation.

Response to the 5-switch bang-bang function in the presence of friction is shown in Fig. 7.8. Fig 7.8(a) gives the position of m1 while Fig. 7.8(b) shows the acceleration plot. Notice that the mass backs up before the end of the move. This is a phenomenon which the accelerometer traces do not show but which actually

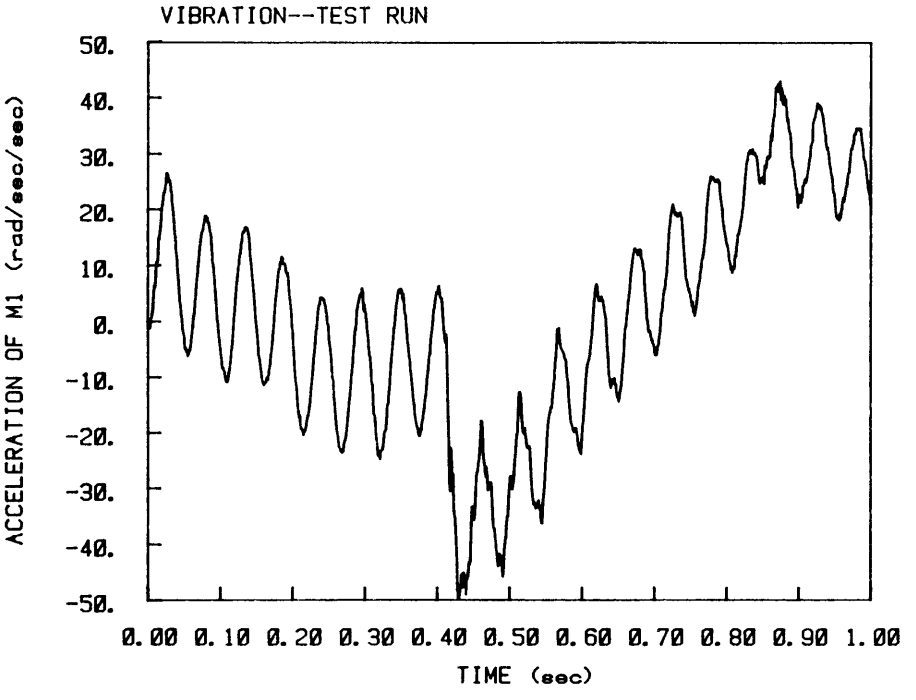

(a)

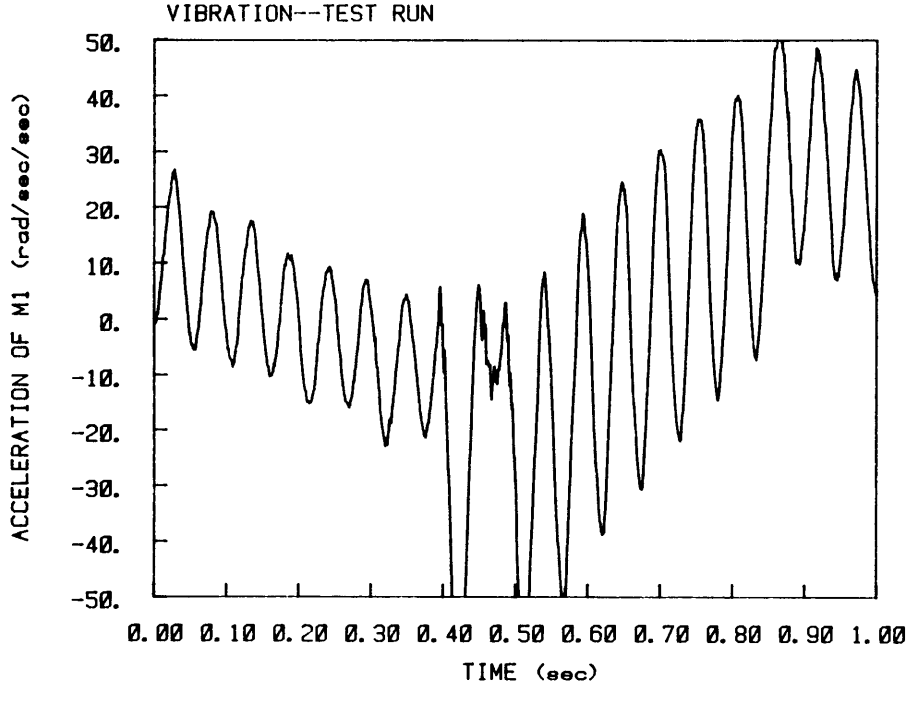

(b)

Figure 7.6: Actual Bang-Bang Acceleration Response.(a)Undamped Switches. (b)Damped Switches.

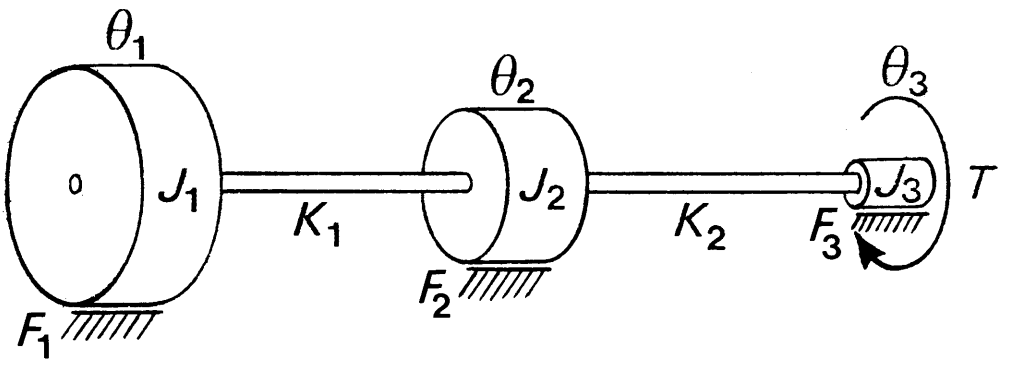

$$F_1 + F_2 + F_3 = 0.2 \text{ lb-in}$$

Figure 7.7: Idealized System Model with Friction

occurs in the experimental system. For the nominal 29 degree rotation, actual measured angular displacement is only 21 degrees because of this reversal. The simulation also predicts some residual vibration as a result of the friction. This suggests that the effect of the friction torque alone could cause the residual vibration which the real system experiences.

An easy way to compensate for this opposing torque is simply to raise the forcing function by the amount of measured frictional drag. This will work since the masses are always moving in the same direction, even though the vibration will increase and decrease the speed periodically. Thus the friction torque always opposes the motion and can be compensated for simply by supplying more torque throughout the move. Using this offset forcing function in the simulation gives encouraging results, as shown in Fig. 7.9. Again Fig. 7.9(a) shows the position response and Fig. 7.9(b) gives the acceleration response. This time the reversal of the mass has been eliminated and the residual vibration reduced, if not totally eliminated.

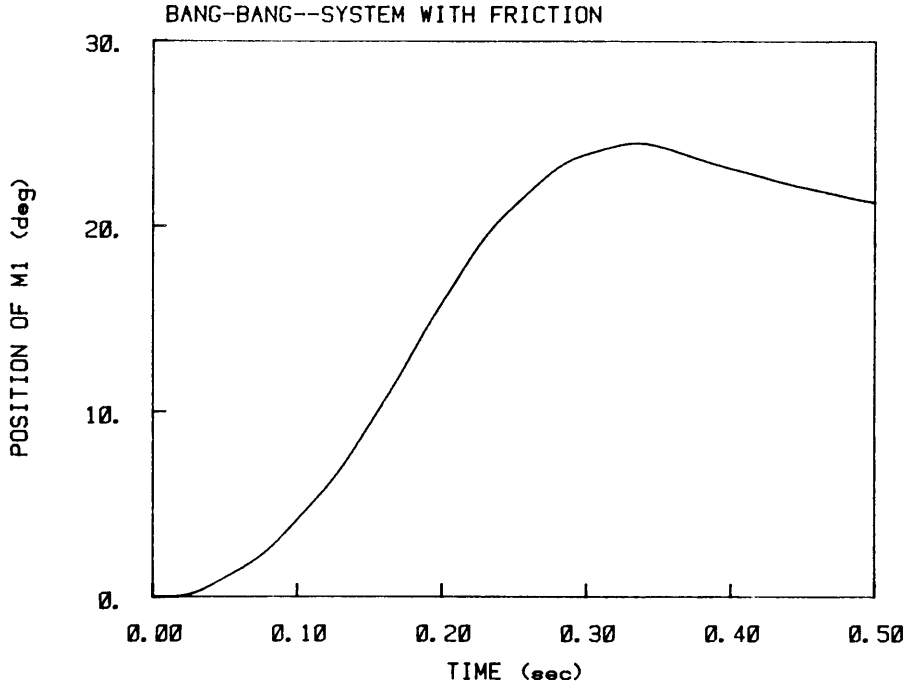

(a)

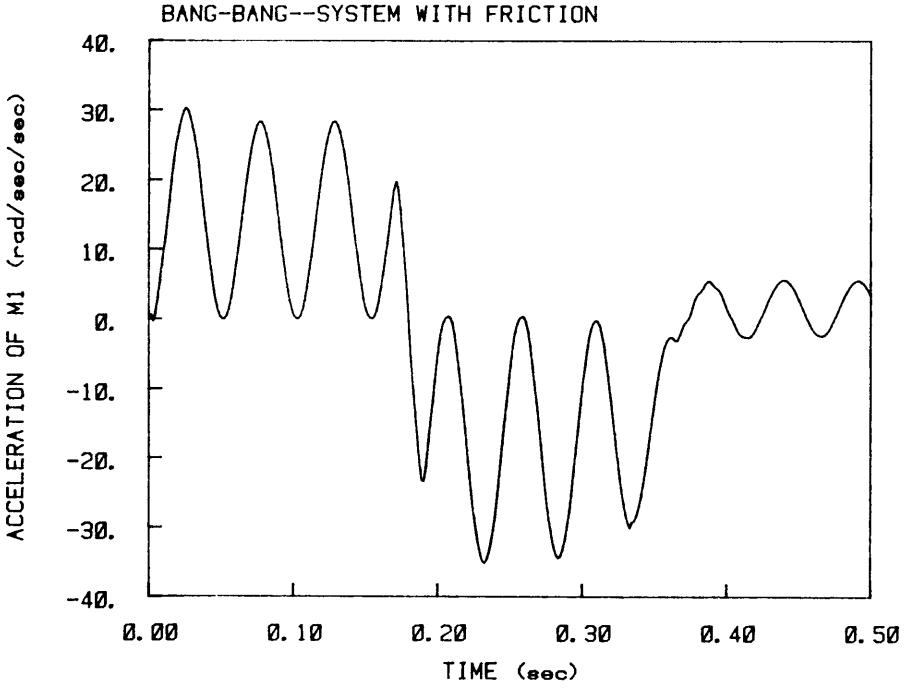

(b)

Figure 7.8: Simulated Bang-Bang Response in the Presence of Friction:(a)Position. (b)Acceleration.

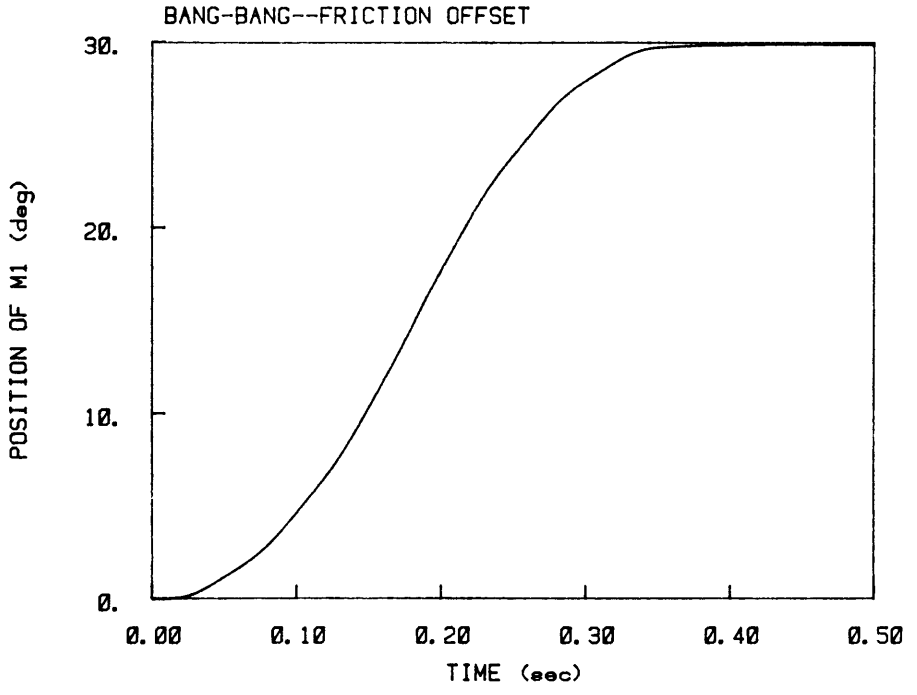

(a)

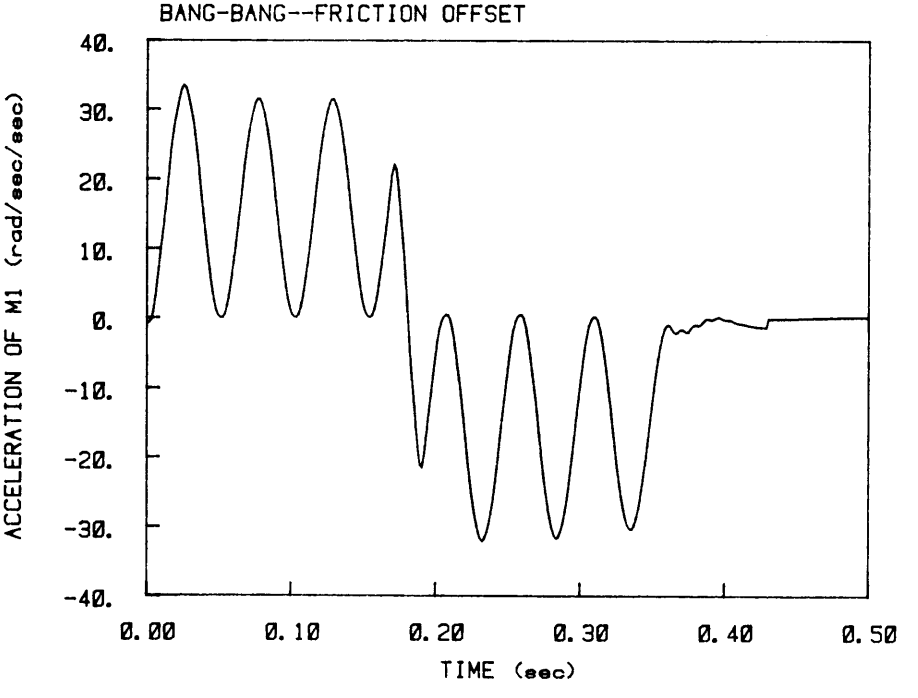

(b)

Figure 7.9: Simulated Bang-Bang Response with Offset for Friction Torque: (a)Position.(b)Acceleration.

To try this offset function on the real system, we need some idea of the friction opposing torque. The tachometer output of the motor during deceleration shows a nearly constant slope. Knowing the combined inertias of the system then determines the opposing torque from the calculated slope of the velocity curve. The friction torque for this system is 0.2 lb-in. Adding this offset to the bang-bang function to drive the real system does in fact prevent it from backing up. This time the nominal 29 degree rotation actually completes 27 degrees, the error possibly due to higher starting friction. However, as Fig. 7.10(b) suggests, the residual vibration is nearly the same as before for the undamped forcing function (see Fig. 6.5(b)).

When this same idea is applied to the ramped sinusoid functions, even more disappointing results appear. As the torque curve of Fig. 7.11(a) indicates, the addition of the offset torque to the waveform introduces small step discontinuities at the start and stop transitions. This generates larger amplitude residual vibration (Fig. 7.11(b)) than the uncompensated ramped sinusoid (see Fig. 6.7(b)). The system does, however, complete the move without backing up, and turns through 25 degrees compared to only 17 degrees without compensation. Increasing the input torque to compensate for friction therefore improves the angular accuracy but is inadequate to significantly reduce the residual vibration of either the bang-bang or the ramped sinusoid functions.

7.3. Hysteresis Damping

Another possible explanation for the observed nonideal behavior is the presence of hysteresis damping in the aluminum shafts. A check on the maximum angular deformations generated using peak torque of 3 lb-in indicates torsional shear stresses of 830 psi. Since the aluminum used here has a 0.2 % yield stress of 8350 psi, the worst operating point is still an order of magnitude smaller than the yield limit. However, if the stress-strain curve begins to deviate from the linear region at a point well below the 0.2 % yield point, then there is a possibility that hysteresis is taking

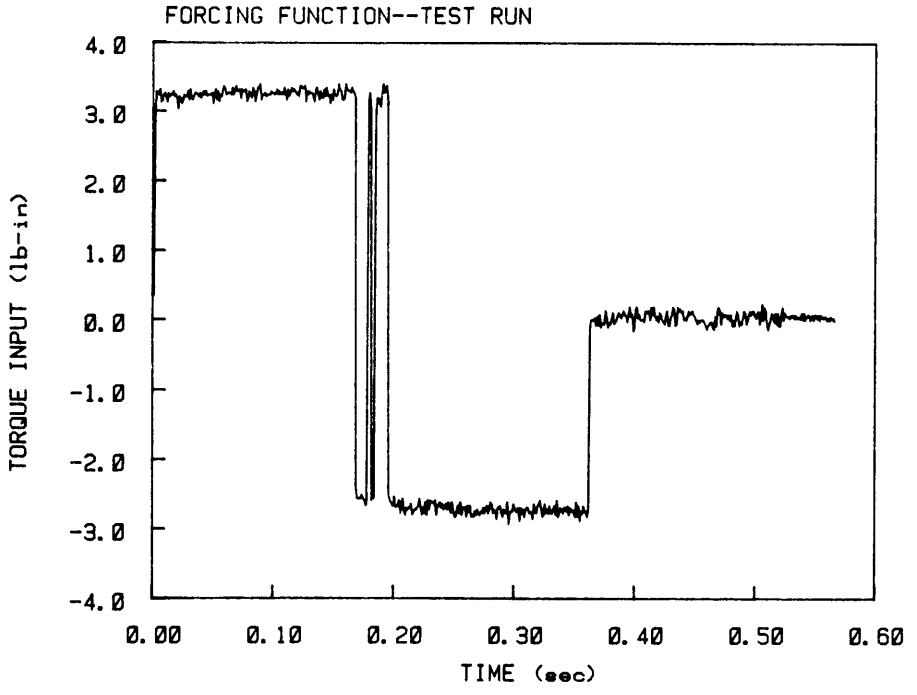

(a)

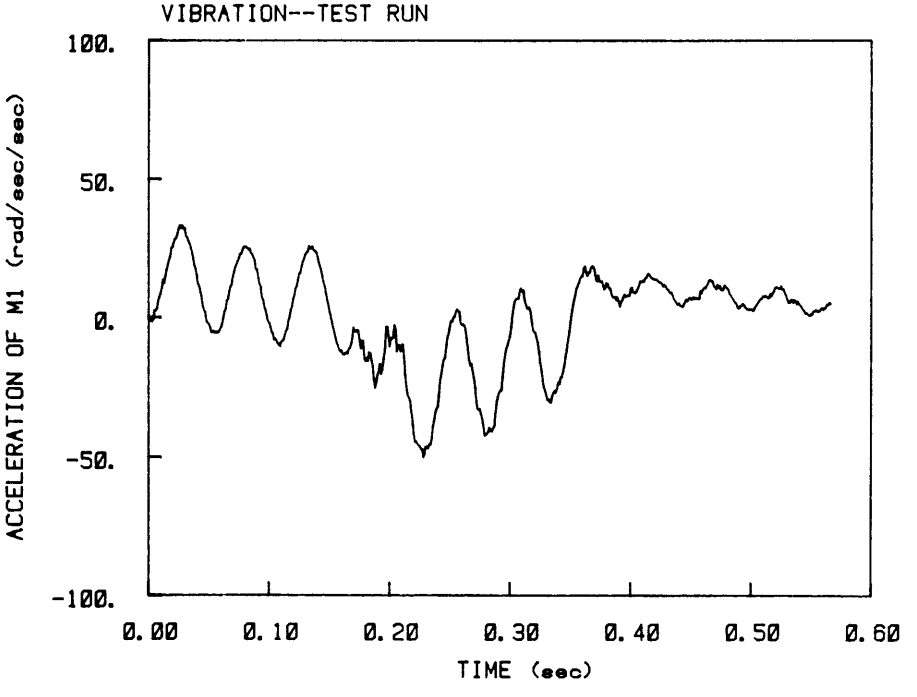

(b)

Figure 7.10: Actual Offset Bang-Bang Response:(a)Torque Input. (b)Acceleration Response.

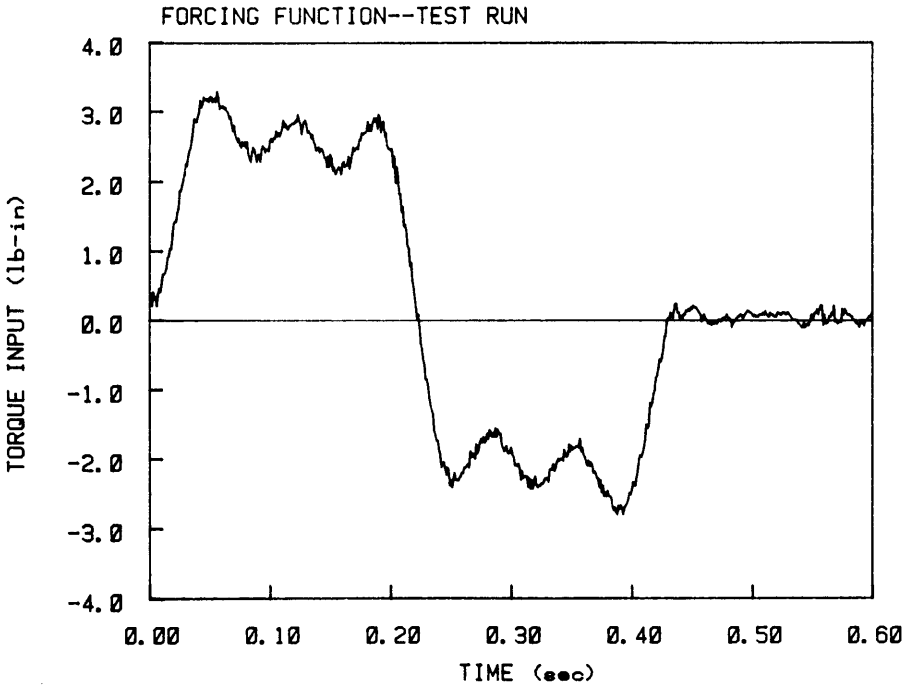

(a)

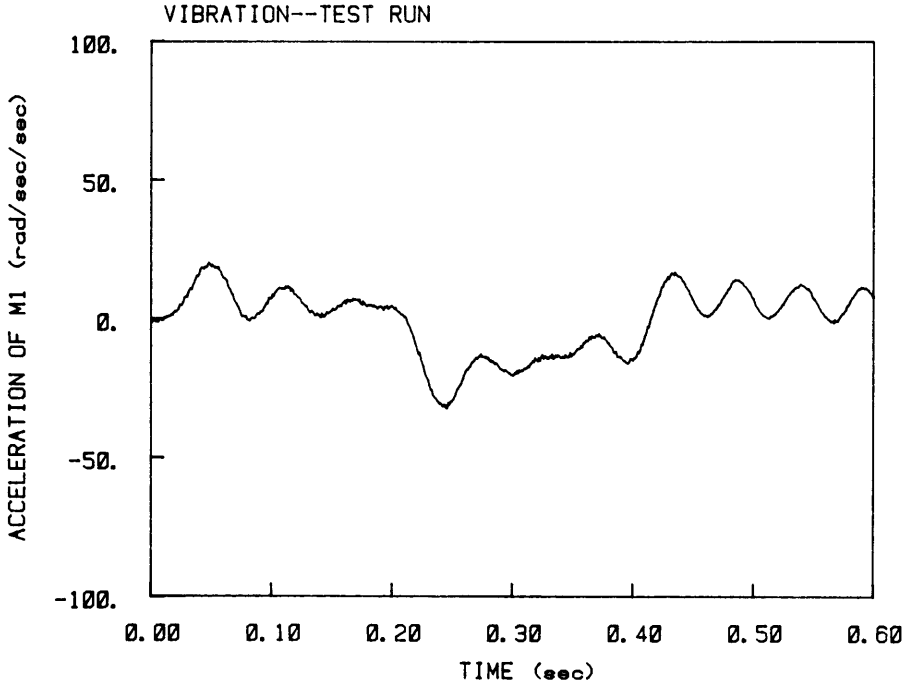

(b)

Figure 7.11: Actual Offset Ramped Sinusoid Response:(a)Torque Input. (b)Acceleration Response.

place. At each torsional oscillation, the shaft would twist back to a position just short of its initial position. It would therefore act as a damper on the oscillation. To the extent that this phenomenon is taking place, it can be improved simply by reducing the peak torque used to drive the system.

Chapter 8.

Adjustment For Parameter Errors

The preceding discussion of system damping indicates that attempts to compensate for dissipation in the test system provide no significant improvement in residual vibration response. The comparisons drawn in chapter 6 between experimental results and theoretical predictions of square wave response indicate that an error in some of the parameters might contribute to the observed residual vibration. The dimensional analysis discussed in chapter 4 revealed that only two dimensionless parameters determined the amount of residual vibration: ωT_s and ω_r. It also turned out that, for $\omega_r > 4$, the response is insensitive to ω_r. Since in the actual system, $\omega_r = 117.3/19.5 = 6.0$, this criterion is satisfied here. So only a variation in ωT_s can cause deviations from predicted response, as long as the linear, undamped model adequately describes the real system.

A plot of the predicted square wave amplitude as a function of ωT_s with $\omega_r = 6.0$ is shown in Fig. 8.1. The vibration amplitude varies periodically with ωT_s and the separation between peaks is given by

$$\omega t = \omega_2 t = 4\pi. \tag{8.1}$$

If the separation time t in the actual data were known, then it would be easy to calculate a value for ω_2 which matches the observed results with the predictions using the linear model. Figure 8.2 shows the experimental square wave amplitude, this time plotted as a function of T_s, rather than move angle, as was the case in Fig. 6.8(a). The separation between peaks is again uniform, as predicted, and

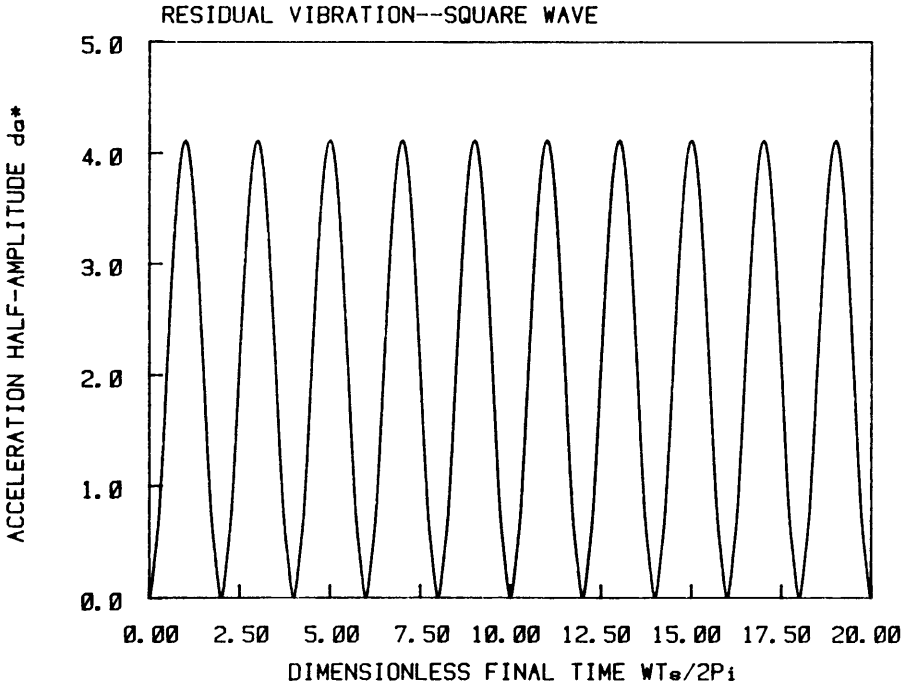

Figure 8.1: Predicted Square Wave Amplitude for the Experimental System

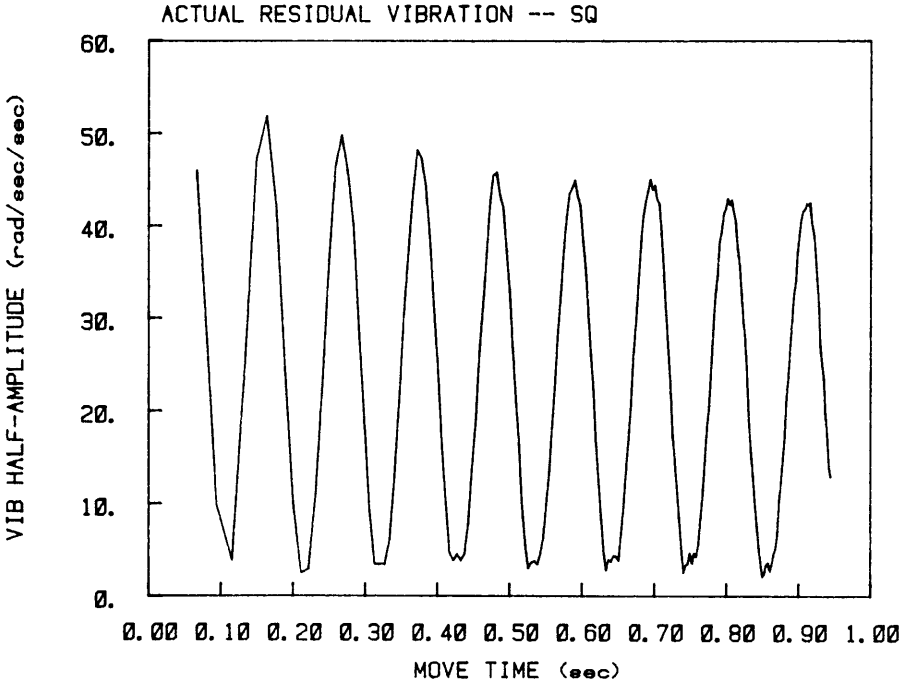

Figure 8.2: Actual Square Wave Amplitude for the Experimental System

measures $t = 0.107$ sec, which gives a predicted value for the fundamental frequency of

$$\omega_2 = \frac{4\pi}{t} = 117.44 \text{ rad/sec} = 18.7 \text{ Hz}. \tag{8.2}$$

This value is 4 % smaller than that suggested by the transfer function plot of Fig. 6.2.

One possible explanation for this discrepancy is the relatively large frequency increments used by the HP Analyzer. When the frequency window is set from 0 to 200 Hz, which was done in order to see the 117.3 Hz resonance, these increments are 0.8 Hz, since the Analyzer subdivides the interval into 256 points. Thus, some of the error can be attributed to lack of sufficient resolution in the transfer function. A new set of data, using a window from 0 to 50 Hz, with a resolution of 0.2 Hz, gives a peak at a frequency of 18.9 Hz, closer to the predicted value. This transfer function, taken while impacting and measuring from the large end disk, is shown in Fig. 8.3(a). Another transfer function, generated with lower impacting forces, is shown in Fig. 8.3(b). Notice that the resonance peak shifts to the left with increasing force. This suggests that a nonlinearity is present in the system, as discussed by Halvorsen and Brown [35]. Nonetheless, the preceding analysis gives an alternative method for calculating the fundamental frequency simply by measuring square wave residual amplitudes over a range of moves.

A new set of forcing functions, determined using this corrected frequency value, give significantly lower residual vibration amplitudes. Response plots and the corresponding torque waveforms are shown in Figures 8.4 to 8.6 using the square wave, bang-bang, and ramped sinusoid functions for a 29 degree rotation. This time, with a more precise value of ω_2, the bang-bang function produces a residual vibration amplitude less than 10 % of the square wave amplitude, while the ramped sinusoid produces less than 7 % of the square wave amplitude. Both response amplitudes represent a 50 % improvement over previous tests using erroneous ω_2.

These results become even more convincing when evaluated over the same 200-degree range of rotations as before. Figures 8.7 to 8.9 show these composite

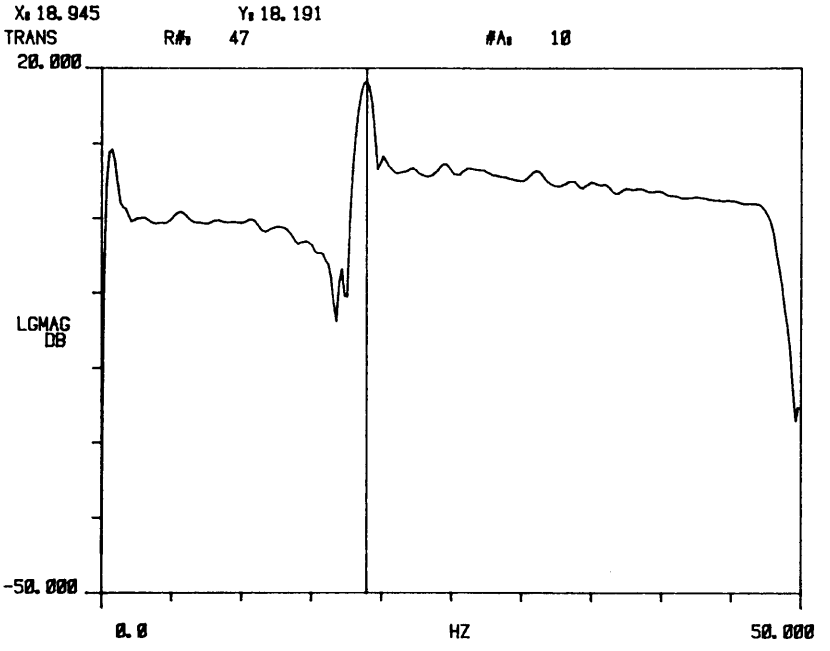

(a)

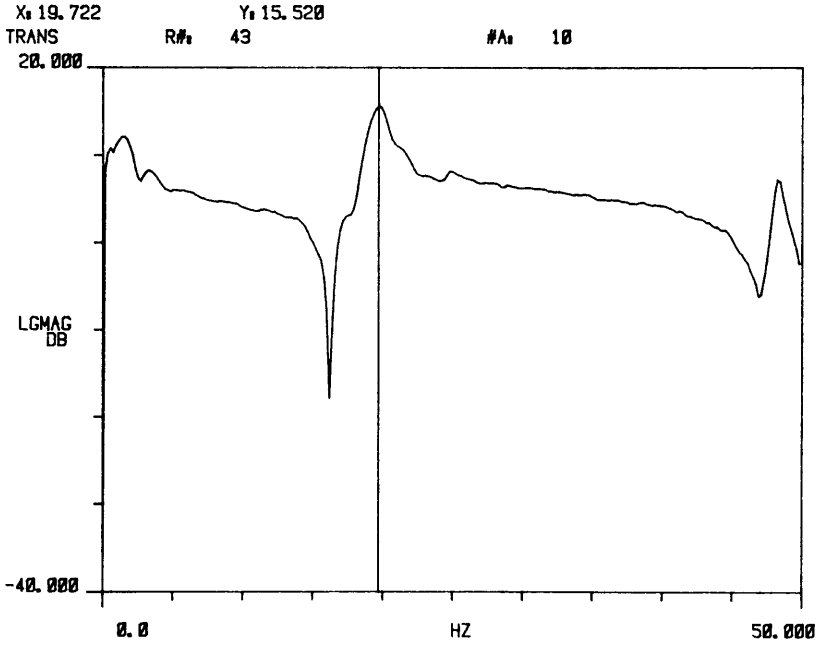

(b)

Figure 8.3: Transfer Function Magnitudes:(a)Large Impacting Force.(b)Small Impacting Force.

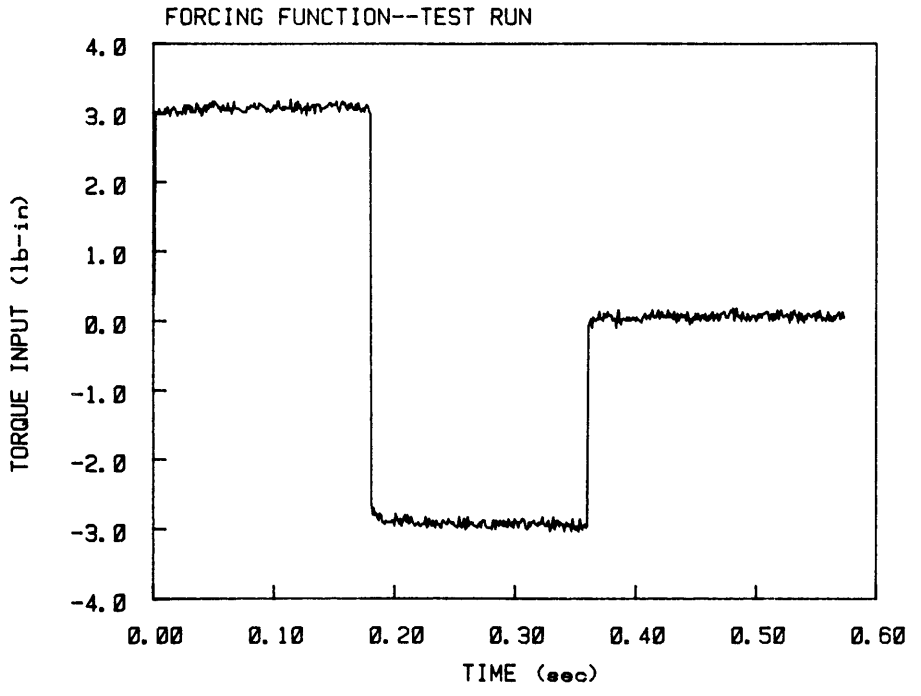

(a)

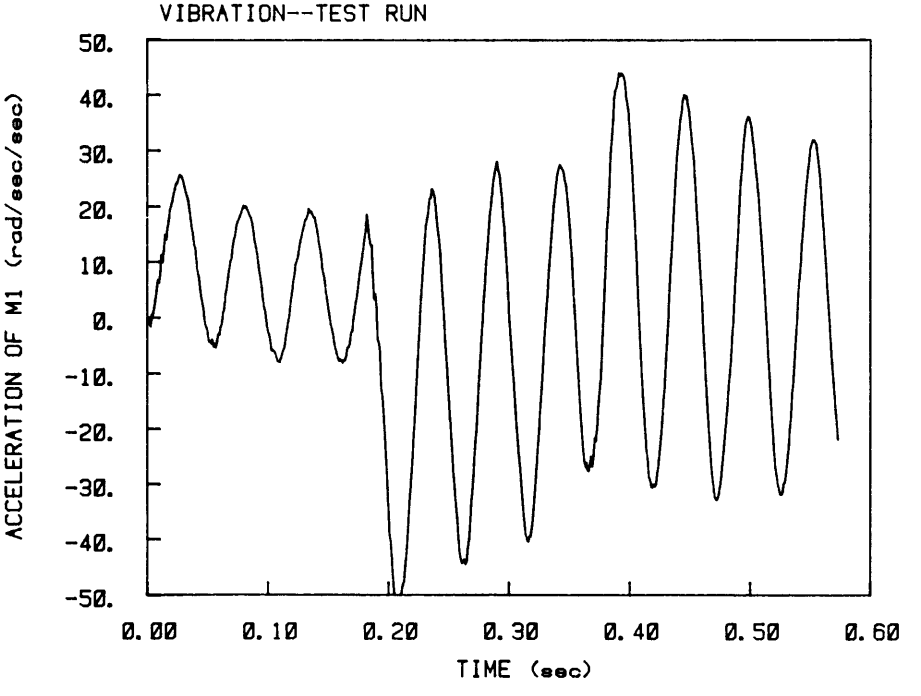

(b)

Figure 8.4: Square Wave Response:(a)Torque Input.(b)Acceleration Response.

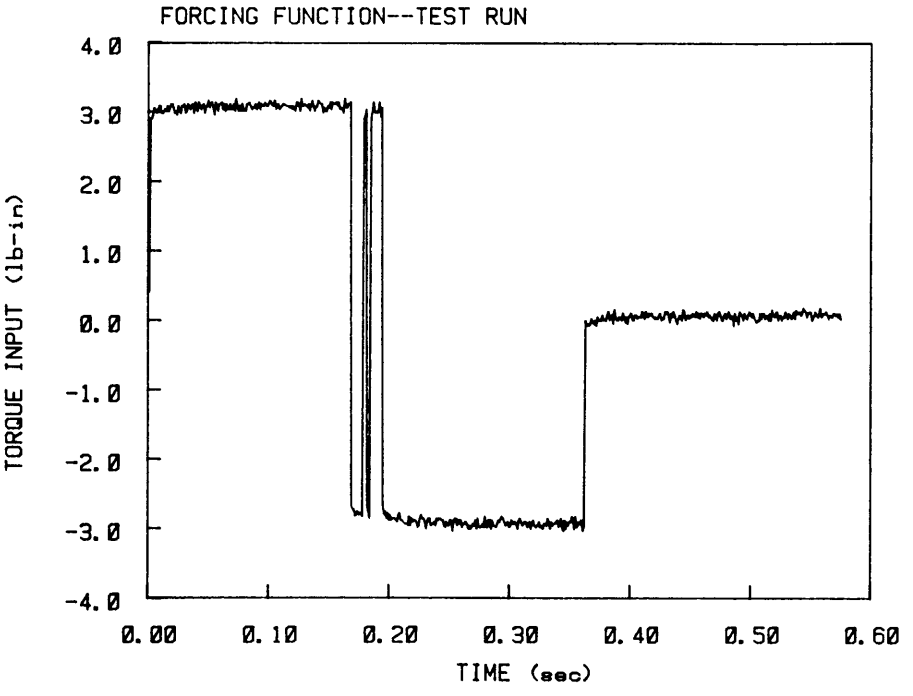

(a)

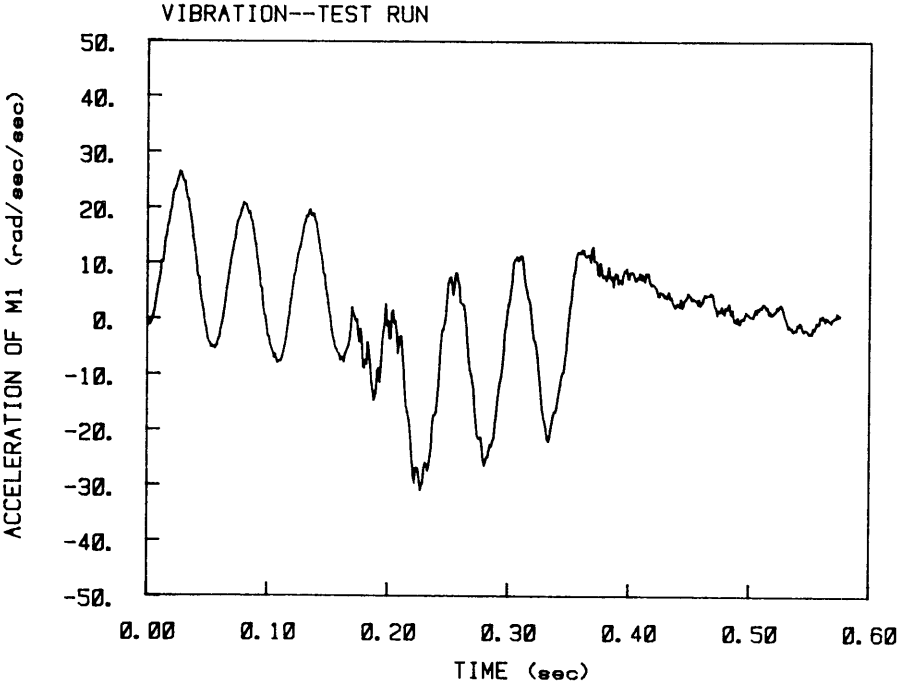

(b)

Figure 8.5: 5-Switch Bang-Bang Response:(a)Torque Input.(b)Acceleration Response.

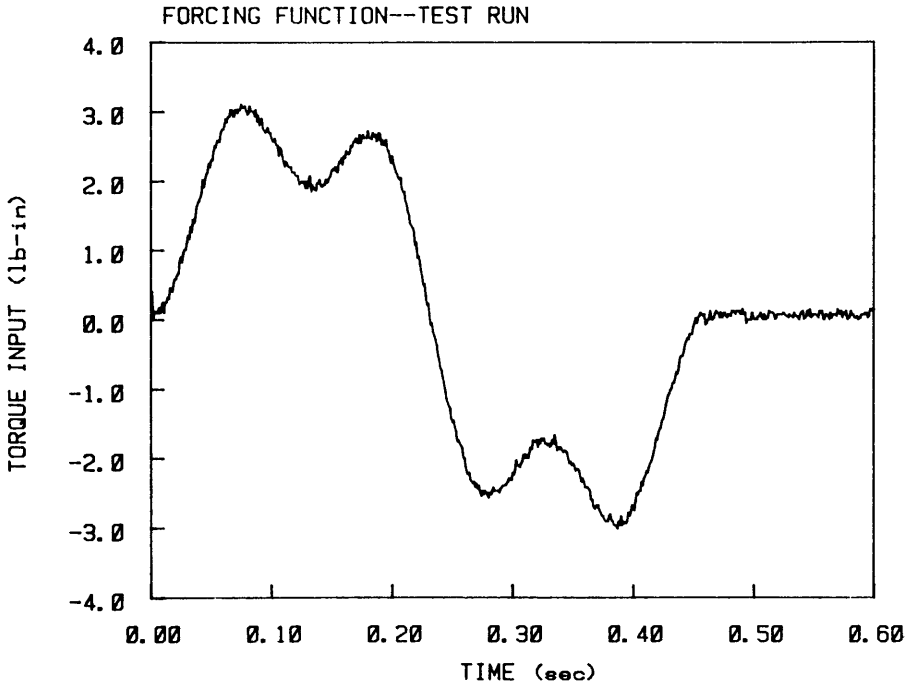

(a)

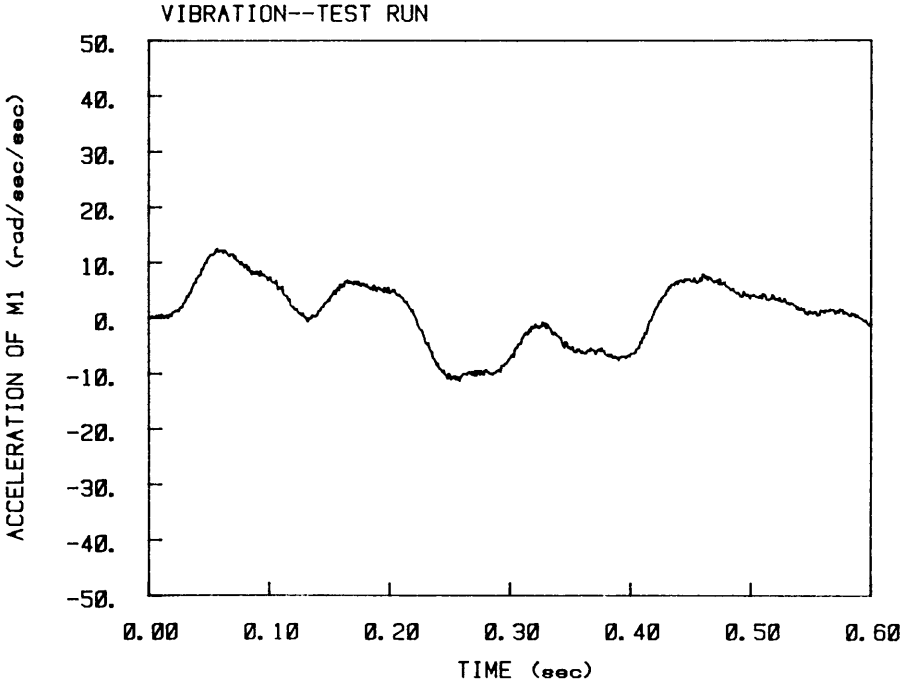

(b)

Figure 8.6: Ramped Sinusoid Response:(a)Torque Input.(b)Acceleration Response.

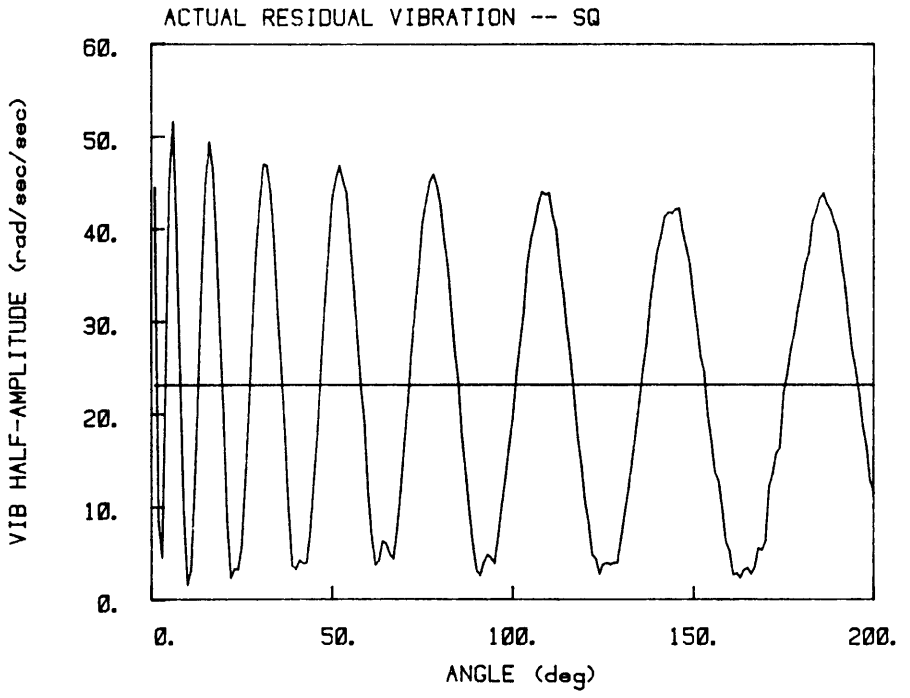

Figure 8.7: Square Wave Vibration

results for the three forcing functions. This time, the mean bang-bang amplitude is significantly lower, only 22.5 % of the mean square wave amplitude, representing a 75 % improvement as a result of fine-tuning ω_2. The ramped sinusoid functions do even better, giving a mean amplitude of only 12 % of the square wave mean, a 60 % improvement on earlier results.

These results emphasize the importance of a precise estimate of the fundamental system frequency to generate forcing functions which minimize residual vibration. But even without any further refinement of the idealized system model, these results show significant attenuation of residual vibration. In other words, factors such as system damping, digitizing error, finite current rise time, or even system nonlinearities have less effect on vibration than the accuracy of measured ω_2. This speaks well for the simplified analysis used here, since it suggests that time is better spent in accurately establishing ω_2 than in complicating the model to incorporate many extraneous factors. In addition, since the square wave response tests the system in its intended mode of operation, it gives precise values of ω_2 despite nonlinearities

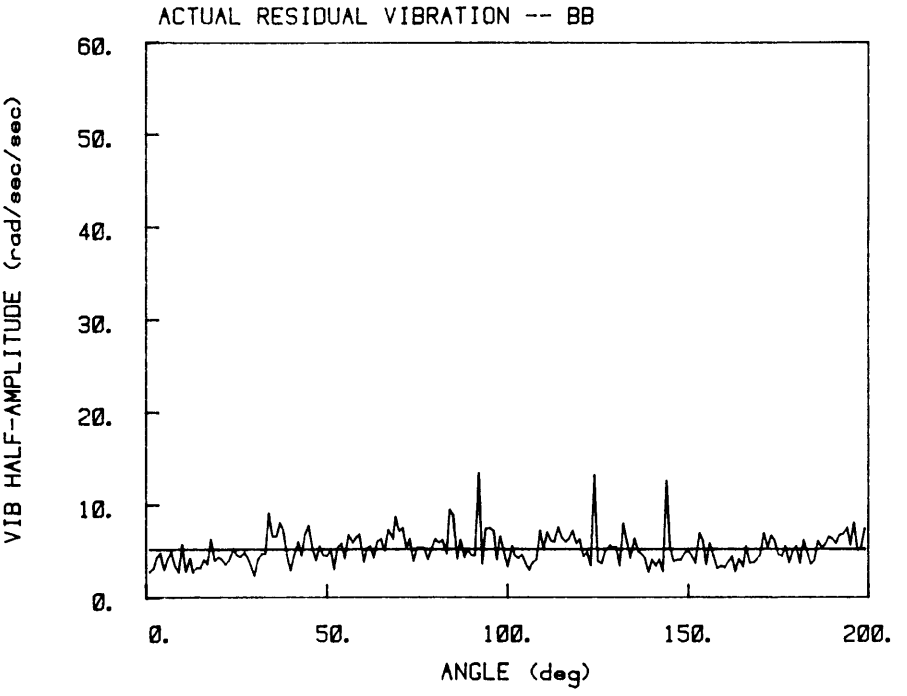

Figure 8.8: Bang-Bang Vibration

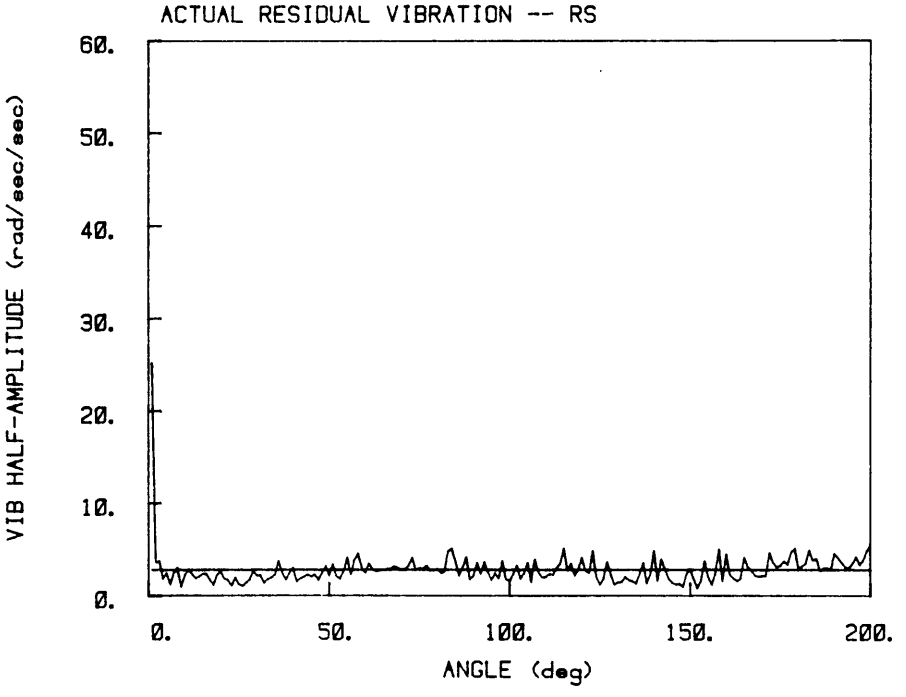

Figure 8.9: Ramped Sinusoid Vibration

which make transfer function determination difficult.

In practice, zero residual vibration is impossible to achieve. But, for each application, an upper bound on allowable residual vibration can be specified. Then a compromise must be made between faster functions which require some additional settling time to come within this bound, and slightly slower functions which will reach the desired position already within the prescribed vibration limits. In the tests presented here, the bang-bang function gives faster move times with slightly higher residual vibration than the corresponding ramped sinusoid functions. Which of these functions ultimately proves to be time-optimal when inherent settling time is included depends on the individual application.

Chapter 9.

Conclusions and Future Work

Two forcing functions have been derived to move a three-mass system quickly from one point to another with a minimum of residual vibration. The first function is a bang-bang function which always switches between peak force in either direction. It can be shown that the required number of switches is $2N - 1$ where N is the number of masses in the system. For the system under investigation, this forcing function is time-optimal and simulations verify that the residual vibration has been eliminated. The other function consists of sums of harmonics of ramped sinusoids chosen to approximate a square wave. The virtue of this function is that it has zero slope at beginning and end of the move, thus minimizing the tendency to excite resonance. This is verified by the simulations. A look at the frequency spectra of sums of different numbers of terms gives an indication of the maximum number of terms to be added without adversely affecting residual vibration. A comparison of these two types of functions shows that the bang-bang is very sensitive to parameter errors. The ramped sinusoid is not only more robust but also very nearly time-optimal, only increasing move times at most by 25 % over most of the working range.

A test fixture which closely matches the theoretical model was designed and built to evaluate these ideas experimentally. It consists of a DC motor actuator and a system consisting of two massive inertias connected by flexible aluminum shafts. Although experimental vibration amplitudes are larger than predicted, both derived

forcing functions are successful at attenuating the residual vibration compared to a square wave. When vibration amplitudes at many moves are averaged, the bang-bang functions reduce residual vibration amplitudes to only 22.5 % of mean square wave amplitude, while the ramped sinusoid functions have residual amplitudes of only 12 % of mean square wave amplitude. Thus, almost an order-of-magnitude reduction in residual vibration is possible in practice, when compared with mean square wave amplitudes.

An investigation of system damping aimed particularly at improving the bang-bang response shows little apparent reduction in residual vibration. A new bang-bang function derived to accomodate viscous damping does not improve the response. Adjusting the input torque to compensate for the friction torque eliminates the observed reversal of the masses but does not reduce the vibration. The effect of hysteresis damping in the shafts is as yet unknown.

Attempts to improve vibration response by including damping in the system model failed. But comparison of predicted and actual square wave vibration amplitudes suggested that the value of ω_2 used for the tests was in error. A new, slightly lower value was calculated from the square wave response data and used to generate new forcing functions. Improving the accuracy of ω_2 by only 4 % improved residual vibration by at least 60 %, indicating that the dominant source of error is inaccuracy in the determination of the fundamental frequency ω_2.

Since some unpredicted vibration still remains, future work should involve generating a more accurate model of the experimental system. A determination of the motor transfer function is important to identify any stray effects such as ripple torque. In order to compensate for disturbances or variations in parameters, the control scheme should be made closed-loop, feeding back at least position information to ensure accurate displacements. Since real systems tend to have higher damping than modeled here, the vibration as a result of an initial step function is almost all decayed before the end of the move. In addition, real systems have velocity limits which preclude using maximum force at all times. One scenario would

thus have the system attain peak velocity with a simple step input function, with any induced vibration decaying while at constant speed. Then a similar analysis as suggested herein would take the system from a constant velocity to its final position at rest with a minimum of residual vibration. The final and most important contribution still to be made is to extend this work to the case when the resonances of a structure are continually changing as the device is moved from one position to another. Since this is what happens when actual cartesian robots are moved, a solution to this problem would go a long way toward accomplishing the goal of high-speed motion with minimum vibration.

Appendix A.

Proof of System Controllability

The bang-bang forcing function always gives time-optimal trajectories from initial state to final state as long as the system is controllable. To check for controllability, the following criterion must be satisfied,

$$\text{Rank}\left[\mathbf{b}, \mathbf{Ab}, \mathbf{A}^2\mathbf{b}, \ldots, \mathbf{A}^{n-1}\mathbf{b}\right] = n \qquad (A.1)$$

where n is the order of the system and the matrices $\mathbf{A}$ and $\mathbf{b}$ are given by

$$\dot{\mathbf{x}} = \mathbf{A}\,\mathbf{x} + \mathbf{b}\,u \qquad (A.2)$$

where

$$\mathbf{A} = \begin{bmatrix} 0 & 1 & 0 & 0 & 0 & 0 \\ -\frac{k_1}{m_1} & 0 & \frac{k_1}{m_1} & 0 & 0 & 0 \\ 0 & 0 & 0 & 1 & 0 & 0 \\ \frac{k_1}{m_2} & 0 & -\frac{k_1+k_2}{m_2} & 0 & \frac{k_2}{m_2} & 0 \\ 0 & 0 & 0 & 0 & 0 & 1 \\ 0 & 0 & \frac{k_2}{m_3} & 0 & -\frac{k_2}{m_3} & 0 \end{bmatrix}, \quad \mathbf{b} = \begin{bmatrix} 0 \\ 0 \\ 0 \\ 0 \\ 0 \\ \frac{1}{m_3} \end{bmatrix}.$$

The controllability criterion to be satisfied by this system is

$$\text{Rank}\left[\mathbf{b}, \mathbf{Ab}, \mathbf{A}^2\mathbf{b}, \mathbf{A}^3\mathbf{b}, \mathbf{A}^4\mathbf{b}, \mathbf{A}^5\mathbf{b}\right] = 6 \qquad (A.3)$$

and when the above matrices are substituted into the controllability matrix, its determinant is positive. Thus the rank of the matrix is full, i.e. rank = 6, and controllability is proved.

Appendix B.

Derivation of Frequency Spectra for Ramped Sinusoids

In order to determine the frequency content of the ramped sinusoid time functions, take their Fourier Transform,

$$\mathcal{F}(\omega) = \int_0^{T_f} F(t) e^{-j\omega t}\, dt \qquad (B.1)$$

where

$$F(t) = \frac{F}{SF} \sum_{l=1}^{L} \frac{B_l}{\alpha_l^2} \left[\lambda_l (t - T_f/2) - \sin \lambda_l t + \frac{\alpha_l}{2} \cos \lambda_l t \right]. \qquad (B.2)$$

Note that the time function is zero everywhere except during the interval $0 < t < T_f$, which gives the limits on the integration. When this integral is solved, the magnitude of the frequency spectrum is given by

$$\frac{|\mathcal{F}(\omega)|}{FT_f} = \left| \frac{2\sin(\omega T_f/2) - \omega T_f \cos(\omega T_f/2)}{SF(\omega T_f)^2} \sum_{l=1}^{L} \frac{B_l \alpha_l}{\alpha_l^2 - (\omega T_f)^2} \right|. \qquad (B.3)$$

This expression can be plotted as a function of ωT_f, where T_f now simply nondimensionalizes a general frequency ω. To be useful for determining the number of terms L, the final move time T_f must be known in order to locate the resonant frequencies in the spectra. But T_f is a function of L:

$$T_f = \sqrt{\frac{-12(m_1 + m_2 + m_3)x_f}{\frac{F}{SF} \sum_{l=1}^{L} B_l/\alpha_l}}. \qquad (B.4)$$

If the factor which depends on L is separated from T_f, the result is an expression in T_s, the square wave move time

$$T_f = \Gamma T_s \tag{B.5}$$

where

$$\Gamma = \sqrt{\frac{-3}{\frac{1}{SF}\sum_{l=1}^{L} B_l/\alpha_l}} \tag{B.6}$$

and

$$T_s = \sqrt{4(m_1 + m_2 + m_3)x_f/F}. \tag{B.7}$$

Replacing dimensionless frequency ωT_f, using these substitutions, gives

$$\omega T_f = \Gamma \omega T_s \tag{B.9}$$

The resulting expression for the frequency spectrum is

$$\frac{|\mathcal{F}(\omega)|}{FT_s} = \left| \Gamma \frac{2\sin(\Gamma \omega T_s/2) - \Gamma \omega T_s \cos(\Gamma \omega T_s/2)}{SF\,\Gamma^2(\omega T_s)^2} \sum_{l=1}^{L} \frac{B_l \alpha_l}{\alpha_l^2 - \Gamma^2(\omega T_s)^2} \right|. \tag{B.10}$$

Thus the amplitude of the frequency spectrum can be plotted as a function of dimensionless frequency ωT_s. So for a given set of masses, input force, and move distance, T_s is specified, which locates the resonant frequencies in the spectra.

Appendix C.

Uniqueness of Solutions to Nonlinear Equations

Since the equations which are to be satisfied by the switch times are both nonlinear and transcendental, it is nearly impossible to determine where solutions should occur. According to equations (2.31) to (2.33), three expressions in ωdt_1, ωdt_2, and ωT_f must be satisfied simultaneously:

$$f(\omega dt_1, \omega dt_2, \omega T_f) = -2\cos\omega dt_1 + 2\cos\omega dt_2 + \cos(\omega T_f/2) - 1 = 0 \qquad (C.1)$$

$$g(\omega dt_1, \omega dt_2, \omega T_f) = -2\cos\omega_r\omega dt_1 + 2\cos\omega_r\omega dt_2 + \cos(\omega_r\omega T_f/2) - 1 = 0 \qquad (C.2)$$

$$h(\omega dt_1, \omega dt_2, \omega T_f) = -2\omega dt_1^2 + 2\omega dt_2^2 + (\omega T_f/2)^2 - (\omega T_s/2)^2 = 0 \qquad (C.3)$$

If it were possible to substitute two of these equations into the third to eliminate two of the unknowns, a single function would result in the single unknown whose zeros would determine the solutions. Unfortunately, it is not possible to do that here. However, one unknown can be eliminated by combining (C.1) and (C.3):

$$\omega dt_2 = \cos^{-1}\left[\cos\sqrt{\omega dt_2^2 + (\omega T_f^2 - \omega T_s^2)/8} - \frac{1}{2}\cos(\omega T_f/2) + \frac{1}{2}\right] \qquad (C.4)$$

For a specified value of ωT_s and a given value of ωT_f, an iteration scheme will converge on the correct value for ωdt_2. Then ωdt_1 is given by

$$\omega dt_1 = \sqrt{\omega dt_2^2 + (\omega T_f^2 - \omega T_s^2)/8}. \qquad (C.5)$$

Using a range of values for ωT_f starting with ωT_s and plotting $g(\omega dt_1, \omega dt_2, \omega T_f)$ as a function of ωT_f will locate the zeros of g. Figure C.1 shows such a plot for

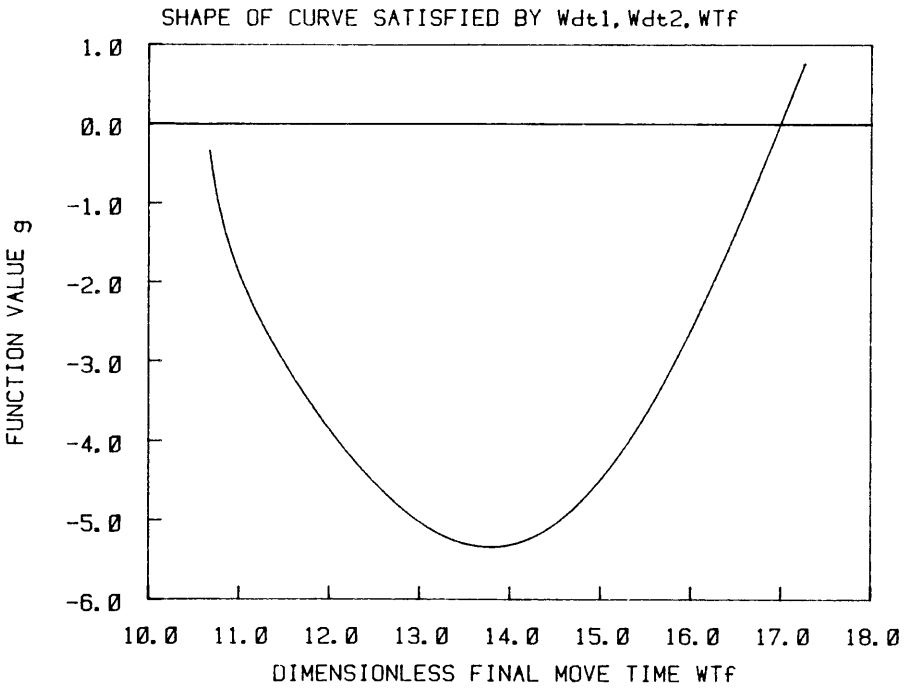

Figure C.1: Solutions for ωT_f with $\omega T_s = 10.5$

a value of $\omega T_s = 10.5$. Notice that this curve does not cross zero until it passes a considerable distance to the right to very large values of ωT_f.

It would seem plausible that perhaps a solution might be found further to the left of the curve. However, when $f(\omega dt_1, \omega dt_2, \omega T_f)$ is plotted as a function of ωdt_2, given that $\omega T_f = 10.6$ and using equation (C.4) to determine ωdt_1, it is apparent that f has no zeros for any acceptable values of ωdt_2 (Fig. C.2).

It turns out that Fig. C.1 is not unique, since the iteration on ωdt_2 involves an arccosine function, which is not unique. Plotting f as above with $\omega T_f = 13.0$ gives the curve shown in Fig. C.3. This indicates that there are two more solutions to ωdt_2 which might conceivably give smaller values for ωT_f with $\omega T_s = 10.5$. However, close consideration will reveal that both of these choices for ωdt_2 give $\omega dt_2 > \omega T_f$, which requires that the switch times occur before the forcing function even begins. Thus, the only solutions to the simultaneous equations (C.1) to (C.3) are those switches which give a very large value for the final time ωT_f.

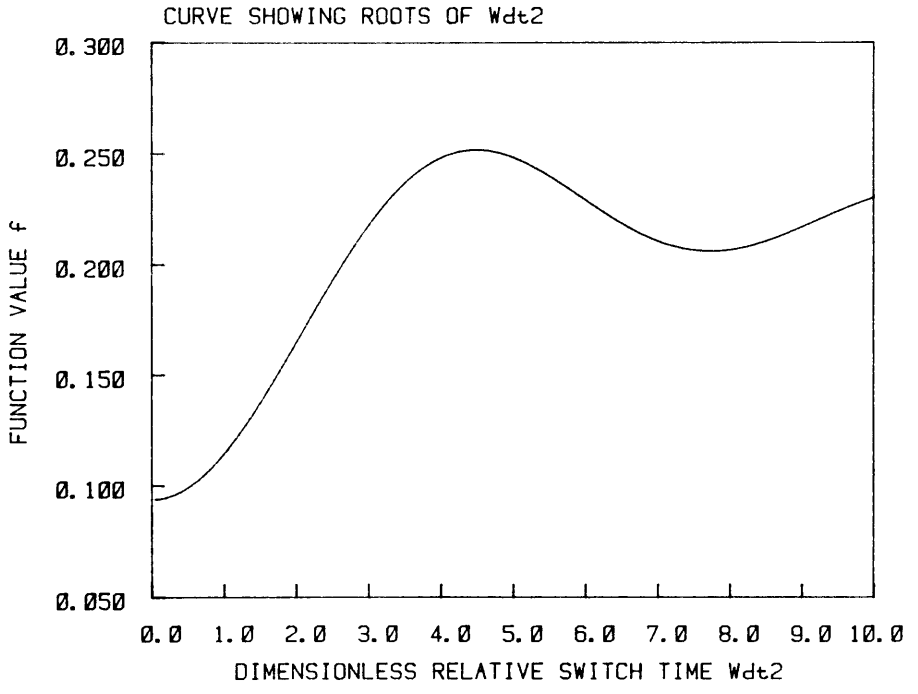

Figure C.2: Solutions for ωdt_2 when $\omega T_f = 10.6$ and $\omega T_s = 10.5$

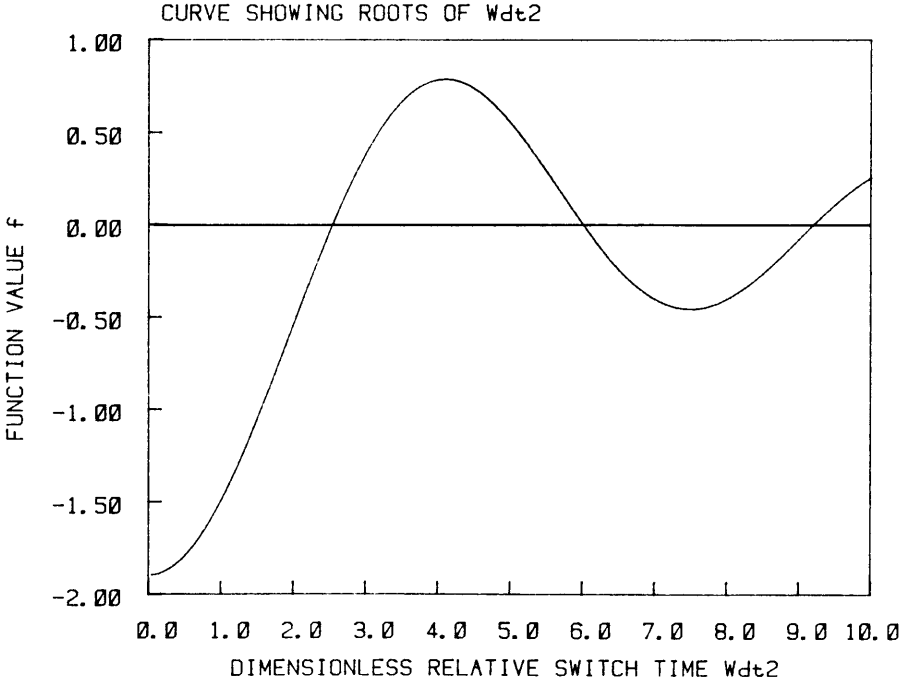

Figure C.3: Solutions for ωdt_2 when $\omega T_f = 13.0$ and $\omega T_s = 10.5$

REFERENCES

[1] Aspinwall, D. M., "Acceleration Profiles for Minimizing Residual Response," ASME *Journal of Dynamic Systems, Measurement, and Control*, Vol. 102, No. 1, Mar. 1980, pp. 3–6.

[2] Swigert, C. J., "Shaped Torque Techniques," *Journal of Guidance and Control*, Vol. 3, No. 5, Sept.–Oct. 1980, pp. 460–467.

[3] Sangveraphunsiri, V. and Book, W. J., "An Approach to the Minimum Time Control of a Simple Flexible Arm," ASME *Winter Annual Meeting*, Boston, Mass., Nov. 1983.

[4] Lin, J. G., et al., "Output Feedback Control of Large Space Structures: An Investigation of Four Design Methods," *Second AIAA Symposium on Dynamics and Control of Large Flexible Spacecraft*, June 1979, pp. 1–18.

[5] Meirovitch, L., Van Landingham, H. F., and Öz, H., "Distributed Control of Spinning Flexible Spacecraft," *First AIAA Symposium on Dynamics and Control of Large Flexible Spacecraft*, June 1977, pp. 249–269.

[6] Balas, M. J., "Active Control of Flexible Systems," *First AIAA Symposium on Dynamics and Control of Large Flexible Spacecraft*, June 1977, pp. 217–236.

[7] Balas, M. J., and Canavin, J. R., "An Active Modal Control System Philosophy for a Class of Large Space Structures," *First AIAA Symposium on Dynamics and Control of Large Flexible Spacecraft*, June 1977, pp. 271–285.

[8] Turner, J. D., and Junkins, J. L., "Optimal Large Angle Single Axis Rotational Maneuvers of Flexible Spacecraft," *Second AIAA Symposium on Dynamics and Control of Large Flexible Spacecraft*, June 1979, pp. 91–110.

[9] Caglayan, A. K., Van Landingham, H. F., and Sathe, S. G., "A Procedure for Optimal Control of Flexible Surface Vibrations," *Second AIAA Symposium on Dynamics and Control of Large Flexible Spacecraft*, June 1979, pp. 129–144.

[10] Gran, R., and Rossi, M., "Closed-Loop Order Reduction for Large Structures Control," *Second AIAA Symposium on Dynamics and Control of Large Flexible Spacecraft*, June 1979, pp. 443–457.

[11] Joshi, S. M., and Groom, N. J., "Controller Design Approaches for Large Space Structures Using LQG Control Theory," *Second AIAA Symposium on Dynamics and Control of Large Flexible Spacecraft*, June 1979, pp. 35–50.

[12] Skelton, R. E., and Hughes, P. C., "Flexible Space Structure Model Reduction by Modal Cost Analysis," *Second AIAA Symposium on Dynamics and Control of Large Flexible Spacecraft*, June 1979, pp. 641–660.

[13] Gibson, J. S., "Convergence and Stability in Linear Modal Regulation of Flexible Structures," *Second AIAA Symposium on Dynamics and Control of Large Flexible Spacecraft*, June 1979, pp. 51–64.

[14] Sesak, J. R., Likins, P. W., and Coradetti, T., "Flexible Spacecraft Control by Model Error Sensitivity Suppression," *Second AIAA Symposium on Dynamics and Control of Large Flexible Spacecraft*, June 1979, pp. 349–368.

[15] Balas, M. J., "Enhanced Modal Control of Flexible Structures Via Innovations Feedthrough," *Second AIAA Symposium on Dynamics and Control of Large Flexible Spacecraft*, June 1979, pp. 677–700.

[16] Strunce, R. R., and Henderson, T. C., "Application of Modern Modal Controller Design to a Large Space Structure," *Second AIAA Symposium on Dynamics and Control of Large Flexible Spacecraft*, June 1979, pp. 661–675.

[17] Johnson, C. R., Jr., "Approaches to Adaptive Digital Control Focusing on the Second Order Modal Descriptions of Large, Flexible Spacecraft Dynamics," *Second AIAA Symposium on Dynamics and Control of Large Flexible Spacecraft*, June 1979, pp. 301–315.

[18] Benhabib, R. J., Iwens, R. P., and Jackson, R. L., "Active Vibration Control of a Flat Plate Using Model Reference Adaptive Techniques," *Second AIAA Symposium on Dynamics and Control of Large Flexible Spacecraft*, June 1979, pp. 317–329.

[19] Potter, J. E., and Ginter, S. D., "A New Concept in Adaptive Structural Control," *Second AIAA Symposium on Dynamics and Control of Large Flexible Spacecraft*, June 1979, pp. 331–348.

[20] Book, W. J., Maizza-Neto, O., and Whitney, D. E., "Feedback Control of Two Beam, Two Joint Systems with Distributed Flexibility," ASME *Journal of Dynamic Systems, Measurement, and Control*, Vol. 97, No. 4, Dec. 1975, pp. 424–431.

[21] Gupta, N. K., and Lyons, M. G., et al., "Frequency-Shaping Methods in Large Space Structures Control", AIAA *Guidance and Control Conference*, August 1981.

[22] Bellman, R., Glicksberg, I., and Gross, O., "On the 'Bang-Bang' Control Problem," *Quarterly of Applied Mathematics*, Vol. 14, No. 1, 1956, pp. 11–18.

[23] LaSalle, J. P., "The Time Optimal Control Problem," *Contributions to Differential Equations*, Vol. 5, 1960, pp. 1–24.

[24] Lee, E. B., and Markus, L., *Foundations of Optimal Control Theory*, Wiley, New York, 1967, pp. 143–145.

[25] Thomson, W. T., *Theory of Vibration with Applications*, Prentice-Hall, Inc., Englewood Cliffs, N. J., 1972, pp. 178–180.

[26] Meirovitch, L., *Elements of Vibration Analysis*, McGraw-Hill Book Co., New York, 1975, pp. 146–148.

[27] Bushaw, D. W., "Optimal Discontinuous Forcing Terms," *Contributions to the Theory of Nonlinear Oscillations*, Princeton University Press, Princeton, N. J., Vol. 4, 1958, pp. 29–52.

[28] Ryan, E. P., *Optimal Relay and Saturating Control System Synthesis*, IEE Control Engineering Series 14, Peter Peregrinus, Ltd., London, 1982, pp. 158–211.

[29] Athanassiades, M., and Smith, O. J. M., "Theory and Design of High-Order Bang-Bang Control Systems," IRE *Transactions on Automatic Control*, Vol. AC-6, May 1961, pp. 125–134.

[30] Smith, F. B., Jr., "Time-Optimal Control of Higher-Order Systems," IRE *Transactions on Automatic Control*, Vol. AC-6, Feb. 1961, pp. 16–21.

[31] Lee, E. B., "Mathematical Aspects of the Synthesis of Linear Minimum Response-Time Controllers," IRE *Transactions on Automatic Control*, Vol. AC-5, Sept. 1960, pp. 283–290.

[32] Lee, E. B., and Markus, L., op. cit., pp. 132–137.

[33] Makino, H., et al., "Research and Development of the SCARA Robot," *Proceedings of the 4th International Conference on Production Engineering*, Tokyo, 1980, pp. 885–890.

[34] Knudsen, H. K., "An Iterative Procedure for Computing Time-Optimal Controls," IEEE *Transactions on Automatic Control*, Vol. AC-9, Jan. 1964, pp. 23–30.

[35] Halvorsen, W. G., and Brown, D. L., "Impulse Technique for Structural Frequency Testing," *Sound and Vibration*, Nov. 1977, pp. 8–21.

[36] Meckl, P. H., Active Damping in a Three-Axis Robotic Manipulator," ASME *Design and Production Engineering Technical Conference*, Dearborn, Mich., Sept. 1983, Paper No. 83-DET-80, accepted for publication in ASME *Journal of Vibration, Acoustics, Stress, and Reliability in Design.*